AN ANALYSIS OF THE SPECTRAL
DISTRIBUTION OF LIGHT QUASIELASTICALLY SCATTERED FROM HIGH
MOLECULAR WEIGHT POLYMER
SOLUTIONS IN THE LOWER CRITICAL
TEMPERATURE REGION

Dissertation for the Degree of Ph. D. MICHIGAN STATE UNIVERSITY SISTO NICHOLAS STISO 1974



This is to certify that the

thesis entitled

An Analysis of the Spectral Distribution of Light Quasi-elastically Scattered from High Molecular Weight Polymer Solutions in the Lower Critical Temperature Region

> presented by Sisto Nicholas Stiso

has been accepted towards fulfillment of the requirements for

Doctoral degree in Physical Chemistry

Major professor

O-7639



The high mole

dependence determine

ments was

Hig

cation-ca

cular wei

separated

according

fractions
polymer t

 ${
m Th}_4$

consisti

and a Ge

 $t_{ ext{emperat}}$

of the s

ABSTRACT

AN ANALYSIS OF THE SPECTRAL DISTRIBUTION OF LIGHT QUASI-ELASTICALLY SCATTERED FROM HIGH MOLECULAR WEIGHT POLYMER SOLUTIONS IN THE LOWER CRITICAL TEMPERATURE REGION

By

Sisto Nicholas Stiso

The spectral distribution of light elastically scattered from high molecular weight polymer solutions has been measured, and the dependence of the power spectrum on temperature and scattering angle determined. The frequency resolution required for these measurements was provided by light-beating spectroscopic techniques.

High molecular weight polyisobutylene was prepared by standard cation-catalyzed polymerization procedures. Fractions having molecular weights of 3.40 million, 6.34 million, and 13.4 million were separated from the bulk polymer by solvent-non-solvent precipitation according to Kamide's theory. Molecular weights of the different fractions were determined by Brillioun Spectroscopy. Solutions of the polymer to be analyzed were prepared in research grade normal pentane.

The light-beating spectrometer was of the laser homodyne type, consisting of a 4 mwatt He-Ne laser, an EMI 9558 photomultiplier tube and a General Radio Model 1910A wave analyzer and recorder. A special temperature control chamber was assembled which held the temperature of the sample constant to $\pm 0.003^{\circ}$ C at 75-80°C while measurements were

ing exp predict particl tempera Moderate point an tions we characte In molecular

being E

S

correlati cated tha

temperatu

manner (I

experiment The

systems ex expression

Where the (of the sam; being made. The performance of the instrument was checked by comparing experimentally determined diffusion coefficients with values predicted by theory for aqueous suspensions of polystyrene latex particles.

Spectra obtained for polymer solutions in the lower critical temperature region exhibited good fit to a single Lorentzian curve. Moderate deviations were observed at temperatures close to the critical point and at scattering angles greater than 45°. However, the deviations were believed to be instrumental artifacts rather than phenomena characteristic of the polymer solvent system.

In analyzing the data, the dependence of spectral halfwidth on molecular wright, scattering angle, and distance from the critical temperature was examined. The angular dependence in the conventional manner (Γ vs K^2), and with a correction term to account for long range correlation near the critical point (Γ/K^2 vs K^2). The results indicated that both analyses are applicable to the data, depending on the experimental conditions.

The diffusion coefficients determined for the polymer/solvent systems exhibited a temperature dependence characterized by the expression

$$D \alpha \left(\frac{T - T_c}{T_c} \right)^{\gamma}$$

where the critical exponent, γ , is function of the molecular weight of the sample.

AN ANALYSIS OF THE SPECTRAL DISTRIBUTION OF LIGHT QUASI-ELASTICALLY SCATTERED FROM HIGH MOLECULAR WEIGHT POLYMER SOLUTIONS IN THE LOWER CRITICAL TEMPERATURE REGION

Ву

Sisto Nicholas Stiso

A DISSERTATION

Submitted to
Michigan State University
in partial fulfillment of the requirements
for the degree of

DOCTOR OF PHILOSOPHY

Department of Chemistry

5 7 7 3 3°

To Kathy and Michael

The for the c

provided

The p

of the gla

gratefully
The as

for allowing company, an

The con

The enc

The sacting through under

will not go

ACKNOWLEDGMENTS

The author wishes especially to thank Professor J. B. Kinsinger for the counseling, support, and many helpful discussions which he provided during the course of this work.

The professional abilities afforded by Keki Mistry and Andy Seers of the glassblowing shop, and Chuck Hacker, Rus Geyer, and Dick Menke of the machine shop in fabricating the light-beating spectrometer are gratefully acknowledged.

The author is indebted to Dr. Jerome Greyson and to Ames Company for allowing him to complete his dissertation while working with the company, and for the use of the secretarial and duplicating facilities.

The comradeship of my fellow workers, Stuart Gaumer, Mary Tannehill, Henry Yuen, and Doug Nordhaus is much appreciated.

The encouragement, patience, and moral support offered by my wife, Kathy, will always be remembered.

The sacrifices endured by the author's parents to support him through undergraduate school and make this work possible, it is hoped, will not go unrewarded.

TABLE OF CONTENTS

	P	age
DE DI CAT	ON	ii
ACKNOWLE	DGMENT	ii
LIST OF	TABLES	v1
LIST OF	FIGURES	11
LIST OF	APPENDICES	Ĺx
CHAPTER		
I.	INTRODUCTION	1
	Historical	1
	Light-Beating	i
		12
.II.	THEORY	14
	Diffusion Equations	15
		16
		17
	Relating Concentration Fluctuations to the	
		18
	Tower operation of the percentage Bight	18
		20
	Considerations at the Critical Point	22
III.	INSTRUMENTATION	24
	General Description	24
	Sample Cells	24
		26
		31
		33
		33
		36

IV.

7.

VI.

MI.

REFERENCES

APPENDICES

		Page
IV.	TEMPERATURE MEASUREMENT AND CONTROL	39
	Equipment	39
	Calibration of Thermocouples	39
	Relationship of EMF to Temperature	43
	Correction for Thermal Lag	44
	Temperature Stability	44
v.	SAMPLE PREPARATION	49
	Preparation of Polyisobutylene	49
	Fractionation of Polymer	50
	Molecular Weight Determination	52
	Viscometry	52
	Brillioun Spectroscopy	58
VI.	EXPERIMENTAL	69
	Polystyrene Spheres	69
	Discussion of Spectra	69
	Statistical Treatment	69
	Measurement of Translational	
	Diffusion Coefficient	74
	Discussion of Results	79
	Polymer Solutions	81
	Critical Solution Temperatures	81
	Measuring Techniques	82
	Discussion of Spectra	83
	Temperature Dependence of Line Shape	83
	Angular Dependence of Line Shape	89
	Molecular Weight Dependence of Line Shape	89
	Determination of Diffusion Coefficients	98
	Summary	102
VII.	CONCLUSIONS	109
	Conclusions	109
	Suggestions for Future Research	111
REFERENCES		114
APPENDICES		117

TABLE

4.1

4.2 4.3

4.4

5.1

5.2

5.3 6.1

6.2

6.3

6.4

6.5

6.6

6.7

6.8

LIST OF TABLES

TABLE		Page
4.1	Calibration of a Copper-Constantan Thermocouple Against a Platinum Thermometer	42
4.2	Stability of Sample Temperature at 25.00°C	46
4.3	Stability of Sample Temperature at 55.00°C	47
4.4	Stability of Sample Temperature at 75.00°C	48
5.1	J Values for Various Concentrations of Polymer in Toluene	64
5.2	Light Scattering Parameters for Toluene	65
5.3	Differential Refractometer Constants Determined for Various Salt Solutions	66
6.1	Experimental Half-widths and Diffusion Coefficients for 0.109 micron Latex Particles	77
6.2	Experimental Half-widths and Diffusion Coefficients for 0.357 micron Latex Particles	78
6.3	Angular Dependence of Spectral Halfwidth, Fraction 1A(2a)	92
6.4	Angular Dependence of Spectral Halfwidth. Fraction 1A(3b)	93
6.5	Angular Dependence of Spectral Halfwidth. Fraction 2A(2)	94
6.6	Temperature Dependence of the Diffusion Coefficient for Fraction $1A(2a)$ $T_C = 76.75^{\circ}C$	99
6.7	Temperature Dependence of the Diffusion Coefficient for Fraction 1A(3b) T _C =77.60°C	99
6.8	Temperature Dependence of the Diffusion Coefficient for Fraction 2A(2) T _b =77.85°C	100

TABLE	Page	
6.9 Diffusion Coefficients and Correlation Lengt Correction for Long Range Correlation Applie		

FIGURE

1.1

1.2

1.3

3.1

3.2

3.3

3.4

3.5

3.6

4.1

4.2

5.1

5.2

5.3

5.4

5.5

5.6

LIST OF FIGURES

FIGURE		Page
1.1	Electromagnetic Beats	2
1.2	Laser Heterodyne Spectrometer	7
1.3	Laser Homodyne Spectrometer	9
3.1	Light Beating Spectrometer and Associated Equipment	25
3.2	Temperature Control Chamber	27
3.3	Sample Cell and Temperature Control Block	29
3.4	Laser and Collimating Optics	32
3.5	Detection System	35
3.6	Photomultiplier Tube Circuit Diagram	37
4.1	Constant Current Supply for Resistance Bridge	41
4.2	Plot of Sample Temperature vs Temperature of Copper Block	45
5.1	Polymer Fractionation Scheme	53
5.2	Determination of Intrinsic Viscosity from Relative Viscosity Data. Fraction 2A(2)	55
5.3	Determination of Intrinsic Viscosity from Relative Viscosity Data. Fraction 1A(2a)	57
5.4	Brillioun Spectrometer	60
5.5	Brillioum Spectrum of Toluene	62
5.6	Brillioun Spectrum of PIB in Toluene. Fraction 1A(2a)-3	63

FIGURE		Page
5.7	Extrapolation of Light Scattering Data to Zero Concentration	68
6.1	Light-Beating Spectra. 0.357 Micron Particles. T = 25.00°C	70
6.2	Light-Beating Spectra. 0.357 Micron Particles. T = 25.00°C	71
6.3	Comparison of Light-Beating Spectrum with Calculate Lorentzian Curve. 0.109 Latex Particles. $\theta = 30^{\circ}$, $\Gamma_{\frac{1}{2}} = 70.3$ Hz	đ 75
6.4	Comparison of Light-Beating Spectrum with Galculate Lorentzian Curve. 0.357 Latex Particles. $\theta = 30^{\circ}$, $\Gamma_{\frac{1}{2}} = 27.9 \text{Hz}$	d 76
6.5	Angular Dependence of Spectral Halfwidth. Latex Particles	80
6.6	Light-Beating Spectra. Fraction 1A (2a)	84
6.7	Light-Beating Spectra. Fraction 2A (2)	85
6.8	Light-Beating Spectra. Fraction 2A (2)	86
6.9	Comparison of Light-Beating Spectrum with Lorentzia Curve. Fraction 2A (2). (Tc-T) = 1.20° C, $\theta = 30^{\circ}$ $\Gamma_{\frac{1}{2}} = 231$ Hz	
6.10	Comparison of Light-Beating Spectrum with Lorentzia Curve. Fraction 1A (3b). (Tc-T) = 1.15 C, θ = 3 Γ_{2} = 218Hz	n 0°, 88
6.11	Comparison of Light-Beating Spectrum with Lorentzian Curve. Fraction 1A (3b). (Tc-T) = 1.15° C, θ = 1. Γ_{2} = 53Hz	n 5°, 90
6.12	Comparison of Light-Beating Spectrum with Lorentzian Curve. Fraction 1A (2a). (Tc-T) = 1.00° C, θ = 45 Γ L ₂ = 366 Hz	
6.13	Angular Dependence of Spectral Halfwidth. Fraction 1A (2a)	95
6.14	Angular Dependence of Spectral Halfwidth. Fraction 1A (3b)	96
6.15	Angular Dependence of Spectral Halfwidth. Fraction 2A (2)	97
6.16	Temperature Dependence of the Diffusion Coefficient	101

FIGURE		Page
6.17	Plot of Γ/K^2 vs K^2 for Fraction 1A(2a)	103
6.18	Plot of Γ/K^2 vs K^2 for Fraction 1A(3b)	104
6.19	Temperature Dependence of the Diffusion Coef- ficient with Correlation Corrections Applied .	108

CHAPTER I

INTRODUCTION

Historical

Light-beating spectroscopy is a relatively new yet powerful technique which has made possible the measurement of optical lineshapes and frequency shifts with a resolution approaching several Hz. The phenomenon of "light-beating" was first discussed by A. Forrester in 1947. He postulated that if two light waves of nearly the same frequency were superimposed, the peak amplitude of the resultant wave would oscillate in magnitude at the difference frequency of the two original waves, generating an electromagnetic "beat" signal.

The effect is analogous to the beats which are heard when sound waves of nearly the same frequency are mixed, or the electrical beats which occur when a.c. signals are mixed in nonlinear circuit elements.

Figure 1.1 illustrates the formation of electromagnetic beats.

Curves 1 and 2 represent two light waves which are to be mixed. The variation of the amplitude of the electric vector for curve 1 is given by

$$E_1 = A \sin(2\pi f t) \tag{1.1}$$

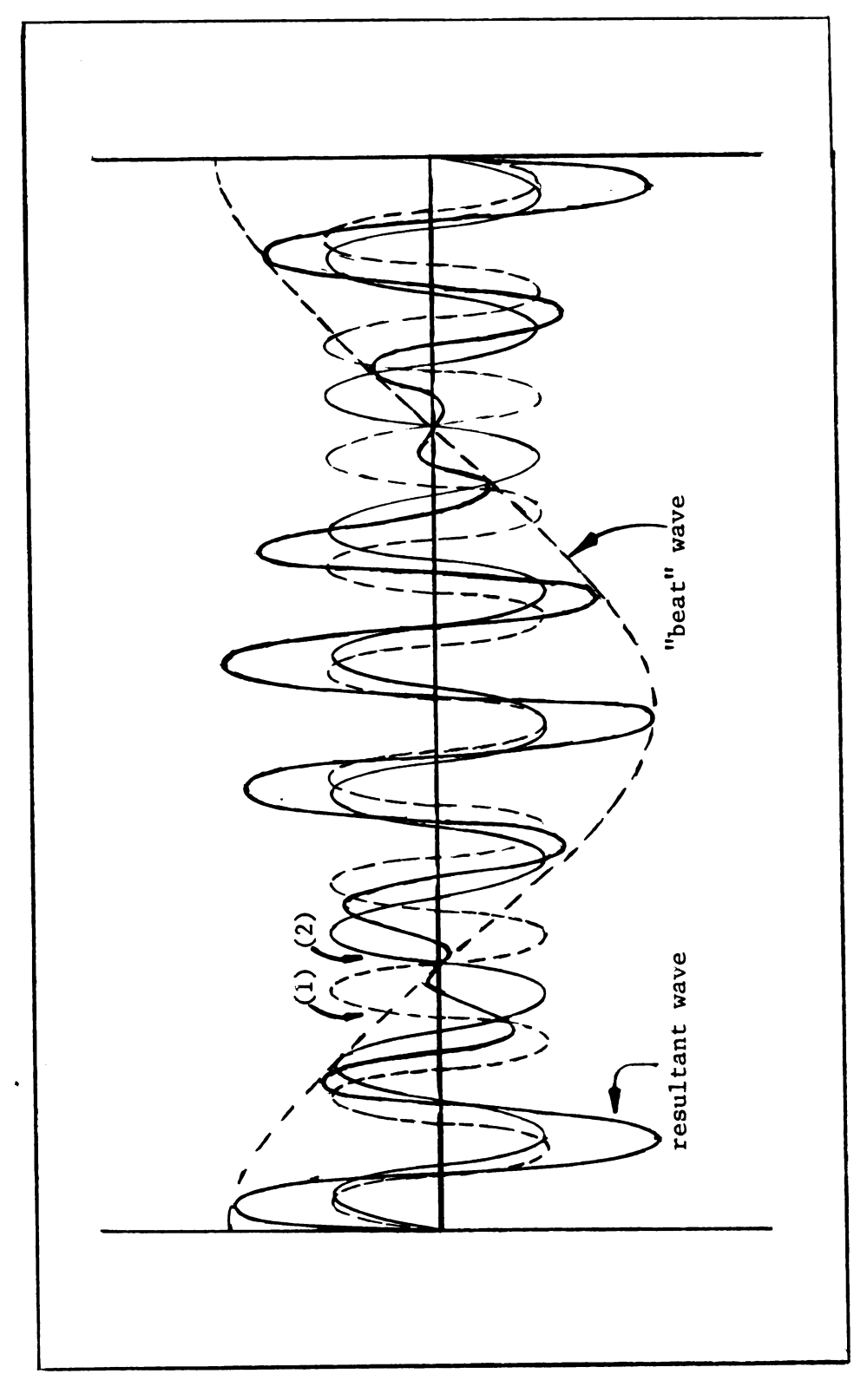


FIGURE 1.1 - Electromagnetic Beats

and by

$$E_2 = A' \sin(2\pi f't)$$
 (1.2)

for curve 2, where A and A' represent the maximum amplitude for each wave. By the principle of superposition, the amplitude of the resultant wave is the sum of the individual amplitudes

$$E = E_1 + E_2 = A \sin(2\pi ft) + A' \sin(2\pi f't)$$
 (1.3)

For simplicity, consider A = A', then

$$E = A \left(\sin(2\pi f t) + \sin(2\pi f' t) \right)$$
 (1.4)

Employing the trigonometric relation for the sum of two sines, one obtains

$$E = (2A\cos(\pi(f-f')t)) \sin(\pi(f+f')t)$$
 (1.5)

which represents a wave of frequency (f+f') whose amplitude is modulated by a wave of frequency (f-f'). The modulating frequency, (f-f'), is referred to as the "beat" frequency.

It can be seen from Figure 1.1 that the average amplitude of the beat signal is zero. Detection of the amplitude fluctuations, therefore, requires a nonlinear device which responds to the square of the amplitude of the beat frequency rather than to the amplitude itself. The ear, which is a nonlinear detector, is capable of detecting sonic beats while a nonlinear circuit element must be used for production of electrical beats. Similarly a photoelectric device, which responds to the intensity of light incident upon it, is necessary for detection of electromagnetic beats.

In an experiment proposed by Forrester to demonstrate the light-beating effect, two of the Zeeman spectral lines from a Hg lamp would be isolated using narrow bandwidth optical filters and mixed on the surface of a photoelectric detector. It was argued², however, that the light waves emanating from such a source are spatially incoherent, and phase cancellation of the beats would result when mixing occurred on the photocathode surface. The resulting signal, therefore, would be undetectable above the shot noise of the detector.

Forrester³, however, maintained that while the intensity of the beat signals may be reduced by phase variations, detection could still be accomplished by suitable signal processing techniques. In 1955, he published⁴ the results of experiments in which he observed the occurrence of beats between lines emitted from the Hg²⁰² atom. This work was significant in that it demonstrated the possibility of measuring narrow spectral lines through analysis of the beat-frequency spectrum of the photocurrent. However, even with the use of phase sensitive detection and amplification the maximum signal to noise ratio obtainable at the time was too low to make photoelectric mixing a useful spectroscopic tool.

The principal obstacle in the development of the technique was the low intensity and broad linewidth of conventional light sources. The introduction of the laser in the late 1950's made available a high intensity beam of light which was both polarized and coherent in space and time. Realizing the potential of the laser in photoelectric mixing experiments, Forrester⁵, in 1961, proposed a design for a light beating spectrometer which could be used to analyze narrow spectral

lines. The instrument consisted of a laser, a photoelectric detector, and a communications receiver. The narrow spectral width and high energy density of the laser beam made it ideal for use as an optical local oscillator in a manner analogous to electronic oscillators employed in conventional receivers. The light from the laser source is beat against each of the frequencies contained in the spectral region by mixing on the cathode surface of the photodetector. The resulting photocurrent oscillates at each of the beat frequencies with an amplitude proportional to the intensity of the wave producing the oscillation. Hence, an analysis performed on the frequency dependent portion of the photocurrent will yield the power spectrum of the beat frequencies centered about the frequency of the laser line.

In the spectrometer proposed by Forrester, the frequency analysis would be performed by a communications receiver. Narrow bandwidth electronic filters incorporated into such instruments provided a frequency resolution four or five orders of magnitude greater than could be obtained with conventional optical monochromators and interferometers. The total instrumental linewidth in modern light beating spectrometers is typically less than 15 Hz.

A further advantage of the light beating technique over conventional optical spectroscopy is the higher signal to noise ratio obtainable. If P_s represents the power contained within the signal to be analyzed and P_o the oscillator power, then the signal current produced by the photodetector is proportional to $(P_sP_o)^{\frac{1}{2}}$. Hence, the local oscillator signal, if properly aligned with the signal being analyzed, can raise the level of a very weak signal above the noise of the detector.

While Forrester was investigating the applicability of the laser to photoelectric mixing experiments, scientists involved in light scattering studies were exploring the possibility of using the laser as a light source. Although angular intensity and polarization measurements on Rayleigh scattered light had been performed for many years, the additional information contained in the spectral distribution of the scattered light was inaccessible because of the limited resolution of conventional light scattering spectrometers.

In 1963, Cummins, Knable, and Yeh⁶, at Columbia University, reported they had measured for the first time, the broadening of the central Rayleigh line due to the diffusional motion of polystyrene lattices in water. The instrument used for the observation was constructed after the design suggested by Forrester, consisting of a laser, a photomultiplier tube and a communications receiver, as illustrated in Figure 1.2.

Optical heterodyning was accomplished by splitting the laser beam along two optical paths, one of which was used as a local oscillator while the other illuminated the sample. The light scattered by the sample at a particular angle was mixed with the unscattered beam on the photocathode surface. The resulting photocurrent was analyzed by a communications receiver which yielded the power spectrum of the beat frequencies.

The successful operation of the instrument was dependent on the amplitude of the beat signal being greater than the level of shot noise generated by portions of the oscillator beam which did not mix with the scattered light. For maximum signal to noise ratio, therefore, it is

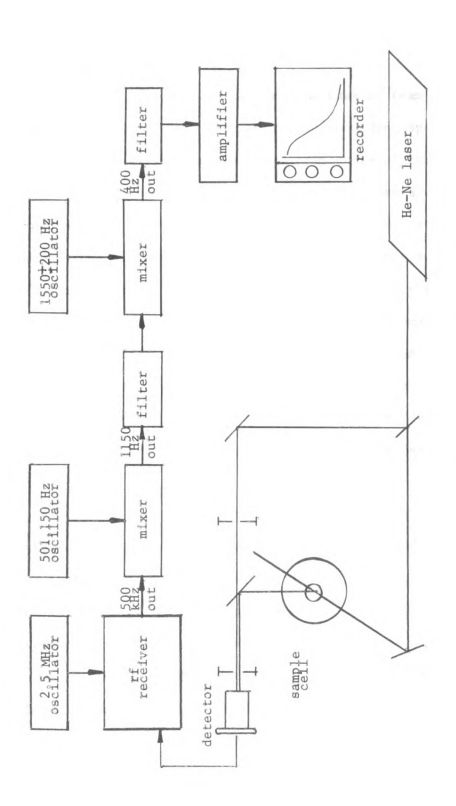


FIGURE 1.2 - Laser Heterodyne Spectrometer

necessary to optimize the beating efficiency by proper alignment of the two beams. This was a difficult procedure inasmuch as the two beams had to have the same direction, curvature, polarization, and phase when mixed at the detector surface.

In an attempt to eliminate the tedious task of beam alignment, G. Benedek developed the "self-beat" or laser-homodyne spectrometer illustrated in Figure 1.3. The essential components of the instrument are the laser, the photoelectric detector, and the wave analyzer. In this spectrometer there is only one optical path so that beating occurs between the different frequency components in the scattered light rather than between the laser and the scattered light. Hence, a difficult alignment procedure is not required. Although the same resolution is possible with this spectrometer as with the optical heterodyne, the S/N ratio is lower inasmuch as the power contained in the signal current is proportional to $(P_s^2)^{\frac{1}{2}}$ rather than to $(P_sP_0)^{\frac{1}{2}}$. Therefore, detection of very low level scattered light may be more difficult.

Most wave and spectrum analyzers employed in this type of spectrometer will rectify the signal after it is filtered and amplified, and before it is recorded. As a result, a power spectrum is not recorded but rather a voltage spectrum, which is the square root of a power spectrum. Therefore, the amplitude obtained from the recorded spectrum must be squared before determination of halfwidth can be made. This feature, characteristic of most homodyne spectrometers, is advantageous in the measurement of extremely narrow spectral lines inasmuch as the voltage spectrum is twice the width of the power spectrum and can, therefore, be measured more accurately.

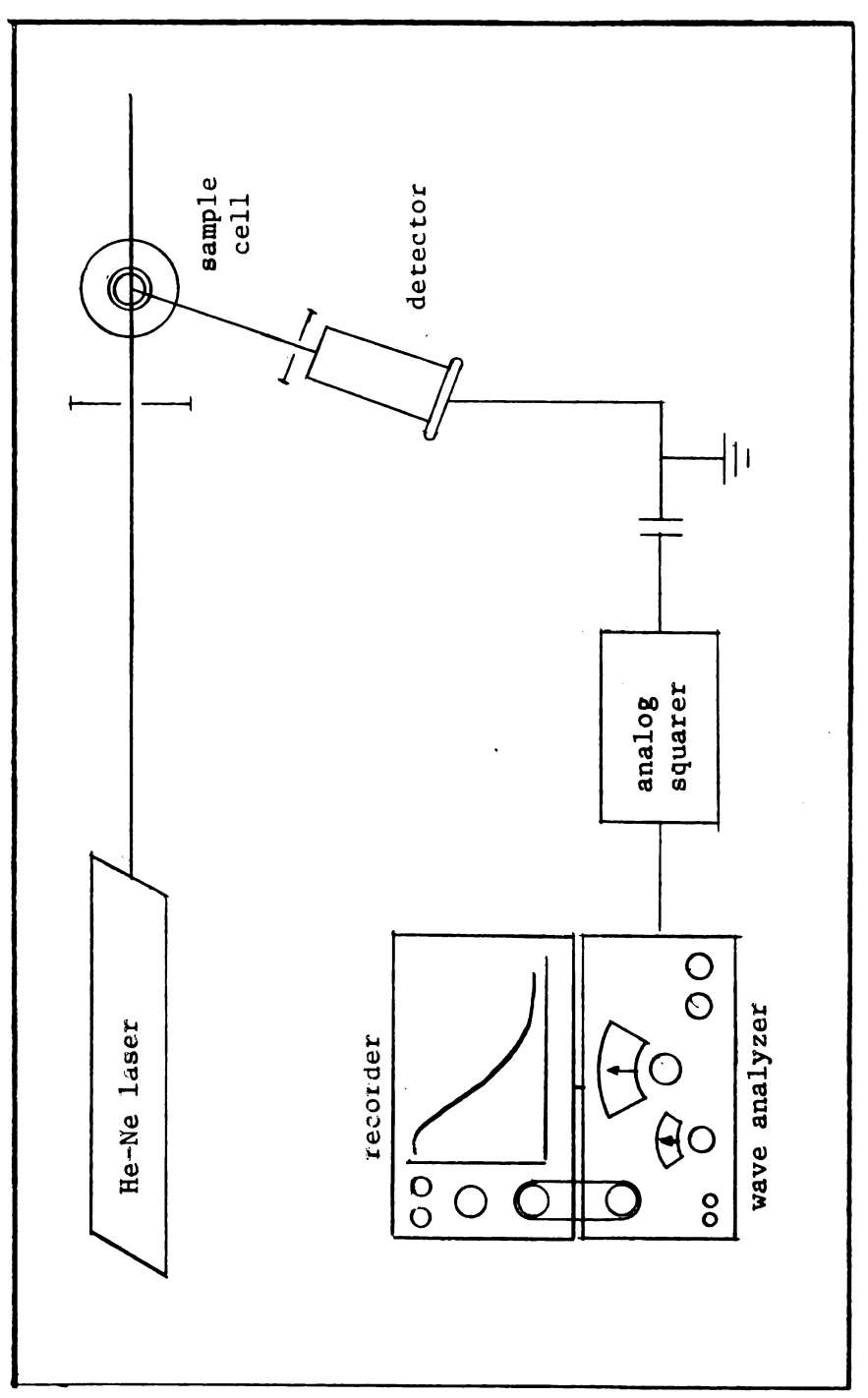


FIGURE 1.3 - Laser Homodyne Spectrometer

The bulk of recent investigations involving light-beating spectroscopy have provided an in-depth study of the translational and rotational motion of proteins and other biological macromolecules in solution 7 - 13. In 1967, Benedek 13 demonstrated that translational diffusion c efficients could be measured accurately for spherical molecules and for macromolecules which were small compared to the wavelength of the incident light. For larger molecules such as deoxyribonucleic acid (DNA) and Tobacco Mosaic Virus (TMV), however, interference from rotational motion and intramolecular motions prevented an accurate measurement of the translational diffusion coefficient.

In 1969, Cummins, et. al. 12, reported that they had resolved the translational and rotational components of the light scattered from solutions of TMV molecules by taking advantage of their different angular dependencies. At angles of observation below 60°, they found that spectra could be fit to a single Lorentzian curve. At angles between 60° and 120°, however, a double Lorentzian term was required to account for the rotational contribution to the scattered light, and at angles greater than 120°, a third term was necessary to account for the beating of the translational spectrum with the rotational spectrum. Their results were in agreement with the theoretical predictions of R. Pecora 14.

Using the homodyne spectrometer, Benedek obtained the first measurements of the spectral distribution of the light scattered from a pure fluid (SF₆) in the region of its critical point. At the same time, S. Alpert reported the results of similar investigations made on a binary sclution of small molecules (cyclohexane-aniline) near the critical solution temperature using an optical heterodyne spectrometer.

In both instances it was demonstrated that the spectral linewidth decreases and approaches zero as the temperature of the system approaches the critical temperature and as the scattering angle approaches zero.

The results of their experiments were discussed 8,15 at the "Conference on Phenomena in the Neighborhood of Critical Points", Washington, D.C., 1965. Their observations were interpreted by P. Debye 16 in terms of the diffusion coefficient which, he indicated, primarily determines the linewidth. According to Debye, the relationship between spectral width, diffusion coefficient, and scattering angle is given by

$$\Gamma = DK^2$$

where Γ is the halfwidth at half maximum, D is the diffusion coefficient, and K is the scattering vector defined by Bragg to be $\frac{4\pi}{\lambda} \sin \frac{\theta}{2}$. Therefore, the linewidth should decrease with decreasing scattering angle and approach zero, as had been observed.

Debye indicated further that the driving force for diffusion is the concentration gradient of the osmotic pressure which is zero at the critical point. Inasmuch as the gradient is proportional to $(T-\Gamma_c)$ from classical theory, then

$$D \propto (T - T_c)^{1.0}$$

and D should approach zero linearly with decreasing distance from the critical point.

The first test of the applicability of Debye's theory to macromolecular systems was by White, Osmundsen, and Ahn 17 in 1966. A laser - hemodyne spectrometer similar to that developed by Benedek was
constructed to observe the spectral broadening from solutions of narrow molecular weight polystyrene in cyclohexane. The broadening a few
tenths of a degree above the critical temperature was found to be an

order of magnitude less than that observed for binary systems of small molecules. Their observations were consistent with the expected persistence of time dependent concentration fluctuations for macromolecular solutions. Furthermore, the broadening of the spectral line conformed moderately well to the \sin^2 ($\frac{\theta}{2}$) dependence predicted by P. Debye¹⁶. However, the temperature dependence was more closely represented by $(T-T_p)^{0.5}$, where T_p is the phase separation temperature, rather by the classical prediction of $(T-T_c)^{1.0}$.

Similar studies by Chu and co-workers 18,19 demonstrated that at temperatures close to the critical point, the simple ${\tt K}^2$ dependence of the linewidth is modified by long range molecular interactions to the form

$$r = DK^2 (1+\xi_r^2K^2)$$

where ξ_{Γ} is the temperature dependent correlation length. Furthermore, the temperature dependence of the extrapolated linewidth, or the diffusion coefficient, was of the form

$$D \propto \left(\frac{T-T_c}{T_c}\right)^{\gamma}$$

with $\gamma \approx 0.77$. They acknowledged, however, the need for further investigations in this area.

The objective of the research described in this thesis was to examine the temperature and angular dependence of light scattered from high molecular weight polymer solutions near the lower critical temperature. It is hoped that the information obtained from the study of additional macromolecular systems will clarify some of the ambiguities associated with critical phenomena.

To obtain the necessary spectral information, a light-beating

spectrometer of the laser-homodyne type was designed and constructed.

A description of the instrument and its performance is given.

Polyisobutylene/n-pentane systems were selected for study because of their relatively accessible lower critical solution temperatures (75°-80°C), and because of the sharpness of the coexistence curve in the region of a lower critical solution temperature relative to that in the region of an upper critical solution temperature. The preparation, fractionation, and molecular weight determination of the polymer samples are described.

Finally, the results of the study and the ensuing data analysis are presented in the text of this thesis.

CHAPTER II

THEORY

The phenomenon of light scattering occurs as a result of inhemogeneities in the optical properties of the scattering medium. These inhomogeneities are induced by such physical processes as the diffusion of mass and the diffusion of thermal energy, which are assumed to fluctuate randomly through the medium. The amplitude of these fluctuations determines the intensity of the scattered light. For example, the simple thermal motion of molecules in a pure liquid is sufficient to scatter low intensity radiation when the temperature of the sample is away from a critical point. However, the increased molecular activity which accompanies a phase transition induces large fluctuations in the optical properties of a medium which results in the scattering of large amounts of light, as evidenced by the well known phenomenon of "critical opalescence."

In a binary solution, concentration gradients created by diffusion of mass will scatter light in addition to that resulting from thermal diffusion. Ordinarily the inhomogeneities produced by mass diffusion are greater in amplitude and decay more slowly than those generated by thermal diffusion, with the result that scattering produced by the former process is more intense. Near a critical solution point this inequality becomes more dramatic as molecules separate into different phases, and the contributions from thermal diffusion can be neglected.

and the state of t

conce

dynan

At the standard At the standar

Where k

We have t

in the cr

Landau and Lifschitz²⁰ have derived the equations for temperature and concentration distributions in a binary system using the linearized hydrodynamic equations of irreversible thermodynamics. Those expressions governing the diffusion of temperature and concentration through a medium are, respectively, the energy transport equation

$$\frac{\partial}{\partial t} \delta T - \frac{k_T}{c_p} \left(\frac{\partial \mu}{\partial C}\right)_{T,P} \frac{\partial}{\partial t} \delta C = \left(\frac{\kappa}{\rho_0 c_p}\right) \nabla^2 \delta T$$
 (2.1)

and the equation of continuity

$$\frac{\partial}{\partial t} \delta C = D \left(\nabla^2 \delta C + \left(\frac{k_T}{T} \right) \nabla^2 \delta T \right)$$
 (2.2)

In the above expressions, D is the binary diffusion constant, k_T is the thermal diffusion ratio, K is the thermal conductivity ($\{\kappa/\rho_0c_p\}$ is the thermal diffusivity), C is the solution concentration, μ is the chemical potential, and c_p is the heat capacity of the mixture. Equilibrium values have been denoted by subscript zero.

Similarly, Landau and Lifschitz have shown that

$$\delta C^2 \propto k_B T \left(\partial \mu / \partial C \right)_{P,T}^{-1}$$
 (2.3)

where $\boldsymbol{k}_{\boldsymbol{B}}$ is the Boltzman constant.

At the critical solution point, the chemical potential and its first and second derivatives vanish²², with the result that δC^2 becomes quite large. From (2.1), however, it is apparent that δT^2 remains finite, and we have the relationship that

$$\delta C^2 >> \delta T^2 \tag{2.4}$$

in the critical region. Under this condition, equation 2.2 simplifies to

$$\frac{\partial}{\partial t} \delta C(\mathbf{r}, t) = D\nabla^2 \delta C(\mathbf{r}, t)$$
 (2.5)

which is the general diffusion equation or Fick's second law. This expression governs the time dependence of concentration fluctuations separated by a distance r in the medium. The solution to equation (2.5) is 8,23

$$-3/2 - \frac{r^2}{4Dt}$$
 $\delta C(r, t) = (4\pi Dt) e$

To obtain the time dependence of concentration fluctuations with the scattering vector, K, it is necessary to take the Fourier transform of equation (2.5), which yields 15,24

$$\frac{\partial}{\partial t} \delta C(K, t) = -DK^2 \delta C(K, t)$$
 (2.6)

where $K = \frac{4\pi}{\lambda} \sin \frac{\theta}{2}$, λ being the wavelength of the incident light and θ the angle of observation of the scattered light.

Concentration fluctuations do not propagate through the medium, but decay exponentially with time. The correlation function for the concentration fluctuations, therefore, will have the form 15,24

$$R_{C}(\tau) = \delta C \star (K, t) \delta C(K, t+\tau) = \langle |\delta C(K, t)|^{2} \rangle e^{-\Gamma(K)\tau}$$
 (2.7)

where $\Gamma(K)$, the experimentally determined parameter, is the inverse lifetime of the concentration fluctuation producing the scattering. $\Gamma(K)$ is defined by

$$\Gamma(K) = DK^2 = D(\frac{4\pi}{\lambda} \sin \frac{\theta}{2})^2$$
 (2.8)

The correlation function $R_{c}(\tau)$ represents the ensemble average of the product of fluctuations separated by time τ .

Assuming that the exciting light source is perfectly monochromatic, i.e., an ideal single mode laser, the electric field of the incident light is defined by

$$E(t) = E_0 e^{-i\omega_0 t}$$
 (2.9)

where $E_{\rm O}$ is the amplitude of the incident plane wave, and $\omega_{\rm O}$ is its frequency.

The scattered field at a distance R away from the illuminated volume is given by 31

$$\delta \xi(K,t) = -E_0 \left(\frac{\omega_0}{c}\right)^2 \frac{\sin \theta}{4\pi R} e^{i(k' R - \omega_0 t)} (2\pi)^{3/2} \delta \varepsilon(K,t) \qquad (2.10)$$

where

$$K = k' - k = \frac{4\pi}{\lambda} \sin \frac{\theta}{2}$$
 (2.11)

In equations (2.10) and (2.11), k is the wave vector of the incident light beam, k' that of the scattered beam, θ is the angle between the direction of polarization of the incident light and the direction of k', and $\delta \varepsilon(K,t)$ is the fluctuation of the dielectric constant responsible for the scattering. The correlation function for fluctuations in the scattered field is, therefore, related to the correlation function for fluctuations in the dielectric constant by

$$R_{\xi}(\tau) = \delta \xi * (K, t) \delta \xi (K, t + \tau) = E_{0}^{2} \left(\frac{\omega_{0}}{C}\right)^{2} \left(\frac{\sin^{2}\theta}{(4\pi R)^{2}}(2\pi)^{3}\right) \delta \varepsilon * (K, t) \delta \varepsilon (K, t + \tau) e^{-i\omega_{0}\tau}$$
(2.12)

Both thermal and mass diffusion will modulate the dielectric constant, although the former process is assumed to be negligible compared to the latter. Hence,

$$(\delta \varepsilon(K,t))_{T} = (\frac{\partial \varepsilon}{\partial C})_{T} (\delta C(K,t))_{T}$$
 (2.13)

From equations (2.7), (2.12), and (2.13), therefore

$$R_{\xi}(\tau) = E_{O}^{2} \left(\frac{\omega_{O}}{c}\right)^{4} \frac{2\pi^{2} \theta}{(4\pi R)^{2}} (2\pi)^{3} \left(\frac{\partial \varepsilon}{\partial C}\right)^{2} \left(\frac{\partial \varepsilon}{\partial C}\right)^{2} \left(\frac{\partial \varepsilon}{\partial C}\right)^{2} e^{-\Gamma \tau} e^{-i\omega_{O}\tau}$$
(2.14)

The Wiener-Khintchine theorem 25 indicates that sufficient information is contained in the correlation function for the scattered field to obtain the power spectrum of the scattered light through a Fourier transform relationship. Hence the scattered power per unit bandwidth at frequency ω is given by

$$p(K,\omega) = (2\pi)^{-1} \int_{-\infty}^{\infty} R_{\xi}(\tau) e^{i\omega\tau} d\tau \qquad (2.15)$$

substituting (2.14) into (2.15) and performing the integration

$$p(K,\omega) = E_0^2 \left(\frac{\omega_0}{c}\right)^4 \frac{\sin^2\theta}{(4\pi R)^2} (2\pi)^3 \left(\frac{\partial \varepsilon}{\partial C}\right)^2 \left(\frac{\partial \varepsilon}{\partial C}\right)^2 \left(\frac{\Gamma(K)/\pi}{(\omega-\omega_0)^2 + \Gamma^2(K)}\right)^3$$
(2.16)

which is the equation for a Lorentzian-shaped spectrum centered at $\omega=\omega_0$ with half width at half maximum $\Delta\omega_{1/2}=\Gamma(K)$.

The average photocurrent resulting from illumination of the photocathode surface by field (2.10) is 26,27

$$i(t) = e\sigma \langle \delta \xi^*(t) \delta \xi(t) \rangle = e\sigma \langle I \rangle$$
 (2.17)

where $\langle \, I \, \rangle$ is the average intensity of the scattered light, e is the charge on an electron, and σ is the quantum efficiency. In actuality, however, the photocurrent consists of a series of discrete pulses which are assumed to be infinitely narrow. If the electrons at time t and at a later time t + τ are distinct, then the current is time dependent and

the correlation function is given by

$$R_{i}^{(1)}(\tau) = i(t)i(t+\tau) = e^{2}\sigma^{2}\langle\delta\xi^{*}(t)\delta\xi(t)\delta\xi^{*}(t+\tau)\delta\xi(t+\tau)\rangle$$

$$= e^{2}\sigma^{2}\langle 1\rangle^{2}G^{(2)}(\tau) \qquad (2.18)$$

where

$$G^{(2)}(\tau) = \underbrace{\langle \delta \xi^*(t) \delta \xi(t) \delta \xi^*(t+\tau) \delta \xi(t+\tau) \rangle}_{\langle \delta \xi^* \delta \xi \rangle^2}$$
(2.19)

However, if the same electron occurs at t and $t + \tau$, the current is time independent or stationary, and the correlation function is given by

$$R_{1}^{(2)}(\tau) = e\sigma \langle \delta \xi^{*}(t) \delta \xi(t) \rangle \delta(\tau) = e\sigma \langle I \rangle \delta(\tau)$$
 (2.20)

Therefore, the total correlation function for the photocurrent is

$$R_{\mathbf{i}}^{(\tau)} = e^{2}\sigma \langle \mathbf{I} \rangle \delta(\tau) + e^{2}\sigma^{2} \langle \mathbf{I} \rangle^{2} G^{(2)}(\tau)$$

$$= e \langle \mathbf{i} \rangle \delta(\tau) + \langle \mathbf{i} \rangle^{2} G^{(2)}(\tau) \qquad (2.21)$$

The correlation function for the scattered field has been defined in (2.14). Basically, it can be represented by

$$R_{\xi}(\tau) = \langle \delta \xi^{*}(t) \delta \xi(t+\tau) \rangle = \langle I \rangle G^{(1)}(\tau)$$
 (2.22)

where

$$I = E_0^2 \left(\frac{\omega_c}{c}\right)^{\frac{4}{3}} \frac{\sin^2 \phi}{(4\pi R)^2} (2\pi)^3 \left(\frac{\partial E}{\partial C}\right)_T \left(\left|\delta C(K, t)\right|^2\right)$$

and

$$G^{(1)}(\tau)=e^{-\Gamma|\tau|}e^{-i\omega_0\tau}$$

The correlation function for the photocurrent is related to the correlation function for the scattered field by

$$G^{(2)}(\tau)=1+|G^{(1)}(\tau)|^2$$
 (2.23)

therefore,

$$R_{i}(\tau) = e(i)\delta(\tau) + (i)^{2}(1+|G^{(1)}(\tau)|^{2})$$
 (2.24)

Finally, the photocurrent spectrum associated with the scattered field is obtained from the Wiener-Khintchine theorem

$$P_{\mathbf{1}}(\omega) = (2\pi)^{-1} \int_{-\infty}^{\infty} \{e(\mathbf{i})\delta(\tau) + \langle \mathbf{i} \rangle^{2} + \langle \mathbf{i} \rangle^{2} e^{-2\Gamma|\tau|} \} e^{\mathbf{i}\omega\tau} d\tau$$

$$= (2\pi)^{-1} e^{\langle \mathbf{i} \rangle} + \langle \mathbf{i} \rangle^{2} \delta(\mathbf{w}) + \langle \mathbf{i} \rangle^{2} \{ \frac{2\Gamma/\pi}{\omega^{2} + (2\Gamma)^{2}} \}$$

$$(2.25)$$

Only the positive frequency portion of the photocurrent spectrum is measured by the wave analyzer. Since $P_i(\omega)$ is symmetric about $\omega=0$, the positive and negative frequency portions can be combined to obtain a spectrum for positive frequencies only.

$$P_{i}^{+}(\omega)_{\omega \geq 0} = (\pi)^{-1} e^{(i) + (i)^{2} \delta'(\omega) + 2(i)^{2}} \left\{ \frac{2\Gamma/\pi}{\omega^{2} + (2\Gamma)^{2}} \right\}$$
 (2.26)

$$P_{\mathbf{i}}^{-}(\omega)_{\omega<0} = 0$$

In equation (2.26), $\delta'(\omega)$ is zero for $\omega < 0$ and twice as large as $\delta(\omega)$ for $\omega \le 0$ so that

$$\int_{0}^{\infty} \delta'(\omega) d\omega = 1$$

The photocurrent power spectrum, therefore, consists of three components: the first, $(\pi)^{-1}e\langle i\rangle$, represents the shot-noise contribution

which arises from the random emission of electrons from the photocathode surface when illuminated. The second, $\langle i \rangle^2 \delta^{\vee}(\omega)$, represents the d-c portion of the photocurrent which is blocked before spectral analysis by an R-C filter network (see Figure 1.3). The final term is the light-beating spectrum. Hence the spectrum is Lorentzian in shape with half-width at half maximum $\Delta \omega_{i_2} = 2\Gamma$, and total power $\langle i \rangle^2$ centered at $\omega = 0$.

The shot noise contribution is subtracted from the total spectrum before the spectral parameters are obtained. The most convenient method of determining the level of shot noise is to measure the amplitude of the voltage spectrum above the frequency range in which the beat signal decays to zero amplitude. Ordinarily, 10-15 kHz is adequate for most liquid systems.

Equation (2.26) also describes the spectrum of light scattered by spherical particles undergoing pure translational diffusion. The translational diffusion coefficient, $D_{\rm t}$, can be determined from equation (2.8) 27

$$\Gamma(K)^2 = D_t K^2 = D_t \left(\frac{4\pi}{\lambda} \sin \frac{\theta}{2} \right)^2$$
 (2.8)

where Γ is the experimentally determined halfwidth and θ is the angle of observation. Furthermore, a graph of halfwidth versus scattering angle is linear with slope proportional to the diffusion coefficient.

Spherical particles such as polystyrene latex beads typically exhibit this type of behavior 9,28 . For this reason, they are often used to calibrate light-beating spectrometers. The value for D_T obtained experimentally from equation (2.8) can be compared to the theoretical value obtained from the Stokes Einstein relationship

$$D_{t} = \frac{k_{B}T}{6\pi nr} \tag{2.15}$$

where $k_{\mbox{\footnotesize{B}}}$ is the Boltzman constant, η is the solution viscosity, and r is the particle radius.

Einstein's fluctuation theory, from which equation (2.14) was derived, was extended by Orstein and Zernike²⁹ to include correlation effects between fluctuations in neighboring volume elements for systems near the critical point. Their theory was formalized by Debye³⁰ such that the relative scattered intensity due to concentration fluctuations within a binary critical mixture can be approximated by the relation

$$I_{C} \alpha = \frac{C}{n} \left(\frac{\partial n}{\partial C}\right)^{2} \frac{T/T_{C}}{T/T_{C} - 1 + K^{2}\phi^{2}/6}$$
 (2.16)

in which C denotes the contentration, n the refractive index of the mixture, T_c the critical mixing temperature, ϕ the Debye interaction parameter, and K the scattering vector defined as in equation (2.11).

The spectral distribution of the elastically scattered light was first investigated theoretically by Landau and Placzek 31 who attributed the scattering to fluctuations in entropy at constant pressure. Their theory was extended by Fixman 32 and Felderhof 33 to include the effect of long range correlation. They indicated that the spectrum of the Rayleigh scattered light should be Lorentzian in shape with half width at half maximum, Γ , defined by

$$\Gamma = DK^{2}(1 + K^{2}L^{2}/6)$$
 (2.17)

where D is the binary diffusion coefficient, and $L^2 \approx \phi^2 (T/T_c - 1)$.

Experimental investigations by Chu 18,19 have demonstrated that at the critical solution consentration and for $\xi_\Gamma K >> 1$, one can write

$$T = DK^2(1 + \xi_1^2 K^2)$$
 (2.18)

where ξ_{Γ} is the temperature dependent correlation length determined from linewidth studies. In terms of the "scaling law" concept 34,35 one can then write

$$D = \lim_{K \to 0} \left(\frac{\Gamma}{K^2} \right) \alpha \left(\frac{T}{T_C} - 1 \right)^{\gamma}$$
 (2.19)

The value for γ determined by Chu was ~0.77.

In the present work, the applicability of equations (2.8), (2.18), and (2.19) to the spectrum of light elastically scattered from high molecular weight polymer solutions in the lower critical temperature region will be examined.

CHAPTER III

INSTRUMENTATION

General Description

The light-beating spectrometer was designed to measure the spectral distribution of light elastically scattered from a test sample as a function of scattering angle and temperature. The essential components of the instrument are illustrated in Figure 3.1. They are: (a) the temperature control chamber and the rotating base, (b) temperature controller and temperature measuring equipment, (c) laser light source, (d) collimating optics, (e) detection system, and (f) wave analyzer and recorder.

In general, light from a collimated laser beam passes through the sample cell at an angle selected on the rotating base. Light scattered by the sample is collected and focused onto the surface of a photomultiplier tube. The resulting photocurrent consists of a d-c signal, which is removed by an RC filter, a shot noise signal, and the light-beating signal. The voltage at each frequency contained in the latter two components is measured by the wave analyzer and displayed on a recorder.

Sample Cells

Light-scattering cells were constructed by one of two methods, depending on the particular experiment to be performed. Line broadening studies on polyisobutylene/n-pentane systems near the lower critical



Figure 3.1 - Light-Beating Spectrometer and Associated Equipment

solution temperature (LCST) required that the solution be heated above the boiling point of the solvent. Under these conditions it was necessary to seal the sample in the cell under reduced pressure. Cells were made from 9 mm (i.d.) Fischer-Porter "Solv-Seal" pyrex glass joints, having a wall thickness of 1 1/2 mm. The bottom end of the joint was sealed, ground flat, and epoxied to a copper disc which would adapt the cell to the temperature control chamber. Polymer solution was forced into the cell through a fine, sintered glass filter under nitrogen pressure. Air was removed from the cell and its contents by repeatedly freezing in liquid nitrogen, evacuating, and warming to room temperature. After sealing, the cell was approximately 2 3/4" in length and contained approximately 4 cc of solution.

Diffusion studies on polystyrene latex spheres were performed in aqueous suspensions at or near room temperature, hence it was not necessary to evacuate and seal the cells, but only to cap them to prevent dust from entering.

Temperature Control Chamber

Near the critical solution point small changes in temperature result in relatively large changes in amplitude and width of the power spectrum, making temperature control of the sample essential for precise measurement of the spectral parameters. To accomplish this at temperatures which were 50-55°C above ambient required the use of two separate temperature control systems, one for the sample itself and a second for the immediate surroundings.

Figure 3.2 illustrates the top view of the temperature control system. The sample cell (Figure 3.2-a) is enclosed in a thermostatic air bath (Figure 3.2-b) by a copper cylinder (Figure 3.2-c and 3.3),

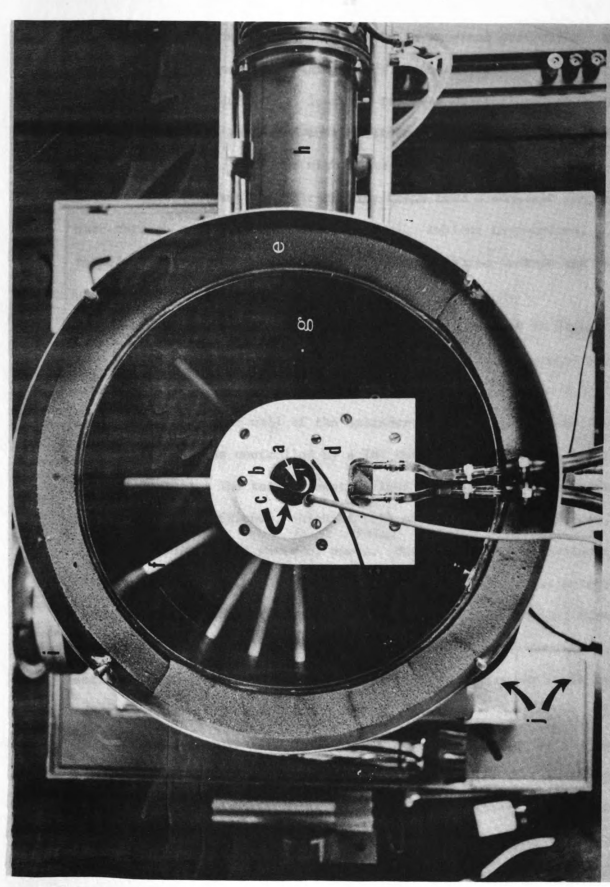


Figure 3.2 - Temperature Control Chamber

the temperature of which is regulated by an external controller. A thermoplastic encasement (Figure 3.2-d) completely surrounding the copper cylinder reduces heat loss and improves controllability. The entire assembly is supported on a platform inside a thermostated stainless steel housing. The air within the housing is maintained near the control point of sample by circulating fluid from a constant temperature bath through copper tubing (Figure 3.2-e). Ambient temperature, therefore, is within a few degrees of the sample temperature and more precise control is possible.

Heat is supplied to the copper cylinder illustrated in Figure 3.3 from a ten-foot length of Nichrome wire, which had been covered with a fiberglass sheath and threaded through 1/8" Cu tubing (Figure 3.3-d) soldered to the outer wall of the cylinder. The voltage across the heating element was controlled by a YSI Model 72 proportional temperature controller. The total resistive load of the wire and contacts was approximately 68 ohms, which at full power (117V) would draw 1.7 amps and dissipate 200 watts of power. This represented considerably more power than required to heat the copper cylinder and was potentially damaging to the Nichrome wire. To limit the amount of current flow through the wire, a 100 ohm, 225 watt power resistor was connected in series with the wire. With this arrangement, heater power could be adjusted between 80 watts and 200 watts.

For cooling purposes, a three-foot length of 1/8" diameter copper tubing (Figure 3.3-e) was soldered to the outer walls of the copper cylinder and fitted with tubing adapters. By adjusting the flow of tap water through the tubing, a proper balance between heating and cooling could be maintained for precise temperature control.

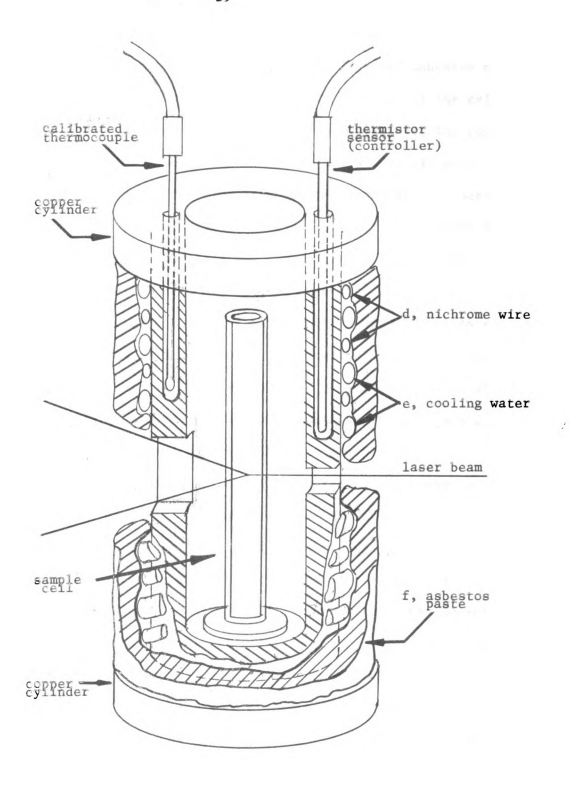


FIGURE 3.3 - Sample Cell and Temperature Control Block

Finally, to increase the effectiveness of heat transfer to the copper cylinder and to reduce heat loss, a 1/8" layer of asbestos paste (Figure 3.3-f) was applied over the entire outer surface of the cylinder.

"Delrin" was used in constructing a thermal jacket for the copper cylinder becasue of its dimensional stability and heat resistance. It showed no visible signs of deterioration after sustaining a temperature of 80°C for periods up to one week. However, since it did expand on heating, it was necessary to align the system (laser beam, sample cell and optics) at the temperature at which measurements were to be made.

"Light-pipes" (Figure 3.2-f) were constructed of 3/8" Delrin rod with a 1/4" hole bored down the center, and positioned at 15° intervals between angles of 0° and 135°. These allowed entrance of the laser beam to the sample cell through the outer stainless steel chamber, insulating foam, Delrin, and copper construction materials of the entire temperature control chamber. All other open areas on the stainless steel housing that would allow passage of room light to the detector were covered with black tape to provide a light-tight system.

The scattered light is collected by optics contained in a Delrin tube (Figure 3.2-g) 2 1/4" diameter x 5" extending from the thermal jacket to the outer stainless steel wall. The outer end of this tube is fitted with an adapter for mounting a copper cylinder (Figure 3.2-h) which may contain lenses, polarizers or other optics.

The photomultiplier tube housing (Figures 3.1 and 3.5) has thirty feet of 1/4" copper tubing soldered to it, through which tap water at 12°C is circulated for cooling purposes. The phototube is supported inside the housing by a 3/8" teflon sleeve (Figure 3.5) which surrounds the dynode portion of the tube. With this arrangement, the efficiency

of the dynode stages of the tube is not impaired by cooling, while the cathode surface, and the electronic circuitry located immediately behind the tube are subjected to the cooling effects of the circulating tap water with the result that the noise level of the photomultiplier is reduced.

The housing for the photomultiplier tube and associated optics is mounted rigidly onto the stainless steel wall, and the entire assembly is centered onto a 15" Bridgeport rotary milling table (Figure 3.2-1). The two are aligned at angles of 0 and 180 degrees and secured together. Angular determinations can be made with a precision of ±5 seconds of a degree.

Alignment of the sample cell and optics with the laser beam is achieved in part by means of a sliding base (Figure 3.2-j) under the rotary table, which permits translation of all components in a direction perpendicular to the laser beam. Vertical alignment is accomplished by movement of the laser mounts (Figure 3.4-b).

Laser Light Source

A Siemens Model LG-64 He-Ne laser (Figure 3.4-a) was used as a light source for scattering experiments. The unit has interchangeable, externally mounted mirrors which allow it to operate at 6328Å in either uniphase mode (TEM00) with a maximum power of 4 milliwatts, or multiphase mode (TEM11) with a maximum power of 10 milliwatts. The laser was used exclusively in the uniphase mode for reasons of stability, narrower beam diameter and greater degree of spatial coherence, although higher intensity would have been advantageous in several experiments.

Laser power was checked periodically with a JEA, Inc. Model 450B optical power meter. Laser output could be optimized by adjustment of

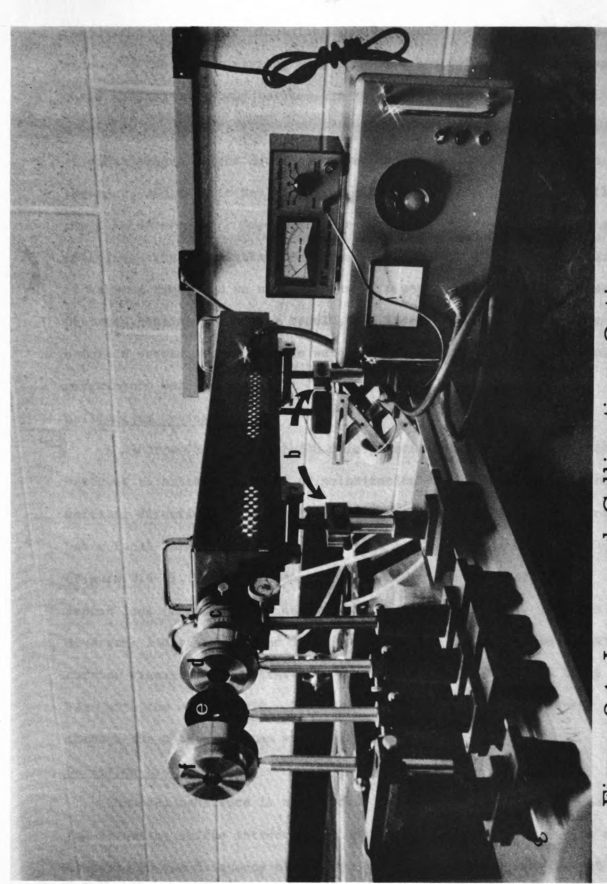


Figure 3.4 - Laser and Collimating Optics

the discharge current. Occasionally, dust would collect on the Brewster windows of the laser cavity, resulting in a loss of power. Cleaning of these optical parts was performed with a water base Collodion solution.

The output of the Model 450B power meter could be monitored on a recorder, and in this way, the time required for the laser to stabilize could be determined. Experiments performed in this respect indicated that intensity fluctuations decreased to less than 1% after six hours of warm-up time, and to a few tenths of a percent when the laser was operated continually. As a result, the laser was turned on the day before a series of experiments were to be initiated and left on until experiments were completed.

Collimating Optics

A Spectra-Physics Model 310 Polarization Rotator (Figure 3.4-c) was used to orient the plane of polarization of the laser beam in the vertical direction. The first lens (Figure 3.4-d) following the rotator has a focal length of 68 mm. It focuses the laser beam onto a pinhole (Figure 3.4-e), having a diameter of 0.020" and a depth of 0.003". A second lens (Figure 3.4-f) having a focal length of 44 mm, collects the divergent light and focuses it at infinity. It is mounted in an Ealing carrier with transverse travel to facilitate alignment of the laser beam with the sample cell. The diameter of the beam after passing through the optical system was 0.022", or approximately 0.5 mm.

Detection System

Temporal coherence is maintained in the scattered light because the frequency shifts introduced by molecular motions are extremely small compared to the frequency of the incident light (approximately $1/10^{12}$).

However, spatial coherence is lost as a result of the fact that the scattered light originates from different sources. Unless this spatial coherence is restored, destructive interference will reduce the level of the beat signal below the shot noise of the detector. Therefore, in addition to collecting the scattered light, the detection system must also restore its spatial coherence.

The coherence length, f, or the distance over which the scattered light is spatially coherent can be approximated by equation $(3.1)^{36}$

$$f = \frac{\lambda}{\Delta \theta} \tag{3.1}$$

where λ is the wavelength, and $\Delta\theta$ is the angular spread in the scattered light. A larger value for f implies a greater degree of spatial coherence. It is evident, therefore, that spatial coherence can be restored by reducing the volume of $\Delta\theta$, which is dependent primarily on the width of the receiver slit. However, stopping down the slit also decreases the amount of scattered light reaching the detector, so that the best design must necessarily be a compromise. Ideally, the aperture size of the receiver slit should be of the same order as the dimensions of the illuminated volume.

A diagram of the detection system is illustrated in Figure 3.5.

The receiver slit (Figure 3.5-b) has dimensions of 0.024" (width) by

0.500" (height), thereby limiting the amount of light collected to that contained within the following angles:

(horizontal) = $0^{\circ}19^{\circ}$ or 5.6 mrad

(azimuthal) = $46^{\circ}30'$ or 0.82 rad

The horizontal angle is kept small to increase angular resolution, while the azimuthal angle is made relatively larger to increase the amount of

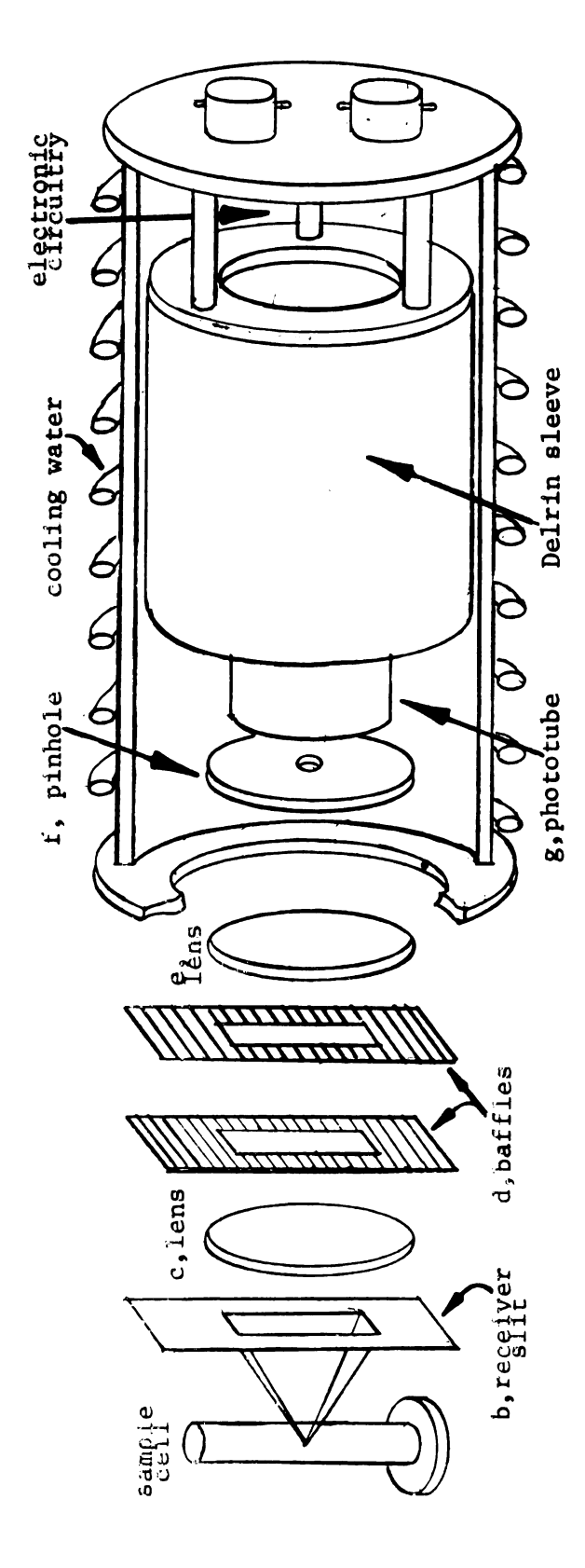


FIGURE 3.5 - Detection System

light collected. The slit is interchangeable if different dimensions would be more suitable for a particular experiment.

Light passing through the slit is collected by a lens (Figure 3.5-c) whose focal point is located at the center of the sample cell. Any stray light entering the slit will not be focused by the lens and should be blocked by a series of two baffles (Figure 3.5-d). The light which is focused by the first lens (Figure 3.5-c) is collected by a second lens (Figure 3.5-e) and focused onto a 2 mm pinhole (Figure 3.5-f) immediately in front of the phototube (Figure 3.5-g).

The detector is an EMI Model 9558C photomultiplier tube, which has an S-20, tri-alkali type cathode surface, and 11 venetian-blind dynodes with CsSb secondary emitting surfaces. The cathode sensitivity is 102uA/L, and the dark current is 5 x 10 A at 1020V. The circuit illustrated in Figure 3.6, recommended by EMI for applications requiring linearity and high gain, was wired onto the phototube socket.

Power for the phototube was supplied by a Kepco Model ABC 1500(M) high voltage, regulated d-c supply.

Wave Analyzer and Recorder

The output of the phototube contains the spectrum of beat frequencies between all components in the scattered light. A General Radio Model 1900-A Wave Analyzer scans the frequency spectrum and measures the amplitude of each component between 0 and 54 kHz.

The input signal to the wave analyzer is adjusted to the proper level, which may be from 30 uv to 300 v, by means of a calibrated input attenuator. Because of the high sensitivity of the wave analyzer, it was not necessary to pre-amplify the signal from the phototube. The analyzer has an input impedance of 1 megohm, and therefore can measure

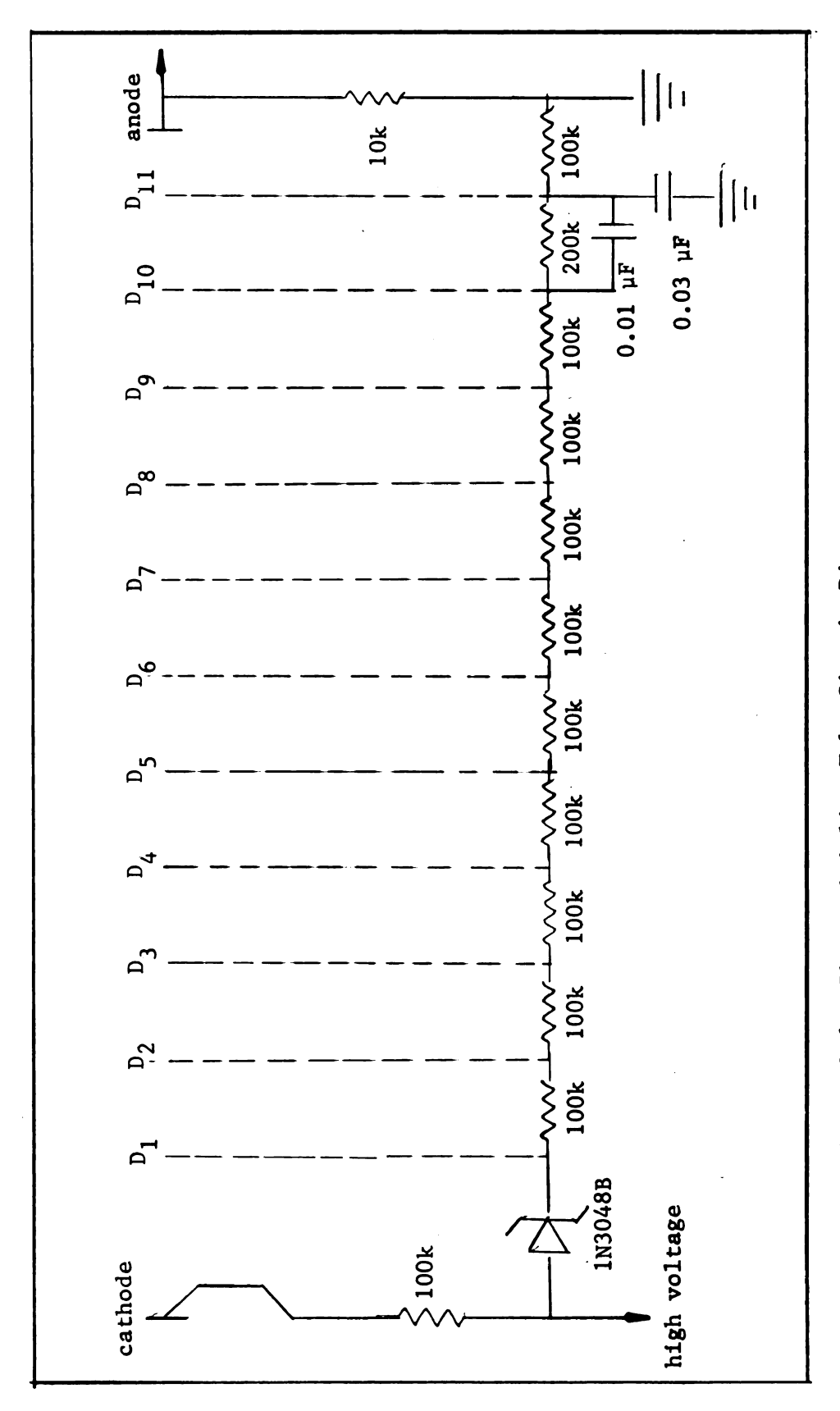
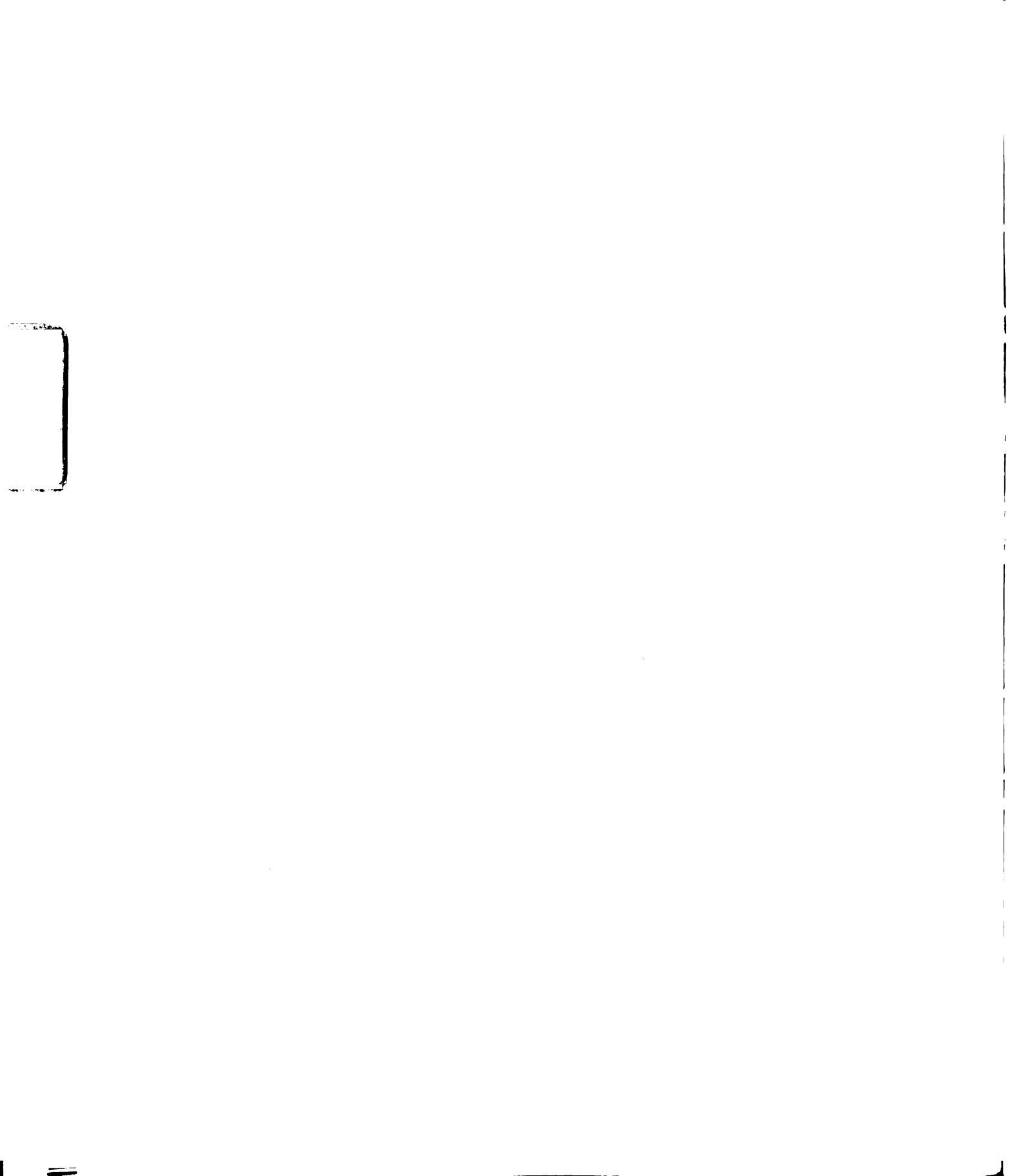


FIGURE 3.6 - Photomultiplier Tube Circuit Diagram



photocurrents lower than 30 picoamps at the 30 $\mu\nu$ setting.

The frequency components in the input signal are scanned by beating them against the signal from a variable local oscillator in a mixer circuit. The oscillator sweeps from 100 kHz to 154 kHz and heterodynes all frequencies in this range to a frequency of 100 kHz. The output transformer of the mixer stage is tuned to the 100 kHz signal, which then is filtered by a 100 kHz crystal filter with a bandwidth adjustable to 3, 10, or 50 Hz. The filtered signal is then amplified and fed to a General Radio Type 1521B Graphic Level Recorder where it undergoes rectification and further amplification before recording. Because the signal is rectified prior to recording, the trace does not represent the actual power spectrum but rather the square root of the power spectrum or the voltage spectrum. To correct for this, values for amplitude obtained from the recorded spectrum are squared prior to use in final calculations.



CHAPTER IV

TEMPERATURE MEASUREMENT AND CONTROL

Sample temperature was measured as a function of the potential difference existing between a thermocouple embedded in the copper block surrounding the sample cell (Figure 3.3) and an identical thermocouple immersed in an ice bath. EMF values were determined with a Portametric Model 300 Potentiometer-Voltmeter Bridge in conjunction with a Keithley Model 155 Null Detector-Microvoltmeter. The use of this particular null detector as an external meter for the bridge extended the range of measurements to ±0.04 µv or ±0.001°C.

Thermocouples were prepared from 20-gauge high-purity copper and constantan thermocouple wire obtained from the Leeds and Northrup Company. Junctions were formed by twisting the ends of the bare wires together and fusing in the flame of an oxygen-methane torch.

Absolute temperature calibration of the thermocouples was performed in a thermostated paraffin oil bath by comparison against a Leeds and Northrup Model 8163 four-terminal platinum resistance thermometer. The temperature of the paraffin oil was regulated to approximately $\pm 0.001^{\circ}$ C with a YSI Model 72 proportional temperature controller and thermistor probe. Temperature fluctuations in the bath were monitored with a thermocouple and a recorder which had been modified to respond to voltage changes of $\pm 0.08~\mu v$, or temperature changes of $\pm 0.002^{\circ}$ C.

The resistance of the platinum thermometer was measured with a Leeds and Northrup Model 8067 Mueller Temperature Bridge, a mercury commutator, and a Keithley null detector. The commutator is a triple pole, double throw, mercury-cup switch which reverses the current flow through the thermometer without having to interchange leads. Measurements are made with current flowing in both the forward and reverse directions to average out errors due to contact potential, which may be significant when accuracy to ±0.001 ohms is desired. Current through the bridge was held constant at 2.0 ma with the supply illustrated in Figure 4.1.

The thermocouple to be calibrated and the platinum thermometer were placed in close proximity in the thermostatic bath. When the recorder indicated that the bath temperature had stabilized, alternate measurements of thermocouple EMF and thermometer resistance were made. Approximately six readings were obtained for EMF and for resistance with current flowing in each direction. This procedure was repeated at 1° C intervals between 30° C and 70° C, and at 0.5° C intervals between 70° C and 85° C. The results at 2° C intervals are listed in Table (4.1). The average deviation for all EMF measurements was ± 0.06 µv or $\pm 0.002^{\circ}$ C, while that for resistance measurements was ± 0.00010 or $\pm 0.001^{\circ}$ C (the temperature coefficient of the platinum thermometer was -0.1 $\Omega/{^{\circ}}$ C).

It was desired to find the relationship between EMF and temperature.

This could be accomplished by first determining the temperature corresponding to each resistance value from the Callendar-Van Dusen equation

$$T = \left(\frac{R_T - R_0}{\alpha R_0}\right) + \delta\left(\frac{T}{100} - 1\right) + \beta\left(\frac{T}{100} - 1\right)\left(\frac{T}{100}\right)^3 \tag{4.1}$$

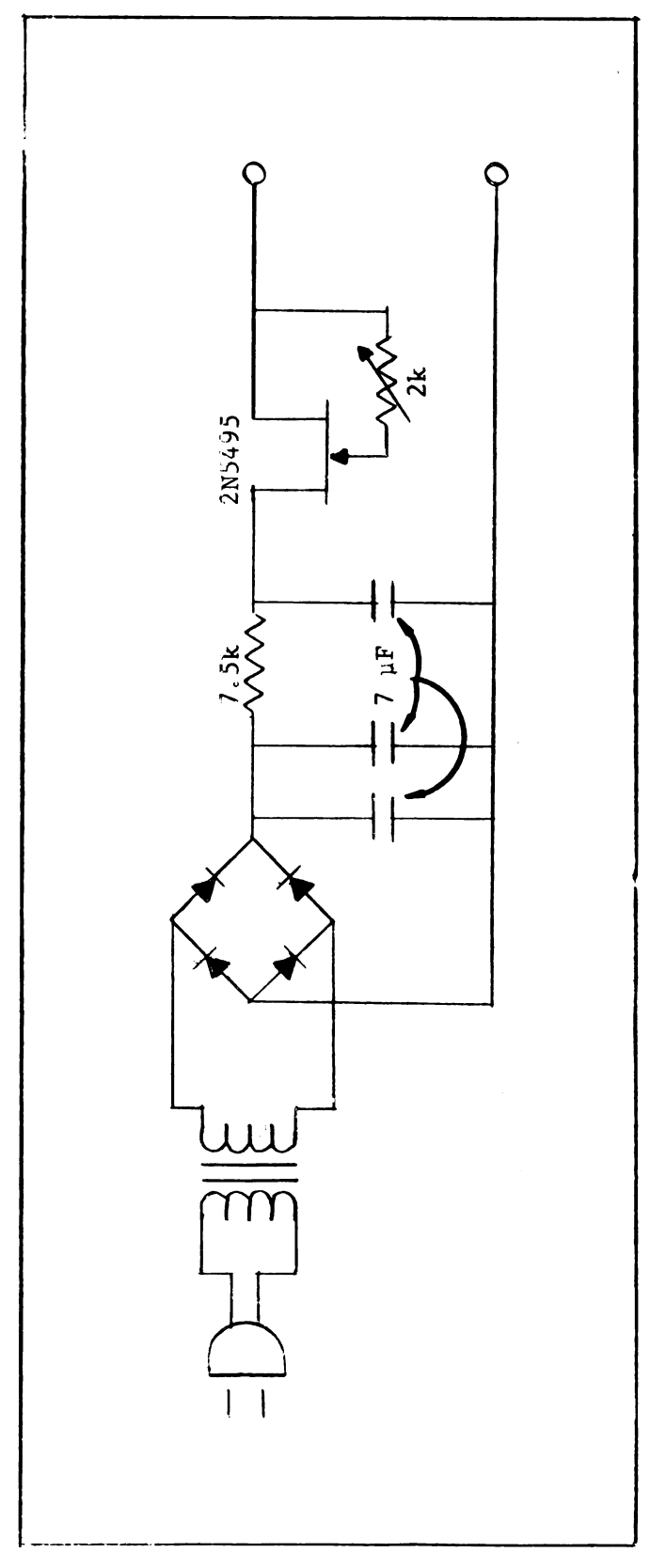


FIGURE 4.1 - Constant Current Supply for Resistance Bridge

TABLE 4.1 - Calibration of Copper-Constantan Thermocouple Against

A Platinum Thermometer

Temp.	EMF	δE	Ravg	δR avg
(°C)	(μV)	(μ V)	(ohms)	(ohms)
0.0	1032.7	0	25.5128	0.00008
30 . 0	1182.9	0.06	28.5418	0.00008
31.0	1226.2	0.06	28.6502	0.00013
32.0	1269.9	0	28.7557	0.00006
33.0	1312.2	0	28.8610	0.00006
34.0	1355.3	0.08	28.9623	0.00011
36.0	1436.0	0	29.1630	0.00007
38.0	1518.1	0.08	29.3575	0.00008
40.0	1598.7	0.09	29.5510	0.00011
42.0	1685.1	0.09	29.7567	0.00013
44.0	1767.6	0.07	29.9598	0.00007
46.0	1852.0	0.10	30.1602	0.00013
48.0	1935.4	0.14	30.3535	0.00016
50.0	2021.9	0.08	30.5524	0.00018
52.0	2149.6	0.04	30.8522	0.00011
54.0	2236.2	0.06	31.0535	0.00012
56.0	2326.5	0.05	31.2532	0.00007
58,0	2413.4	0.08	31.4523	0.00008
60 ، 0	2499。9	0.10	31.6518	0.00014
62.0	2586。 5	0	31,8500	0.00013
64,0	2677.0	0.04	32.0402	0
66.0	2765.5	0	32。2534	0.00013
68.0	2355.1	0.04	32.4557	0.00007
70 ₂ 0	2946.0	0.09	32,6600	0.00013
72.0	2997。3	0 。 05	32.7746	0,00012
74.0	3110 25	0	33 。0280	0.00012
76.0	3200。2	0.04	33,2279	0.00008
78.0	3293.3	0.10	33.4333	0.00008

where

T = temperature in OC

RT = measured value of resistance at 2.0 ma bridge current

 $R_0 = 1.4884$ ohms

 $\alpha = 0.00392604$

 $\beta = \begin{cases} 0.1106, T < 0^{\circ}C \\ 0, T > 0^{\circ}C \end{cases}$

 $\delta = 1.4919$

A Fortran IV program, RESTEM (Appendix A), was written which would perform the necessary calculations. The values for T obtained from the program were combined with their corresponding EMF values, and by means of another Fortran program, EMFFT (Appendix A), which was written for use with a multinomial regression analysis routine, the equation for the best smooth curve through the experimental points was determined

EMF =
$$0.02440 + 0.03671T + 0.67467 \times 10^{-4}T^2 - 0.14709 \times 10^{-10}T^5$$
(4.2)

The standard errors of the coefficients of T, T^2 , and T^5 are, respectively, 3.78×10^{-4} , 4.82×10^{-6} , and 2.73×10^{-12} . The average temperature coefficient (slope of curve) obtained from the above expression is 0.042 mV/deg, which is in good agreement with CRC Handbook value of 0.040 mV/deg for a copper-constantan thermocouple.

To facilitate the conversion of EMF values to temperature, the Fortran program TEMF (see Appendix A) was written to print out the corresponding values of temperature and EMF for all temperatures between 30°C and 85°C at 0.01°C intervals. Interpolation to 0.002°C was easily accomplished, although this exceeds the accuracy to which temperature

could be measured.

Due to the thermal lag which existed between the sample cell and the copper block, it was found necessary to calibrate the temperature of the sample against that of the copper block. Previously calibrated thermocouples were placed in the copper block and in the sample cell containing paraffin oil. EMF measurements were made at 1°C intervals between 25°C and 75°C, and at 0.5°C intervals between 70°C and 85°C. The results obtained for each three-degree interval were plotted on 1 mm graph paper, providing temperature resolution to 0.02°/mm. Therefore, having measured the temperature of the copper block, the temperature of the sample could be found from the graph. Results for the interval between 77°C and 80°C are illustrated in Figure (4.2).

Similar experiments were performed to determine the temperature stability of the system in several temperature ranges. Using the thermocouple arrangement described above, a series of temperature measurements were made at three controller settings; 25.000°C, 55.000°C, and 75.000°C. A minimum time of six hours was allotted for the system to come to thermal equilibrium at each setting. The voltage of each thermocouple was measured every five minutes for one hour and the mean and the average deviation determined. The results listed in Tables (4.2), (4.3), and (4.4) illustrate that stability to ±0.04 µv or ±0.001°C can be obtained at temperatures below 55°C. At higher temperatures, however, stability decreases to ±0.13 µv or ±0.003°C. This represents more than adequate control for studies on polymer solutions at the critical solution temperature inasmuch as molecular weight polydispersity will broaden the range over which the phase transition occurs to several tenths of a degree.

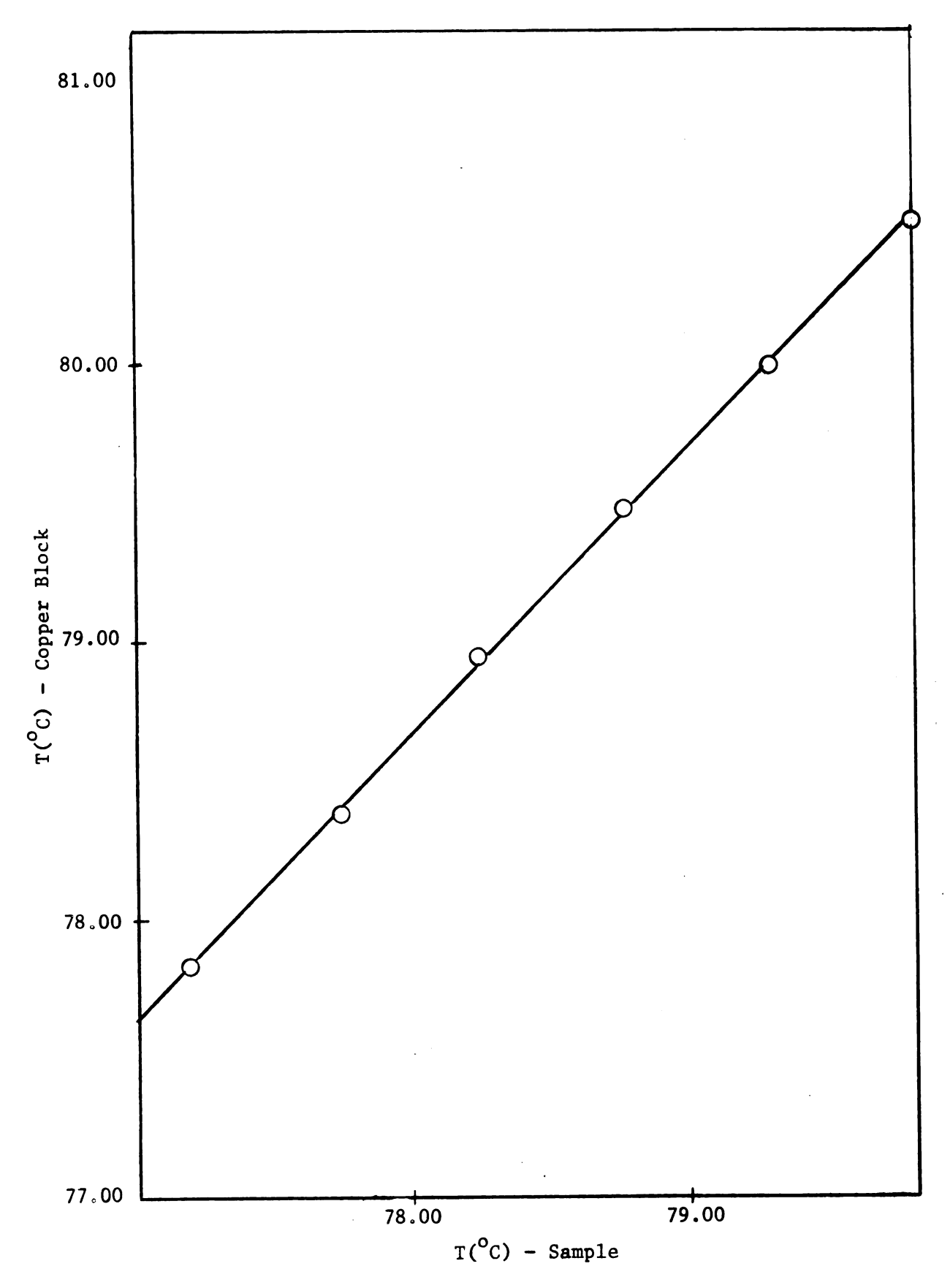


FIGURE 4.2 - Plot of Sample Temperature vs. Temperature of the Copper Block,

TABLE 4.2 - Stability of Sample Temperature at 25.00°C

Time (min.)	Thermocouple Voltage (mV)	Mean Deviation (mV)
0	1.04616	+0.00008
5	1.04606	-0.00002
10	1.04602	-0.00006
15	1.04610	+0.00002
20	1.04612	+0.00004
25	1.04608	0
30	1.04602	-0.00006
35	1.04606	-0.00002
40	1.04600	-0.00008
45	1.04608	0
50	1.04610	-0.00008
55	1.04604	-0.00004
60	1.04610	+0.00002
Average	1.04608	±0.00004

TABLE 4.3 - Stability of Sample Temperature at 55.00°C

Time (min.)	Thermocouple Voltage (mV)	Mean Deviation
0	2.27982	-0.00002
5	2.27990	+0.00006
10	2.27982	-0.00002
15	2.27985	+0.00001
20	2.27988	+0.00004
25	2.27980	-0.00004
30	2.27975	-0.00009
35	2.27982	-0.00002
40	2.27990	+0.00006
45	2.27984	0
50	2.27978	-0.00006
55	2.27985	+0.00001
60	2.27988	+0.00004
Average	2.27984	+ 0.00004

TABLE 4.4 - Stability of Sample Temperature at 75.00°C

Time (min.)	Thermocouple Voltage	Mean Deviation (mV)
0	3.16342	-0.00018
5	3.16364	+0.00004
10	3.16380	+0.00020
15	3.16344	-0.00016
20	3.16378	+0.00018
25	3.16356	-0.00004
30	3.16388	-0.00022
35	3.16348	-0.00012
40	3.16365	+0.00005
45	3.16374	+0.00014
50	3.16382	-0.00022
55	3.16346	-0.00014
60	3.16362	+0.00002
Average	3.16360	±0.00013

CHAPTER V

SAMPLE PREPARATION

Preparation of Polyisobutylene

Polyisobutylene was prepared from C.P. grade (99.0% pure) gaseous isobutylene by cation-catalyzed polymerization techniques ^{37,38}. The reaction involved has been known to proceed with explosive violence, and, consequently, several precautions were observed in preparing the polymer. To dissipate the heat generated by the reaction at a faster rate, the liquified isobutylene was diluted 1:4 with propane, and the reaction was carried out at liquid nitrogen temperatures. In addition, the entire reaction assembly consisting of the reaction flask and liquid nitrogen dewar, was housed in a 3/8" Plexiglas shield. Although the reaction was performed many times, however, no difficulties associated with the explosiveness of the reaction were encountered.

The bulk polymer obtained from the reaction was dissolved in 100 ml of benzene, and reprecipitated by adding the solution slowly to 200 ml of cold methanol (-20°C) with continuous agitation. This procedure was followed by several washings with cold methanol, which gave the polymer a less swollen, more rubber-like texture. The material was dried in a vacuum oven at 45°C to constant weight. Yield was approximately 9 gms of polymer per 20 ml of liquid isobutylene. Total polymer obtained by this procedure amounted to 39.8 gms.

Fractionation

Precise line-broadening measurements on polymer solutions near a critical solution point requires that the molecular weight distribution of the sample be as narrow as possible. Fractionations were performed according to Kamide's ^{39,40,41} method of fractional precipitation which is based on the solution theories of Flory and Huggins. Basically, Kamide's theory predicts that a high fractionation efficiency will be obtained provided that the initial solution is very dilute and/or the amount of precipitate collected in the first fraction is not too small. This prediction has been experimentally confirmed by Koningsveld and Staverman ⁴² on a polyethylene/diphenylether system, and by Kamide, Ogawa, Nakayama and Kawai ⁴³ on an atactic polystyrene/methylcyclohexane system.

The first fraction was separated from the bulk polymer by precipitation from a thermodynamically poor solvent (i.e., one for which ΔH_{mix} is very large). The system chosen was a 57.9:42.1 mixture of methylcyclohexane in n-butanol ⁴⁴. Approximately 5 liters of solvent in a 6-liter Erlenmeyer flask were placed in an oil bath heated to 70° C. The temperature of the bath was controlled to $\pm 0.01^{\circ}$ C using a YSI model 72 proportional temperature controller and thermistor probe. The polymer, in a swollen form, was added to the solvent mixture under continuous agitation and left for 24 hours to insure that the flask and contents were in thermal equilibrium with the bath. The temperature of the bath was then lowered gradually at the rate of 1 degree per hour or 10 degrees per day until a final temperature of 25°C had been reached. Stirring of the polymer solution, which was now quite turbid, was discontinued to allow the polymer to settle.

After 48 hours, the solvent phase was drawn off into another 6-liter Erlenmeyer flask, leaving the precipitated polymeric mass at the bottom of the flask. Several washings with cold methanol gave the polymer a rubber-like texture which could be easily transferred to a beaker for drying in a vacuum oven. Weight of the first fraction was 17.0 grams. Recovery of polymer in the solvent phase was accomplished by evaporation of the solvent followed by treatment with cold methanol. The polymer obtained from this process was designated as fraction 2, and amounted to 20.5 grams.

The polymer needed to make samples for light scattering experiments was obtained by refractionation of the first and second fractions obtained above. The separations were performed in a 4-liter separatory funnel using solvent-nonsolvent precipitation techniques. The funnel was positioned in a thermostated oil bath which held the temperature of the polymer solution constant to $\frac{1}{2}0.01^{\circ}$ C during fractionation.

The 17.0 gram polymer fraction was added to the separatory funnel in a swollen form and dissolved in 2.5 liters of benzene under continuous stirring at 30°C. Methanol was added drop-wise via a buret until the solution became turbid. At this time, the addition of methanol was stopped, although agitation of the solution at constant temperature was continued for 4 to 6 hours. The stirring motor was then turned off and the polymer allowed to settle out overnight.

The polymer which had gelled in the bottom of the funnel could easily be separated from the solvent phase by decanting the latter into a 4-liter Erlenmeyer. Two hundred ml of warm benzene was added to the funnel and swirled to dissolve the polymer. The solution was then

filtered twice through a fine sintered glass filter (pore size 4-5.5µ) under nitrogen pressure to remove dust and other impurities which might interfere with light scattering measurements. The polymer was recovered by precipitating in 300 ml of cold methanol, followed by several rinsings with portions of cold methanol. The polyisobutylene was transferred to a beaker and dried to constant weight in a vacuum oven. Final weight of the polymer, designated as fraction 1A, was 4.8 gms.

The polymer remaining in the solvent phase from the above separation was recovered in two additional fractionation procedures, yielding fractions 1B and 1C which weighed 12.2 and 10.5 gms, respectively.

Similarly, fraction 2 was separated into subfractions 2A, 2B and 2C.

The polymer fractions ultimately used in line-broadening studies were obtained by refractionation of fractions 1A and 2A according to the fractionation scheme given in Figure 5.1. The hexagonal enclosures in Figure 5.1 indicate those fractions selected for examination.

Molecular Weight Determination

The conventional method for molecular weight determination is via the Mark-Houwink expression

$$[n] = KM^{\alpha}$$
 (5.1)

where $\left[\eta\right]$ is the intrinsic viscosity, M is the molecular weight, and K and α and constants for the polymer-solvent system at a particular temperature. Values for K and α for several systems are available in the Polymer Handbook 45 .

The intrinsic viscosity can be found from expressions derived by Huggins and Kraemer relating the relative viscosities to the concentrations at which they were measured,

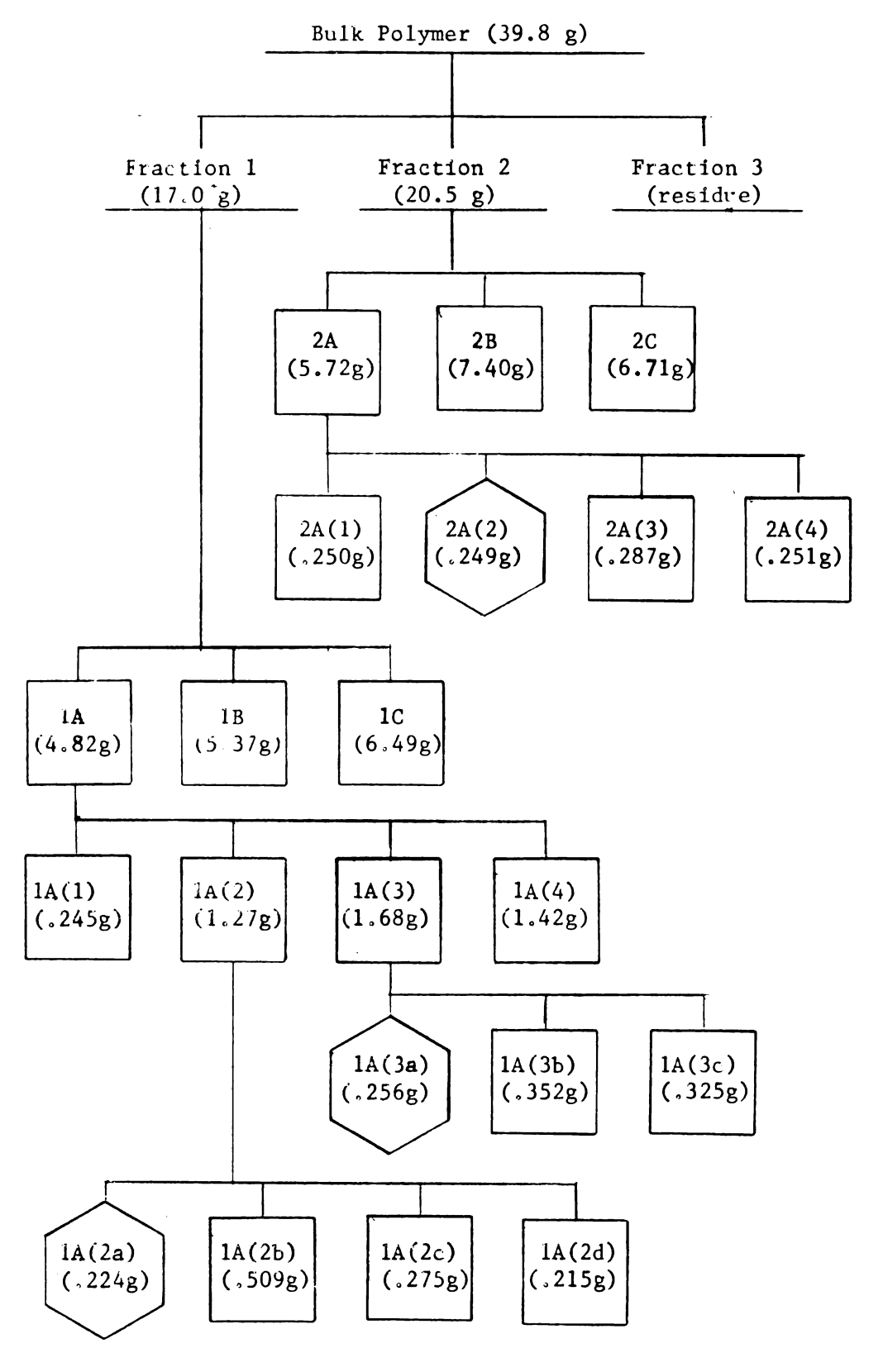


FIGURE 5.1 - Polymer Fractionation Scheme

Huggins equation

$$\frac{(\eta_r - 1)}{C} = \left[\eta\right] + k_1 \left[\eta\right]^2 C \tag{5.2}$$

Kraemer equation

$$\frac{\ln \eta_{\mathbf{r}}}{C} = \left[\eta\right] - k_2 \left[\eta\right]^2 C \tag{5.3}$$

where n_r is the relative viscosity at concentration C, and k_1 and k_2 are constants. Expression (5.2) is the equation for a straight line with slope $k_1[\eta]$ and intercept $[\eta]$. Similarly, equation (5.3) has a slope of $-k_2[\eta]$ and an intercept $[\eta]$. Therefore, extrapolation of relative viscosity terms to zero concentration will yield the value of $[\eta]$ (see Figure 5.2).

Values for n were determined using a Cannon-Ubbelohde semi-micro dilution viscometer. The instrument is designed so that there is a constant pressure head on the solution as it flows through the capillary, thereby eliminating the need to charge the viscometer with the same volume of fluid for each run. As a result, dilutions can be made directly in the viscometer reservoir.

The temperature of the viscometer and its contents was controlled to the better than $\pm 0.01^{\circ}$ C using a thermostated water bath. The viscometer was aligned vertically in the bath with the aid of a cathetometer and held securely in place by a three-finger clamp.

A Breiting stopwatch with an accuracy of 0.1 second was used to measure flow rates. Readings were taken until at least three values were obtained which agreed within 0.1 second, usually requiring from four to six runs. Kinetic energy corrections were considered unnecessary

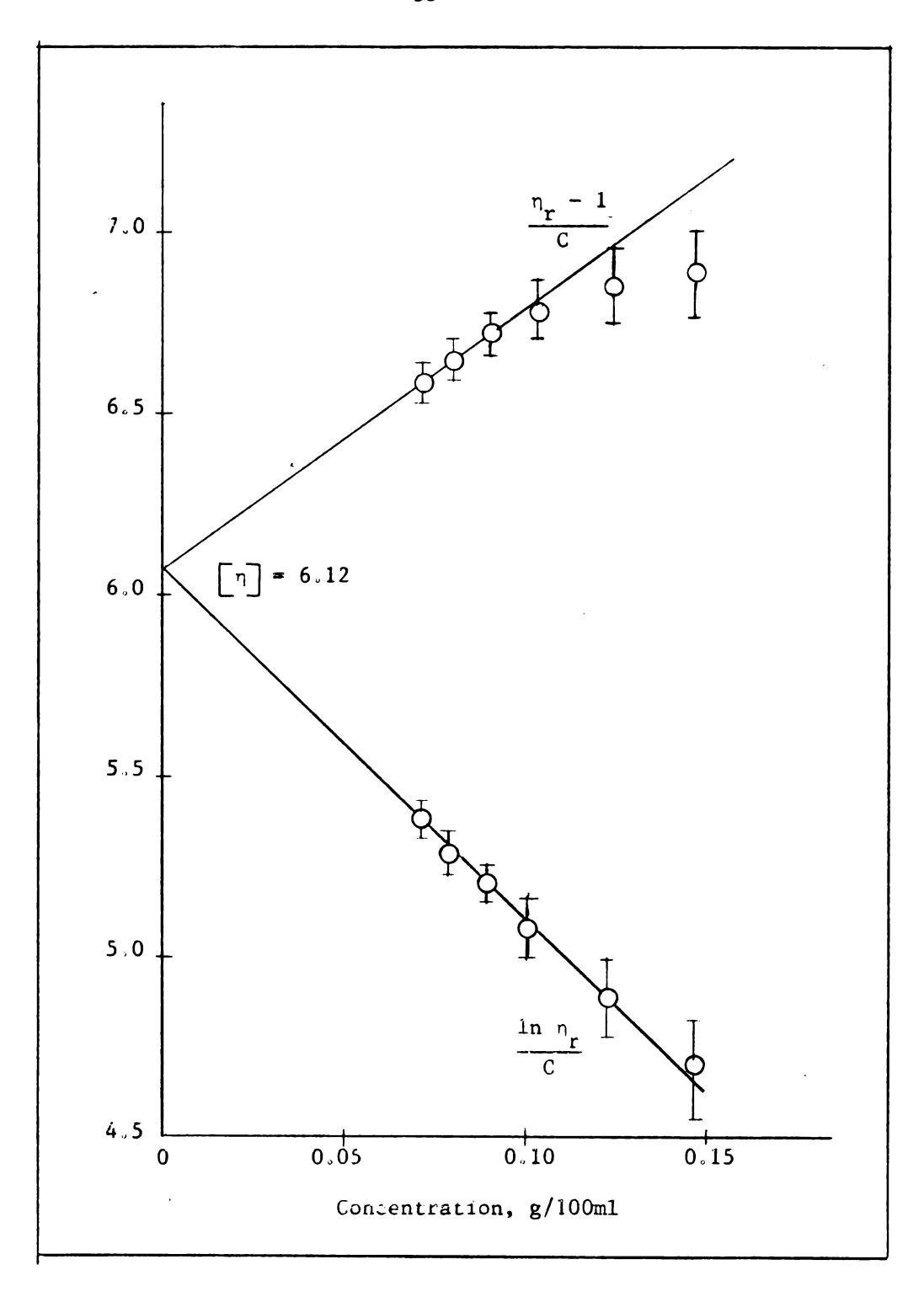


FIGURE 5.2 - Determination of Intrinsic Viscosity from Relative Viscosity Data, Fraction 2A(2).

as all times were above 250 seconds (efflux time for pure solvent, cyclohexane). The molecular weight of fraction 2A(2) determined by this method was $2.14 \times 10^6 \text{g/mol}$. Results are illustrated in Figure 5.2.

An attempt to determine $[\eta]$ for higher molecular weight samples produced results similar to those shown in Figure 5.3. The behavior of $\frac{(\eta_r-1)}{C}$ as a function of C is clearly opposite to what would be expected. Fox, Fox and Flory have demonstrated, however, that specific viscosities, (η_r-1) , of dilute solutions of high molecular weight polymer fractions are proportional to rate of shear when measured in conventional viscometers, and that if accurate determinations are desired, it is necessary to correct the measured viscosities to zero rate of shear. The following empirical expression was derived by the authors from a plot of $\ln(\eta_r-1)$ vs rate of shear:

$$\ln(\eta_r^{-1}) = \{\ln(\eta_r^{-1})\}_0 - \{\frac{\Phi}{100}\} \gamma$$
 (5.4)

where $\{\ln(\eta_r-1)\}_0$ is the value of $\ln(\eta_r-1)$ at zero rate of shear, Φ is the shear coefficient defined by $100 \times \frac{d\{\ln(\eta_r-1)\}}{d\gamma}$, and γ is the rate of shear defined by

$$\gamma = \frac{\text{rhgd}}{2s\eta_r\eta_o}$$
 (5.5)

In equation 5.5, r and s are, respectively, the radius and length of the viscometer capillary, h is the distance between upper and lower levels of liquid in the viscometer, g is the acceleration of gravity, and d is the liquid density. When shear corrected values for $\frac{(\eta_r - 1)}{C}$ were plotted as a function of C, however, little improvement in behavior

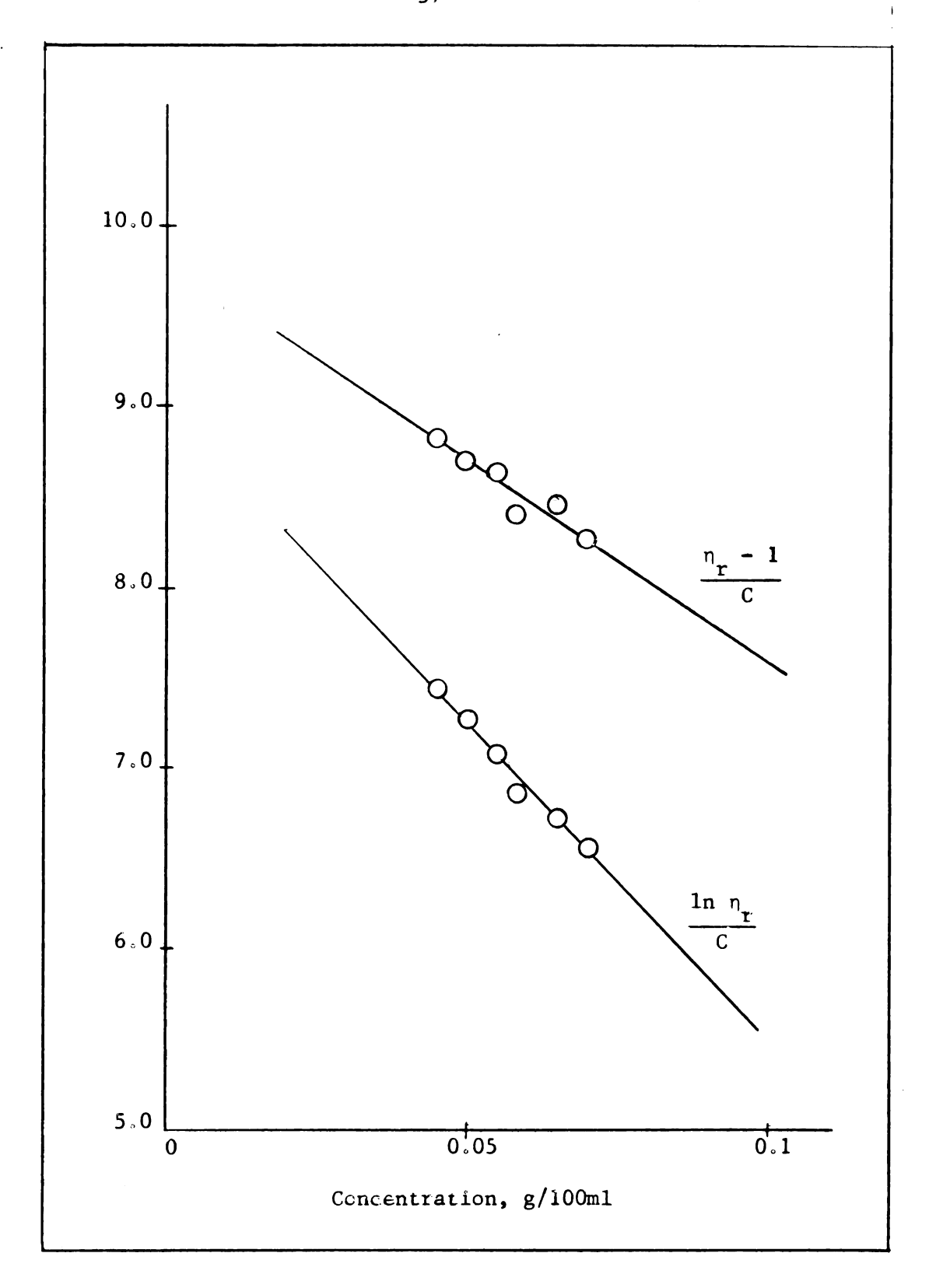


FIGURE 5.3 - Determination of Intrinsic Viscosity from Relative Viscosity Data. Fraction 1A(2a)

was observed. It was concluded, therefore, that the polyisobutylene fractions were of too high a molecular weight to be determined using viscometric methods.

An alternate method for determining polymer molecular weights has been suggested by Miller, San Filippo and Carpenter 49. It involves the resolution of the spectrum of light scattered by the polymer solution into its three components, i.e., the two Brillioun side peaks and the central Rayleigh peak. Although the intensity of the Rayleigh scattered light is dependent on polymer concentration and molecular weight, the area under the Brillioun components is a function of solvent properties alone. As a result, measurement of the ratio of the intensity of the central peak to the sum of the intensities of the side peaks, J, can be related to the weight average molecular weight, M, in an ideal dilute solution by the following expression

$$J = J_0 + BKMC$$
 (5.6)

In equation (5.6), J_{o} is the J value of the pure solvent, C is the concentration of polymer and K a constant given by

$$K = \frac{c_p}{RT^2} \left(\frac{\partial n/\partial C}{\partial n/\partial T} \right)^2$$
 (5.7)

where n is the refractive index. For "nonrelaxing" solvents, i.e., solvents in which little or no energy is transferred from the propagating pressure waves, which are responsible for Brilloun scattering, to non-propagating modes of energy, the constant B in equation (5.6) is equal to J_o. For relaxing solvents B is somewhat more complex, and for this reason, molecular weight determinations were performed in toluene, which is a nonrelaxing solvent.

For real polymer solutions, the chemical potential of the solvent, μ_1 , is expressed in the form of a virial equation

$$\mu_1 - \mu_1^0 = -RTV_1C (M^{-1} + A_2C + A_3C^2 + \cdots)$$
 (5.8)

where V_1 is the partial molar volume of the solvent, and A_2 and A_3 are the second and third virial coefficients, respectively. Equation (5.6) for non-ideal solutions then assumes the form 47,48

$$\frac{BKC}{J-J_0} = (M^{-1} + 2A_2C + 3A_3C^2 + \cdots)$$
 (5.9)

and the molecular weight, M, of the sample can be determined from a plot of $BKC/(J-J_0)$ versus C, assuming A_3 is small.

The Brillioun spectrometer which was used for determination of molecular weights by this method is illustrated in Figure 5.4. A complete description of the instrument is available in reference 49. The light source is a Spectra Physics model 165 Argon Ion laser having a maximum power output of 400 mwatts at 5145Å. The light scattered from the sample at an angle of 90° is collected and focused onto the mirrors of a scanning Fabry-Perot interferometer. The output from the interferometer is focused by a long focal length lens onto a pinhole in front of an EMI 9558B photomultiplier tube. The signal from the phototube is then amplified and the spectrum of the scattered light recorded on a strip chart recorder.

Three solutions were prepared for each of the polymer fractions 1A(2a), 1A(3a), and 2A(2). Concentrations of the solutions varied between 0.01 and 0.05 gms polymer per 100 ml toluene. Typical spectra obtained for the pure solvent and polymer solutions are illustrated in

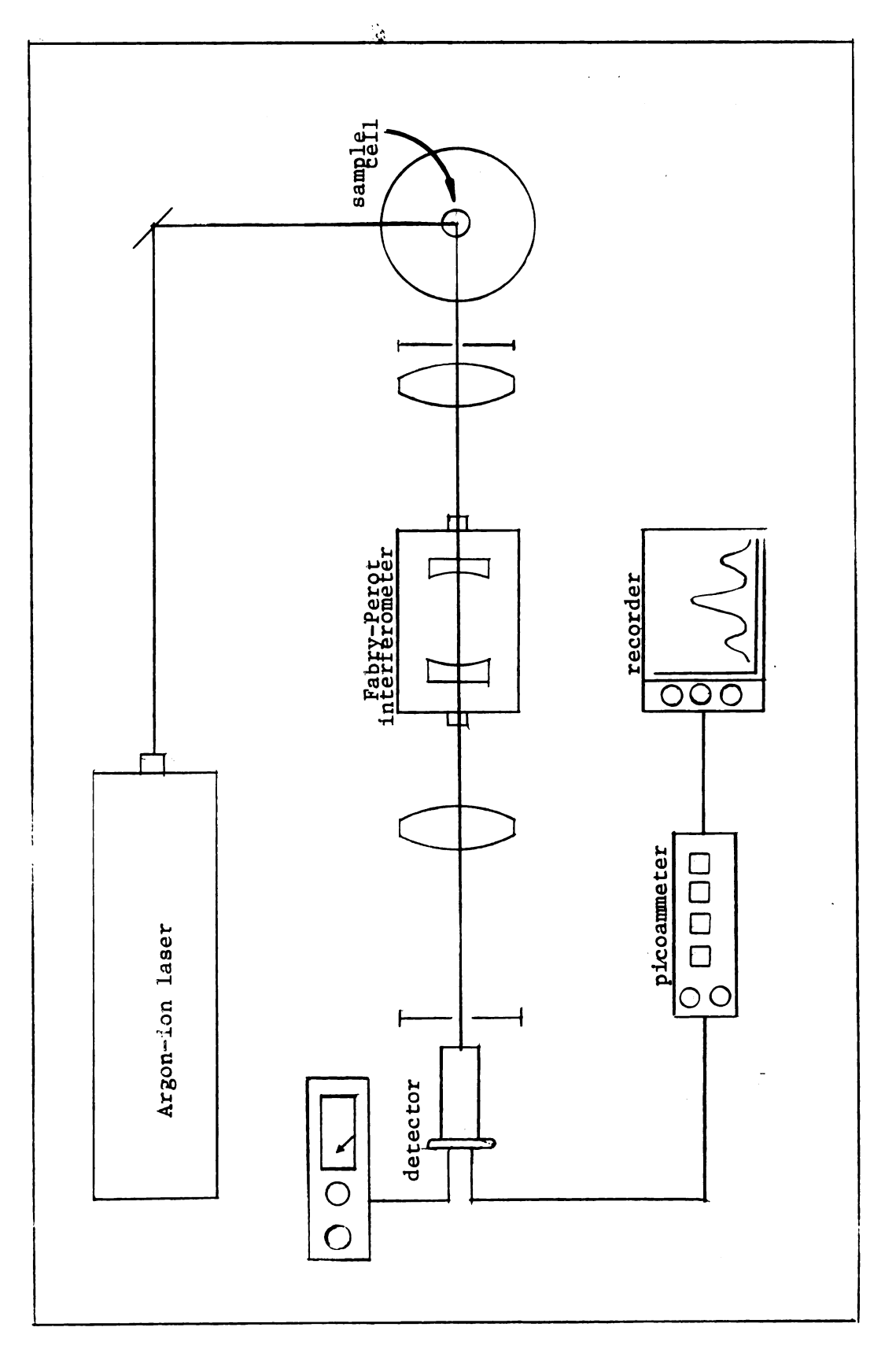


FIGURE 5.4 - Brillioun Spectrometer



Figures 5.5 and 5.6. The central, Rayleigh peak is the result of light which is elastically scattered by polymer and solvent, and is situated at the frequency of the laser line (5145Å). The symmetrically displaced Brillioun peaks are the result of light scattered by pressure waves which propagate through the medium and thereby shift the frequency of the incident light upon interaction. The frequency shift and amplitude of the Brillioun peaks, as previously indicated, are independent of polymer concentration.

The area under each of the peaks was measured with a planimeter.

Values for J were calculated from

$$J = \frac{I_R}{(I_{B_1} + I_{B_2})}$$
 (5.11)

where I_R , I_{B_1} , and I_{B_2} represent the area under the Rayleigh peak and the two Brillioun peaks, respectively. The values for J and J_o obtained from the spectra are listed in Table 5.1. Other parameters required for evaluation of equations 5.6 and 5.7 are given in Table 5.2 with appropriate literature references.

The specific refractive index, $\partial n/\partial C$, for the PIB/toluene system had to be determined experimentally inasmuch as it was not available in the literature. A Brice-Halwer differential refractometer 52 was employed for the measurements. Calibration of the instrument involved determination of an instrument constant, which was a function of the relative positions of the optical components. Solutions of NaCl and KCl of varying concentration having known $\partial n/\partial C$ values were used for this purpose. The results of the calibration experiments are given in Table 5.3. The average value determined for the instrument constant was 1.68 x 10^{-5} .

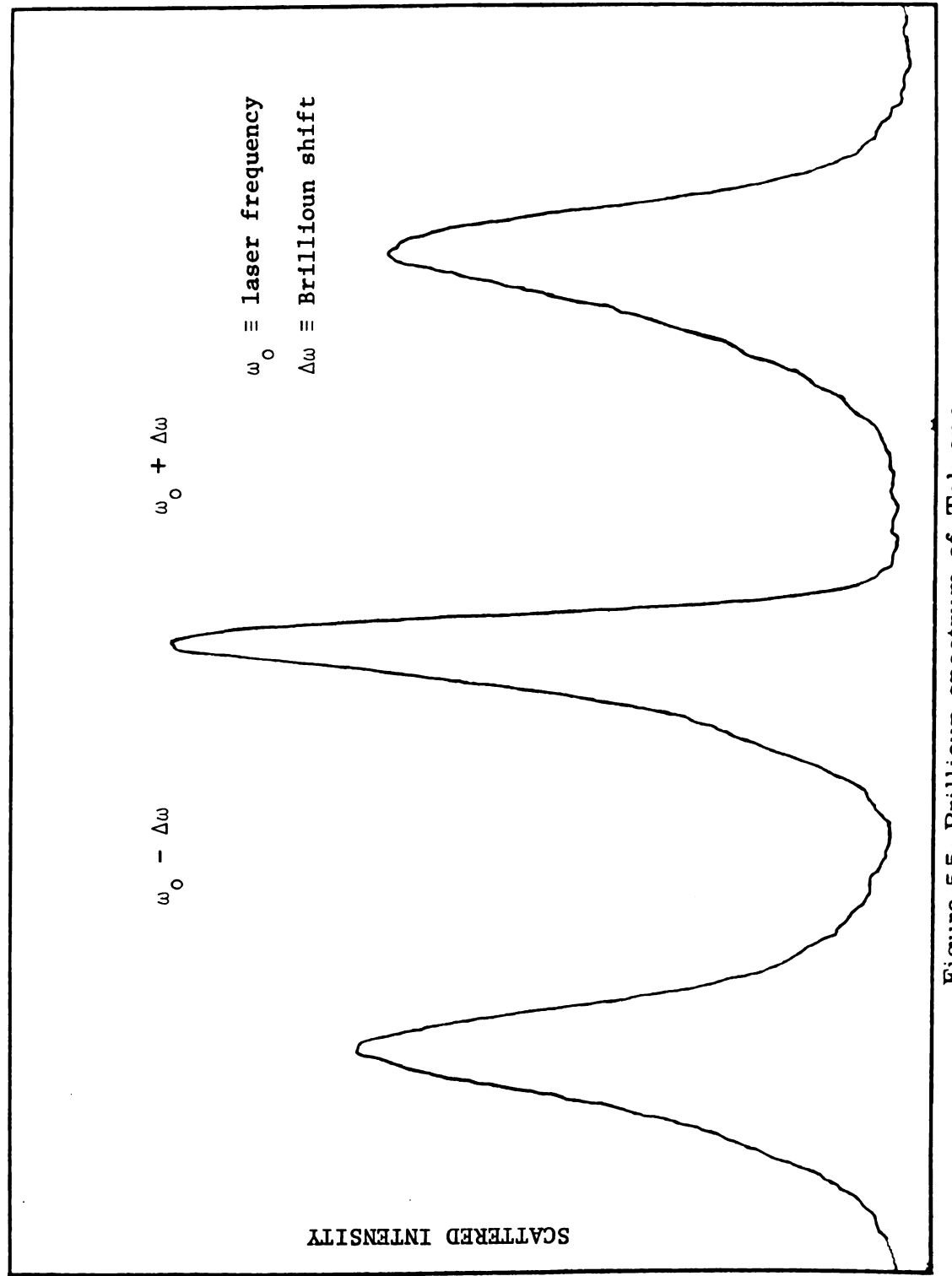


Figure 5.5-Brillioun spectrum of Toluene

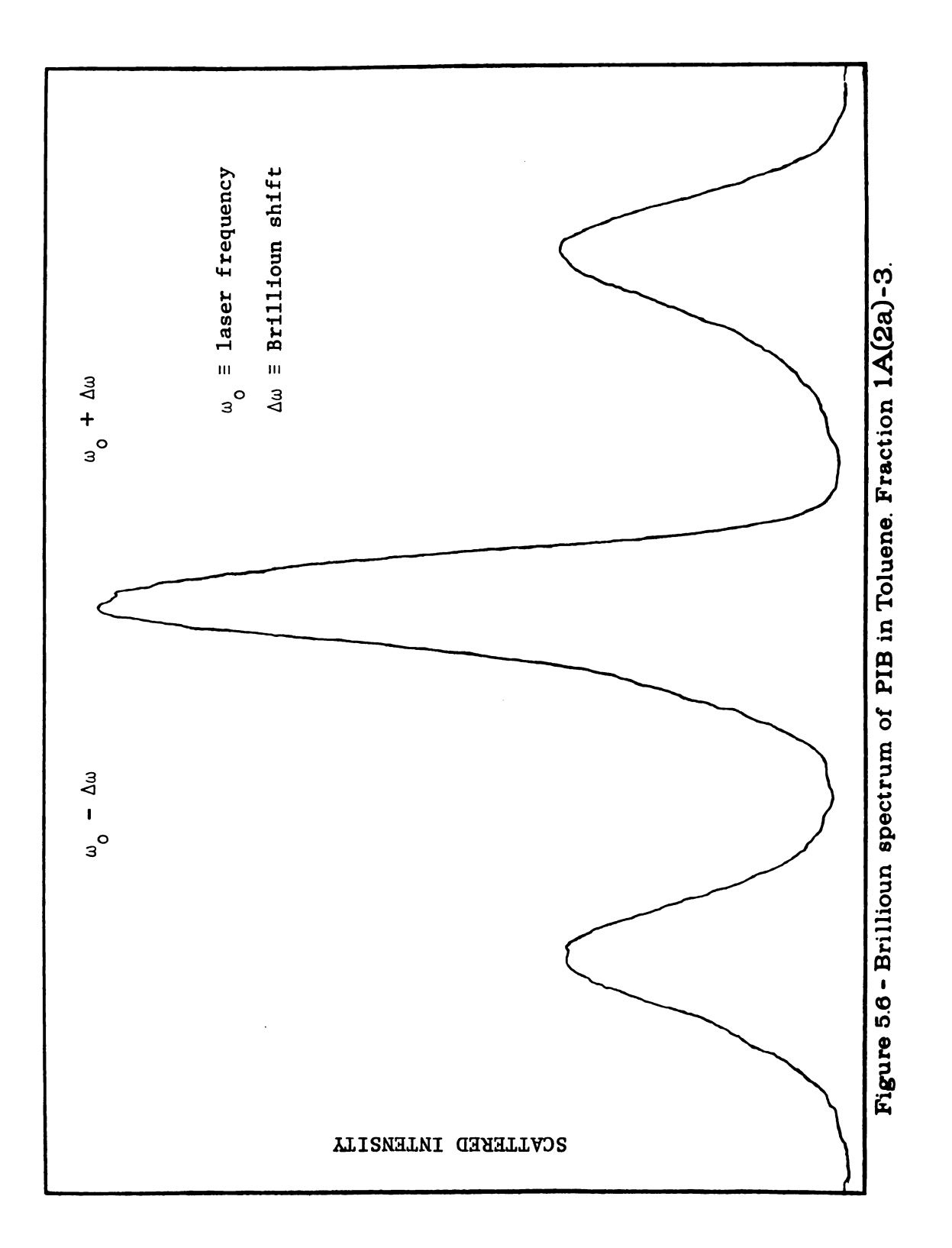


TABLE 5.1 - J Values for Various Concentrations of Polymer in Toluene.

Sample	Concentration (g ml ⁻¹ x 10 ⁴)	J	10 ⁴ C J-Jo
Toluene		0.44±0.02	
1A(2a)-1	1.32	0.98±0.03	2.44±0.05
1A(2a)-2	4.44	1.57±0.06	4.19±0.08
îA(2a)-3	6.93	1.73±0.06	5.50±0.08
1A(3b)-1	1,84	0 ° 84 7 0 ° 01	4.61±0.03
1A(3b)-2	4.51	1 ° 27 ±0 ° 05	6.27±0.07
1A(3b)-3	7.08	1,41±0,05	7 ° 38 ± 0 ° 07
2A(2) -1	1,68	0,63±0,02	8 ° 85 ∓0 ° 04
2A(Z) -2	4.40	0.84±0.03	10.9±0.05
2A(2) -3	7.00	0.98±0.03	13.0±0.05

TABLE 5.2 - Light Scattering Parameters for Toluene

В	0.360 *
c _p	$0.3580 \text{ cal mol}^{-1} \text{ deg}^{-1} *$
∂n/∂T	$-5.51 \times 10^{-4} \text{ deg}^{-1} *$
∂n/∂C	$\begin{cases} 0.0112 \text{ m1 g}_{-1}^{-1}, & \lambda=4358+\\ 0.0043 \text{ m1 g}_{-1}, & \lambda=5145\\ 0.0015 \text{ m1 g}, & \lambda=5461 \end{cases}$
K	$1.22 \times 10^{-3} +$
Jo	0.44†
R	$1.987 \text{ cal mol}^{-1} \text{ deg}^{-1}$

^{*} reference 48

[†] experimentally determined

TABLE 5.3 - Differential Refractometer Constants Determined for Various Salt Solutions.

Position of Optical Components

Scope - 37.35 cm

Lens - 68.05 cm

Cell -103.00 cm

Slit -113.45 cm

Lamp -145.00 cm

Salt	Concentration	Δnxl	10 ³	L	/d	kx1	.0 ⁵
	(g salt/kg H ₂ 0)	54618	4358Å	54618	4358Å	54 61 Å	4358Å
NaC1	3.375	0.5925	0.6140	33.3	36.0	1.78	1.71
NaC1	6.900	1.201	1.246	72.7	76.6	1.65	1.65
NaC1	11.311	1.955	2.030	116.2	121.4	1.68	1.67
KC1	1.0829	1.468	1.520	90.6	89.0	1.62	1.72

The $\partial n/\partial C$ values for the polymer solutions were obtained from equation 5.12

$$\partial n/\partial C = \frac{k\Delta d}{C}$$
 (5.12)

where k is the instrument constant, C is the solution concentration, and d is the differential measurement of slit deviation when the cell is oriented at 0° and 180° to the incoming beam (see reference 50). Measurements were made at two wavelengths of a Hg vapor lamp, 4358Å and 5461Å, with the required value of 5145Å determined by interpolation.

The graphs of BKC/(J-J $_{o}$) illustrated in Figure 5.7 were constructed from the values for J and C given in Table 5.1. The molecular weights determined from equation 5.9 are 3.40 x 10^{6} , 6.34 x 10^{6} and 13.4 x 10^{6} for fractions 2A (2), 1A (3b), and 1A (2a), respectively. It is interesting to note that the molecular weight of fraction 2A(2) determined by this method is in relatively good agreement with the value determined by viscometry, considering the experimental complexities involved in obtaining the light scattering measurements, and the independence of the two measuring techniques.

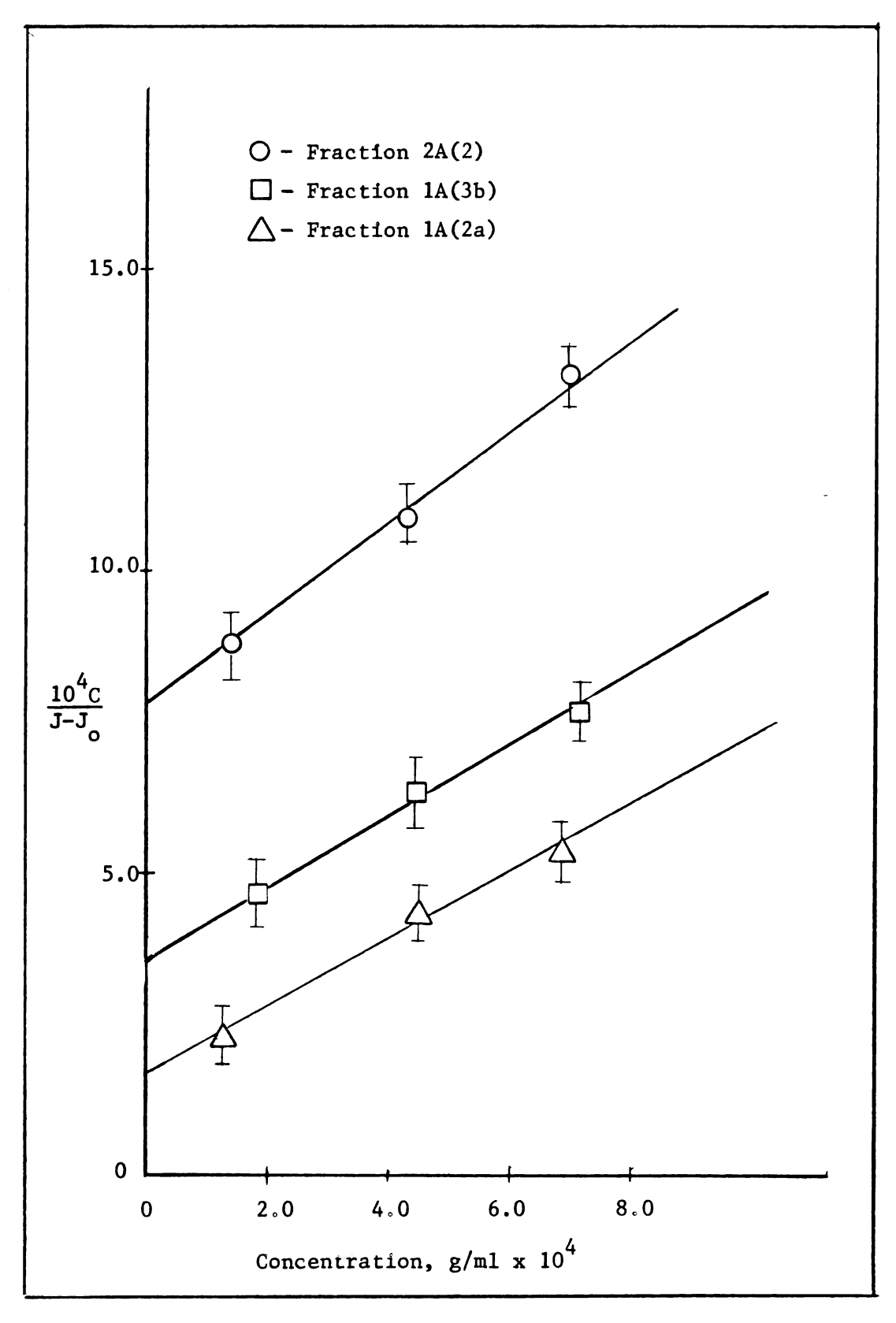


FIGURE 5.7 - Extrapolation of Light Scattering Data to Zero Concentration

CHAPTER VI

EXPERIMENTAL

Polystyrene Spheres

Stock samples of 0.109 µ and 0.357 µ diameter polystyrene latex spheres were obtained as a gift from the Bioproducts Division of the Dow Chemical Company. Suspensions of the particles were prepared with triply distilled water which had been filtered to remove dust and other foreign material. Concentration of the latex suspensions was kept low (0.03-0.05 mg/cc) to avoid multiple scattering effects from the strongly scattering systems. Stamm⁵¹ has shown that the diffusion coefficient of latex particles in aqueous suspensions is independent of concentration in this region.

Diffusion studies on latex systems were conducted at 25.00°C.

Spectra were recorded at angular intervals of 15° between 0° and 90°.

Typical spectra obtained for the latex suspensions are illustrated in Figures 6.1 and 6.2.

The peaks occurring at 60 and 120 Hz are noise components which were traced to the poorly regulated laser power supply. They were evident primarily in spectra obtained at low scattering angles, where more of the unscattered laser light reaches the detector, and also in spectra obtained for weakly scattering systems (polymer solutions). Filtering was not possible inasmuch as the ripple components occur in that region of the spectrum (near d-c) under investigation.

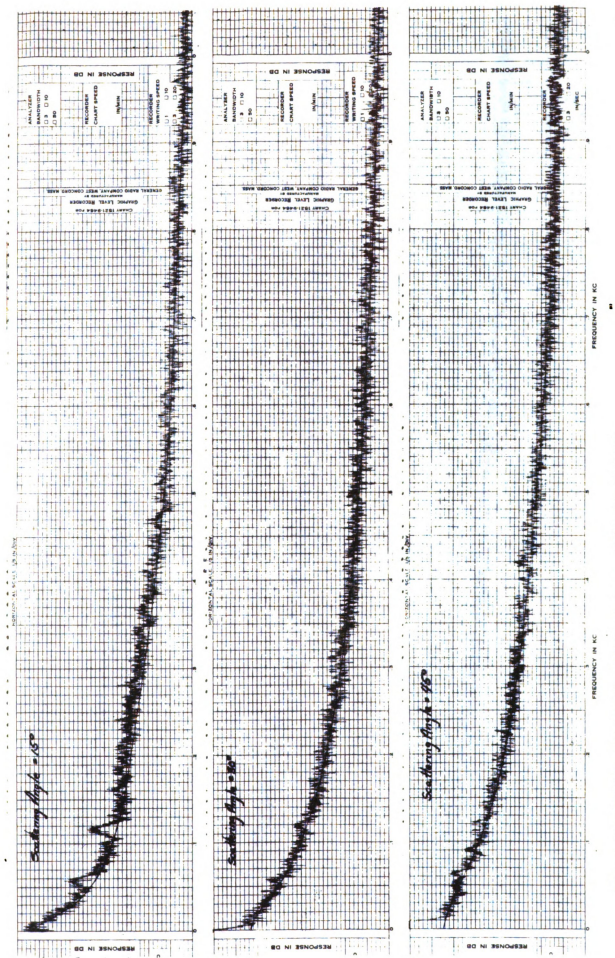
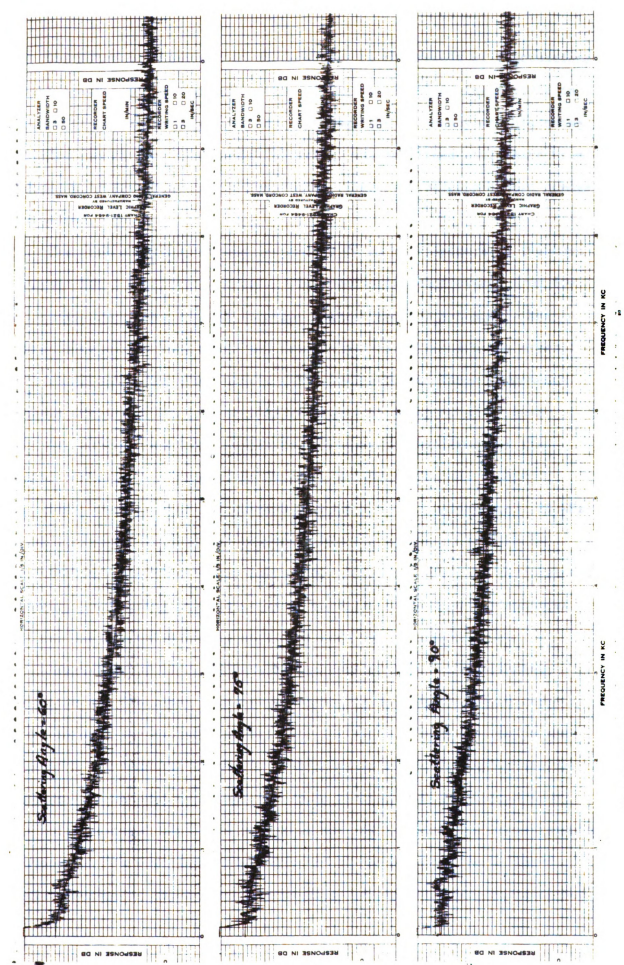


Figure 6.1 - Light-Beating Spectra. 0.357 micron particles. T = 25,00°C



gure 6.2 - Light beating spectra, 0.357 micron particles, T=25.00°C

The noise superimposed on the spectrum is the result of fluctuations in the scattered light intensity created by particles moving rapidly in and out of the illuminated volume. Although the frequency of this noise was also too low for electronic filtering, the amplitude could have been reduced by stirring the latex suspension, thereby producing a more homogenous medium.

The peak observed between d-c and 20 Hz on most spectra is the wave analyzer local oscillator signal. The local oscillator sweeps from 100 kHz to 154 kHz to haterodyne incoming signals between d-c and 54 kHz to a frequency of 100 kHz, which can then be passed by the 100 kHz crystal filter following the mixer stage. When analyzing for those components between d-c and 20 Hz, the oscillator signal is sweeping at or near 100 kHz, and is passed by the filter. Because the amplitude of the oscillator signal is significantly greater than the beat-frequency amplitude, the spectral information between d-c and approximately 20 kHz is obliterated. This is unfortunate since the amplitude at 0 Hz is critical for determination of halfwidth. The problem can be circumvented, however, by treating this point as a variable and letting the computer routine float a value for it until the best one is found.

Approximately 20 to 30 data points consisting of corresponding amplitude and frequency coordinates were obtained from a smooth curve drawn through the spectral noise. The amplitude of the shot noise contribution was measured in the 10-15 kHz region where the light-beating spectrum was non-existent, and the value obtained was subtracted from the total spectral amplitude to obtain the amplitude of the beat-frequency components. In addition, this value had to be converted to a linear scale, because of the logarithmic response of the recorder, and also had

to be squared if the power spectrum rather than the voltage spectrum were desired.

Statistical treatment of the data was performed with a general purpose curve fitting routine, KINFIT⁵², and a Control Data Corporation 6500 computer. The equation to be fit describes a Lorentzian curve

AMP =
$$\frac{U(1)}{1.0 + \left[\frac{XX(1)}{U(2)}\right]^2}$$
 (6.1)

where AMP is the calculated spectral amplitude at frequency XX(1), U(1) is the value for AMP at frequency $\omega = 0$, and U(2) is the halfwidth.

In operation, the program minimizes the function

$$\Phi = \sum_{i=1}^{\eta} W_i F_i^2 \tag{6.2}$$

where η is the number of points, and F_i is a residual function defined in such a way that it would approach zero for all i as the parameters approach their "best" values. For equation (6.1), the residual is defined as

$$RESID = AMP - XX(2)$$
 (6.3)

where XX(2) is the experimentally determined value for the amplitude corresponding to a particular XX(1) value.

Also in equation (6.2), W₁ is a "weighting" term which can be set to unity for all points (referred to as "not using weights") or can be calculated by the program as

$$W_{i} = 1/\sigma_{F_{i}}^{2} \tag{6.4}$$

where

$$\sigma_{\mathbf{F}_{1}^{2}} = \sum_{\mathbf{k}=1}^{m} \left(\frac{\partial \mathbf{F}}{\partial \mathbf{X}_{\mathbf{k}}}\right)^{2} \sigma_{\mathbf{k}_{1}^{2}}$$
(6.5)

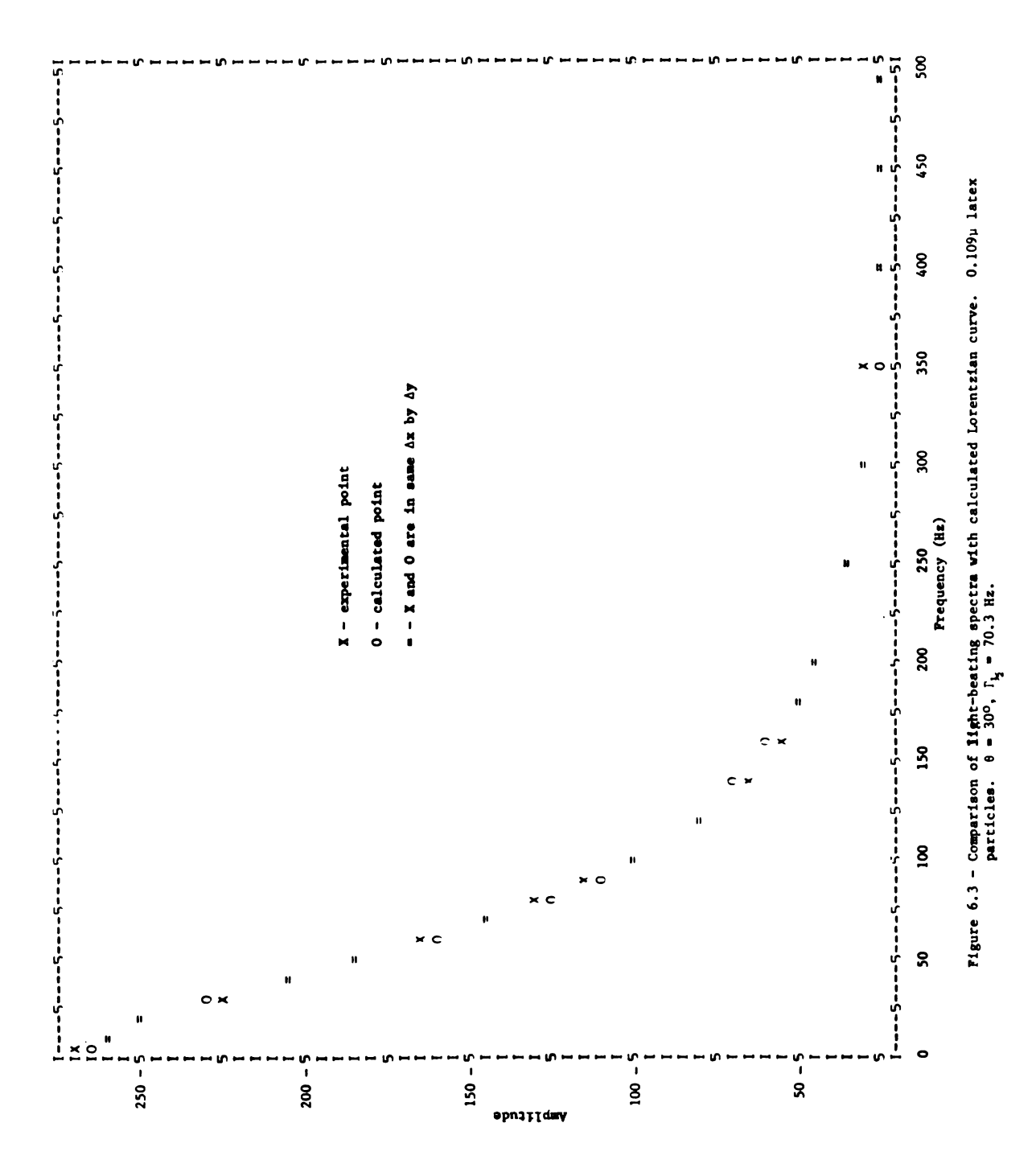
In equation (6.5), m is the number of variables, X_k is the k_{th} variable, and the partial derivative is evaluated at the ith data point. $\sigma_{k_1^2}$ is the variance of the k^{th} variable at the ith point.

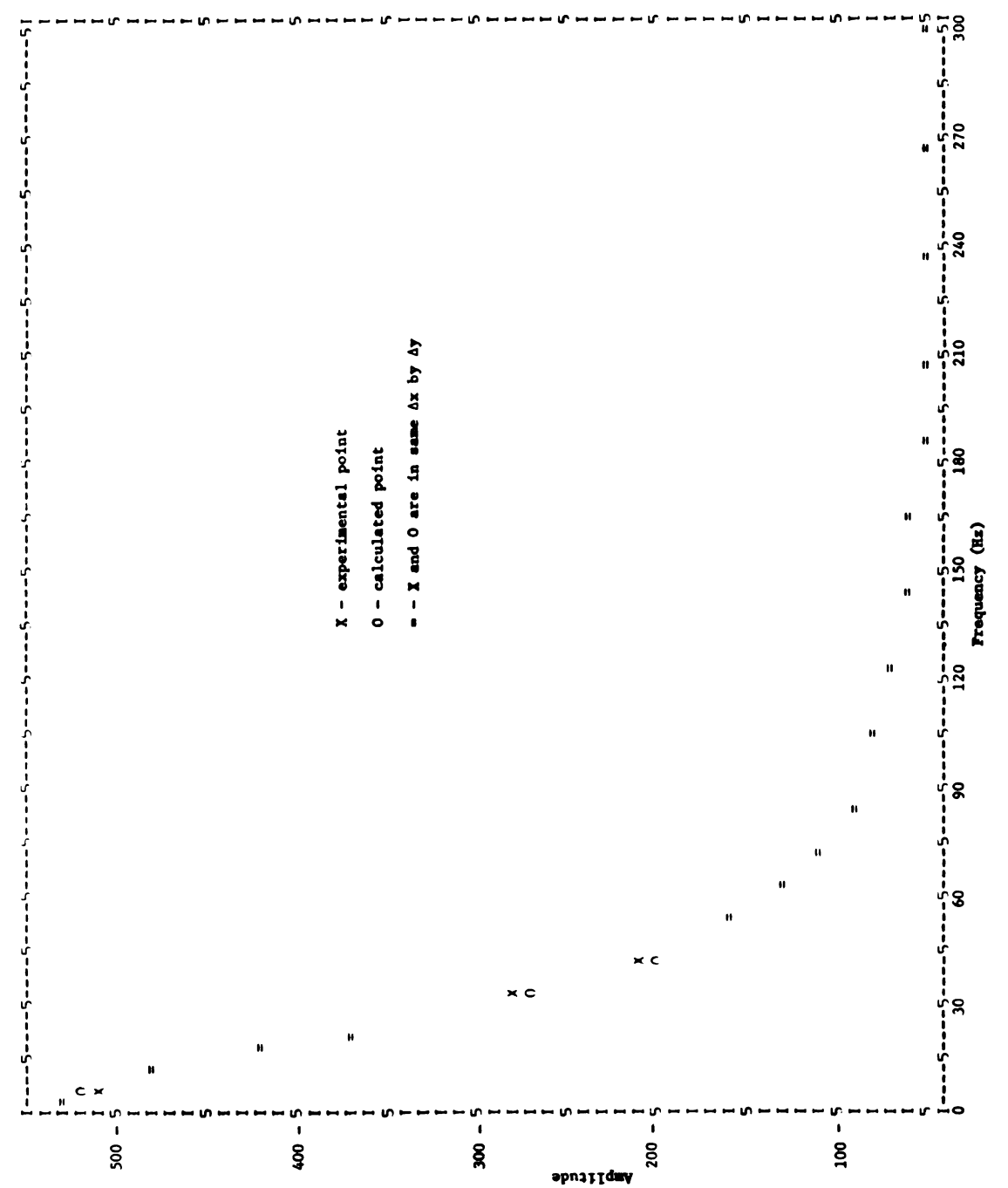
The computer calculates the best values and the corresponding standard deviation for the parameters U(1) and U(2). The residue and weight assigned to each data point is also supplied at the end of the program. The quality of fit between the experimentally determined spectra and the spectra calculated from the best values of U(1) and U(2) can be evaluated from the magnitude of the residues and also from a plot of experimental and calculated values. Figures 6.3 and 6.4 illustrate the excellent fit to a Lorentzian curve which was generally observed for the latex suspensions.

The results for measurements of the translational diffusion coefficient for each size latex particle are given in Tables 6.1 and 6.2. Experimentally determined values were calculated from the expression

$$D = \frac{\Gamma(\lambda_0/n)^2}{16\pi \sin^2(\theta/2)}$$
(6.6)

where Γ is the measured spectral halfwidth, λ_0 is the frequency of the laser line, n is the refractive index of the latex suspension, and θ is the angle of observation. These values were compared with those predicted by the Stokes-Einstein relationship for sphreical particles





Pigure 6.4 - Comparison of light-beating spectra with calculated Lorentzian curve. 0.357 μ latex particles. 8 = 30°, $\Gamma_{\rm k}$ = 27.9 Hz.

TABLE 6.1 - Experimental Halfwidths and Diffusion $\mbox{Coefficients for 0.109$${}_{\mu}$ Latex Particles}$

θ (deg)	Γ _{1,2} (Hz)	D x 10 ⁸ (cm ² sec ⁻¹)	D-D _{SE} x 100 (%)
15	18	4.78 ± 0.02	+6.7
30	64	4.32	-3.6
45	145	4.43	-1.1
60	255	4.59	+2.5
75	365	4.42	-1.3
90	508	4.57	-2.0
	Average	4.51 ± 0.02	+0.9

θ (deg)	Γ _{1,2} (Hz)	D x 10 ⁸ (cm ² sec ⁻¹)	$\frac{D-D_{SE}}{D_{SE}} \times 100 (2)$
15	4	1.04 ± 0.01	-17.5
30	18	1.27	- 0.8
45	33	1.01	-19.8
60	61	1.09	-11.9
75	81	0.98	-22.6
90	124	1.11	-11.9
	Average	1.08 ± 0.01	-14.1

$$^{D}SE = \frac{kT}{6\pi nr}$$
 (6.7)

where k is the Boltzman constant, T is the absolute temperature, η is the solvent viscosity, and r is the radius of the particle. D_{SE} values determined for the 0.109 μ and 0.357 μ latex particles were 4.48 x 10⁻⁸ and 1.28 x 10⁻⁸ cm²sec⁻¹, respectively.

The accuracy of light-beating spectroscopy_in_measuring diffusion coefficients is illustrated by the excellent agreement between the experimentally determined value and the Stokes-Einstein value for 0.109 μ particles. Although the agreement between the two values is somewhat less for the 0.357 μ particles, it is interesting to note that Chu and Schones ²⁴ obtained the same value for D (1.08 x 10⁻⁸ cm²/sec) in identical experiments performed on 0.357 μ particles_obtained from Dow. Lee ⁵³ also reports measured particle dimensions differing from those specified.

Equation (6.6) can be rearranged into the form

$$\Gamma = DK^2 = D\left(\frac{16\pi n^2 \sin^2(\theta/2)}{\lambda_0^2}\right)$$
 (6.6)

which describes a straight line of slope $\frac{\Delta\Gamma}{\Delta\sin^2(\theta/2)} = D \; (\frac{16\pi n^2}{\lambda o^2})$ and intercept zero. The values obtained for the halfwidth, Γ , at various angles of measurement were plotted against $\sin^2(\theta/2)$, and KINFIT used to determine the best straight line. The results are illustrated in Figure (6.5). The slope of the line was evaluated by the computer and then used to calculate an average value for the experimentally determined diffusion coefficients. The values for D obtained by this method were 4.47 * 10^{-8} and 1.07 x 10^{-8} cm²/sec for the 0.109 μ and 0.357 μ particles, respectively.

The intercepts of the plots did not pass through the origin as expected, because of instrumental contributions to the light-beating spectrum. The average intercept value determined by the computer for

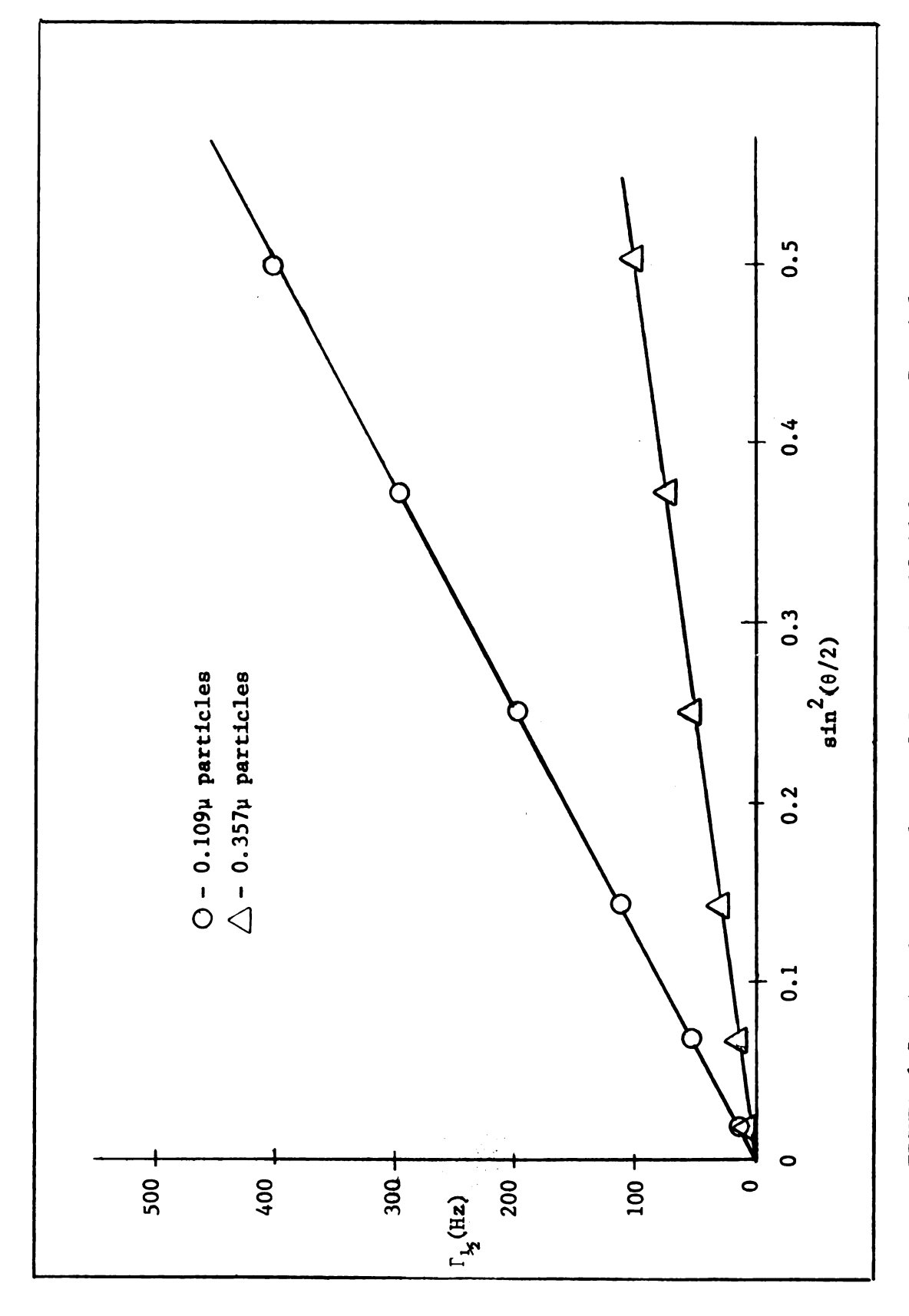


FIGURE 6.5 - Angular Dependence of Spectral Halfwidth. Latex Particles.



all measurements was 8 Hz. Consequently, this value was subtracted from the spectral halfwidth before calculation of the diffusion coefficients.

The resolving power of the instrument, which can be calculated from the instrumental linewidth and the frequency of the laser line (5 x 10^{14} Hz), is better than 1 part in 10^{13} . Hence, the light-beating spectrometer can analyze spectral lines with resolution that is four to five orders of magnitude greater than the best conventional optical techniques.

Polymer Solutions

Polymer solutions containing 0.05% polyisobutylene (PIB) were prepared with research grade n-pentane. Samples from each of fractions to be investigated were weighed directly into a 25 ml volumetric flask which had previously been cleaned in aqua regia and thoroughly rinsed to remove dust. Solvent was added to the flask through an ultrafine sintered glass filter, and the flask and contents brought to thermal equilibrium in a 20°C water bath. Additional pentane at 20°C was added to the mark, after which the flask was stoppered and the contents mechanically stirred for twenty-four hours.

The solution was poured through a course grade sintered glass filter into a sample cell which had also been cleaned in aqua regia. The cell and contents were degassed to a pressure of 5×10^{-7} mm Hg and sealed under vacuum with a torch. After testing for fissure at elevated temperatures, the cell was mounted on a copper base for positioning in the instrument.

At least two preliminary runs were made on each sample to determine the critical temperature and the temperatures at which spectra would be recorded. The change in scattered light intensity with temperature was monitored on a separate recorder as the temperature of the sample approached the critical solution point. When the strip-chart recorder indicated that the scattered intensity had stabilized, it was assumed that thermal equilibrium had been reached and that an accurate spectrum could be obtained. The onset of critical opalescence was marked by rapid fluctuations in the recorder trace. The amplitude of these fluctuations would increase in magnitude up to the critical point, and then die off rapidly as the solution separated into two stable phases.

The lower critical solution temperatures determined for the three polymer fractions by this method were 77.85° C, 77.60° C and 76.75° C for fractions 2A(2), 1A(3a), and 1A(2a), respectively. The accuracy of the measurements was considered to be approximately $\pm 0.05^{\circ}$ C, although the critical points were not sharply defined due to the apparent polydispersity of the samples.

Due to the large difference in densities between PIB and n-pentane at elevated temperatures, sedimentation of polymer was a major problem. It was determined that approximately one-half hour remained after the temperature of the sample had stabilized during which spectra could be recorded. After this time, the scattered intensity would fluctuate as polymer settled out of solution, and an accurate spectrum could not be obtained. Because of this time limitation, only four spectra could be recorded at each temperature. Hence, measurements were made at angles of 15°, 30°, 45° and 60°. At angles of observation greater than 60° it was found that the intensity of the light-beating signal was too low to be distinguishable from detector noise, and a spectrum could not have been obtained in any case. The total time required for the four measurements was approximately twenty minutes, after which the instrument was returned to the original scattering angle of 15° to determine if the scattered intensity had remained constant. If the intensity had changed,

the experiment was repeated from the beginning, although it was generally found that the intensity had remained stable.

Typical spectra obtained for the polymer solutions are illustrated in Figures 6.6 through 6.8. A complete spectrum, normally requiring forty minutes, was not possible because of the time limitation imposed by the polymer sedimentation problem. Instead, portions of each spectrum were recorded at various frequency intervals and a smooth curve connecting the successive portions was drawn to complete the spectrum. This procedure has successfully been used by Dubois and Berge 4 in diffusion studies on binary systems of small molecules. In the low frequency region (near d-c) of the spectra, where the amplitude decreases sharply with increasing frequency, it was necessary to record at intervals of 50 Hz or less to obtain an adequate amount of spectral information. At higher frequencies (greater than 300-500 Hz) the amplitude decays more slowly and a sufficient amount of spectral information could be obtained by recording at 100-200 Hz intervals.

Figure 6.6 illustrates the dependence of spectral shape on temperature. The decrease in width and increase in amplitude as the temperature of the sample approaches the critical solution point is evident. For spectra recorded near the critical point it was necessary to switch recorder range part way through the scan to accommodate the large amplitude changes which were encountered. Most spectra exhibited good fit to a single Lorentzian curve (Figures 6.9 and 6.10) in the low frequency region of the spectrum but deviated from Lorentzian behavior at higher frequencies (greater than 800-1000 Hz) where signal intensity was low compared to detector noise.

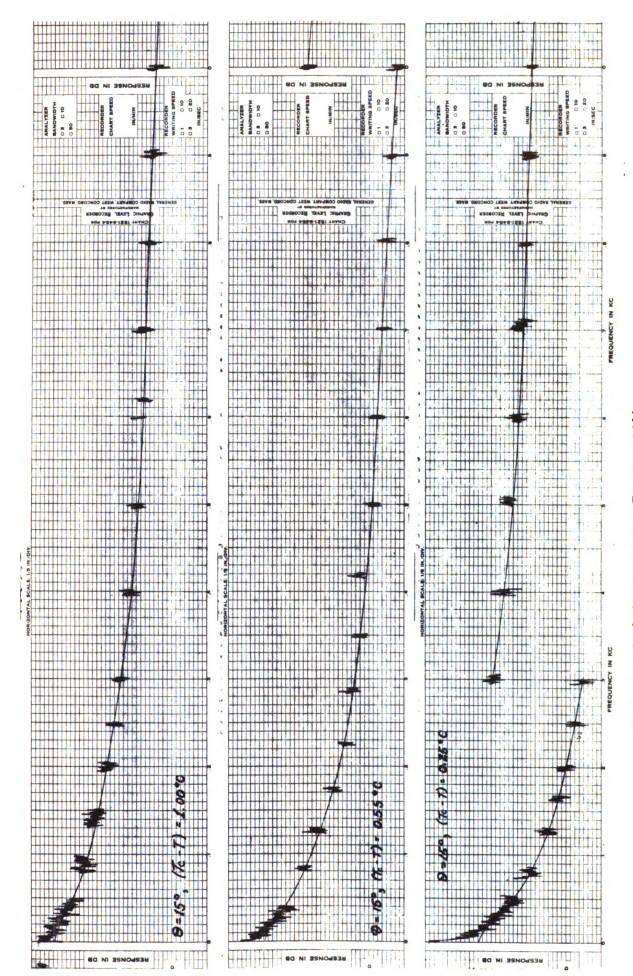


Figure 6.6 - Light-beating spectra. Fraction 1A2(a)

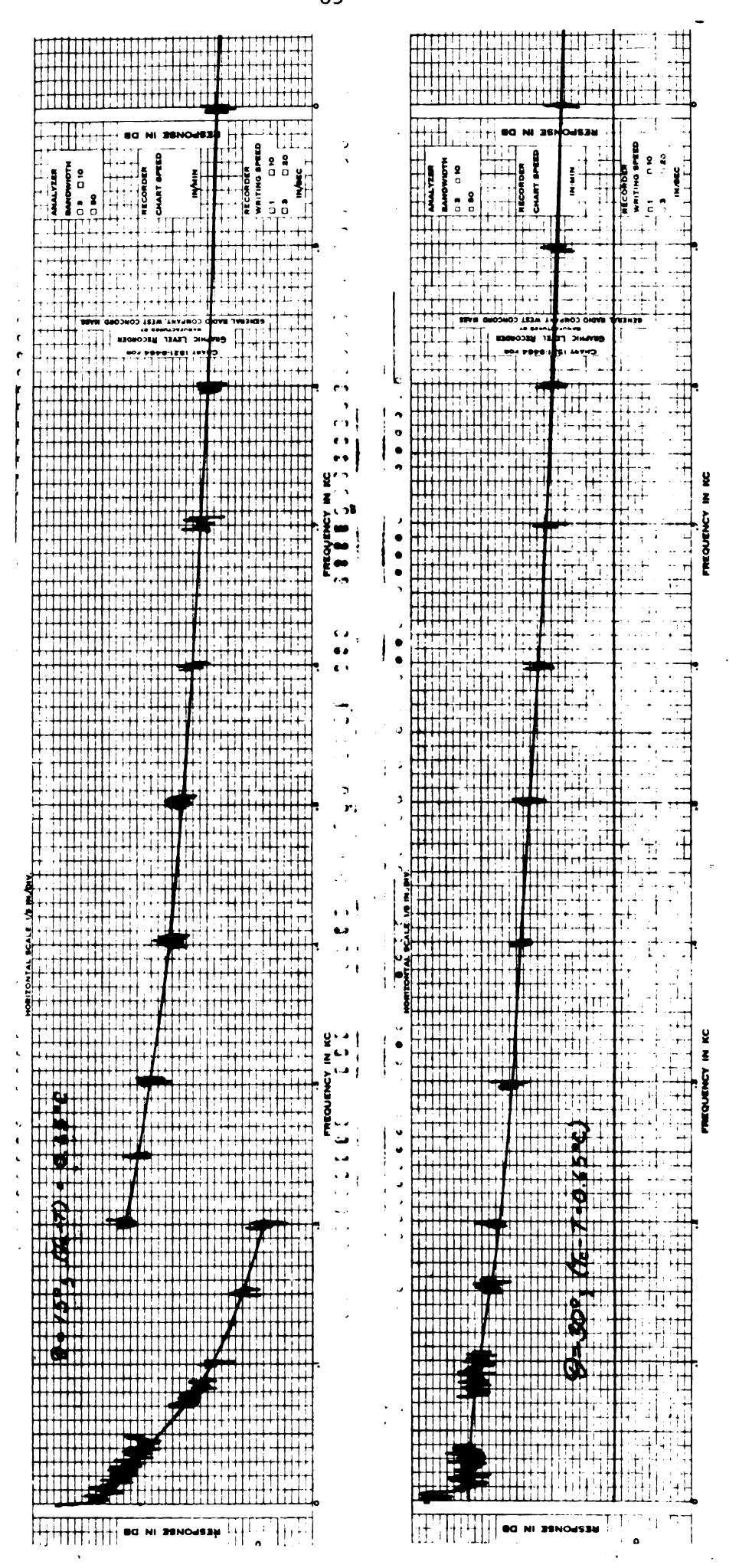


Figure 6.7 - Light-beating spectra. Fraction 2A(2)

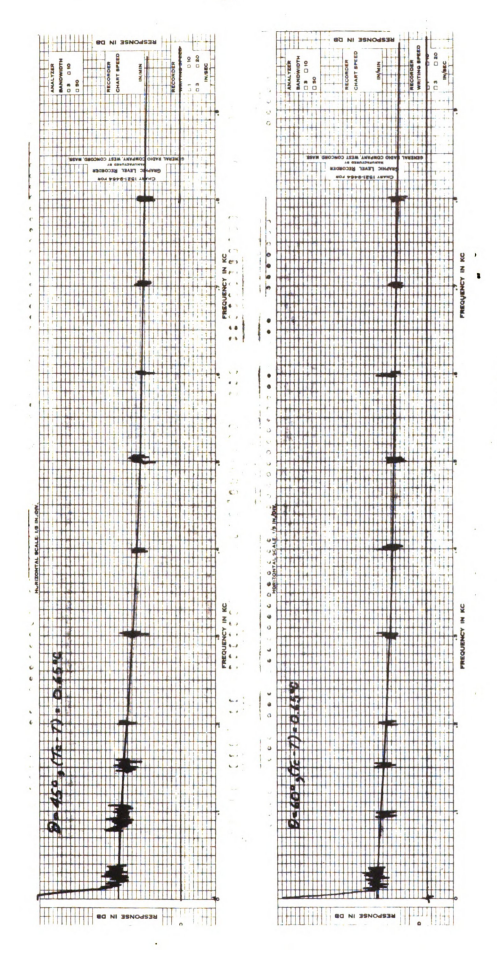
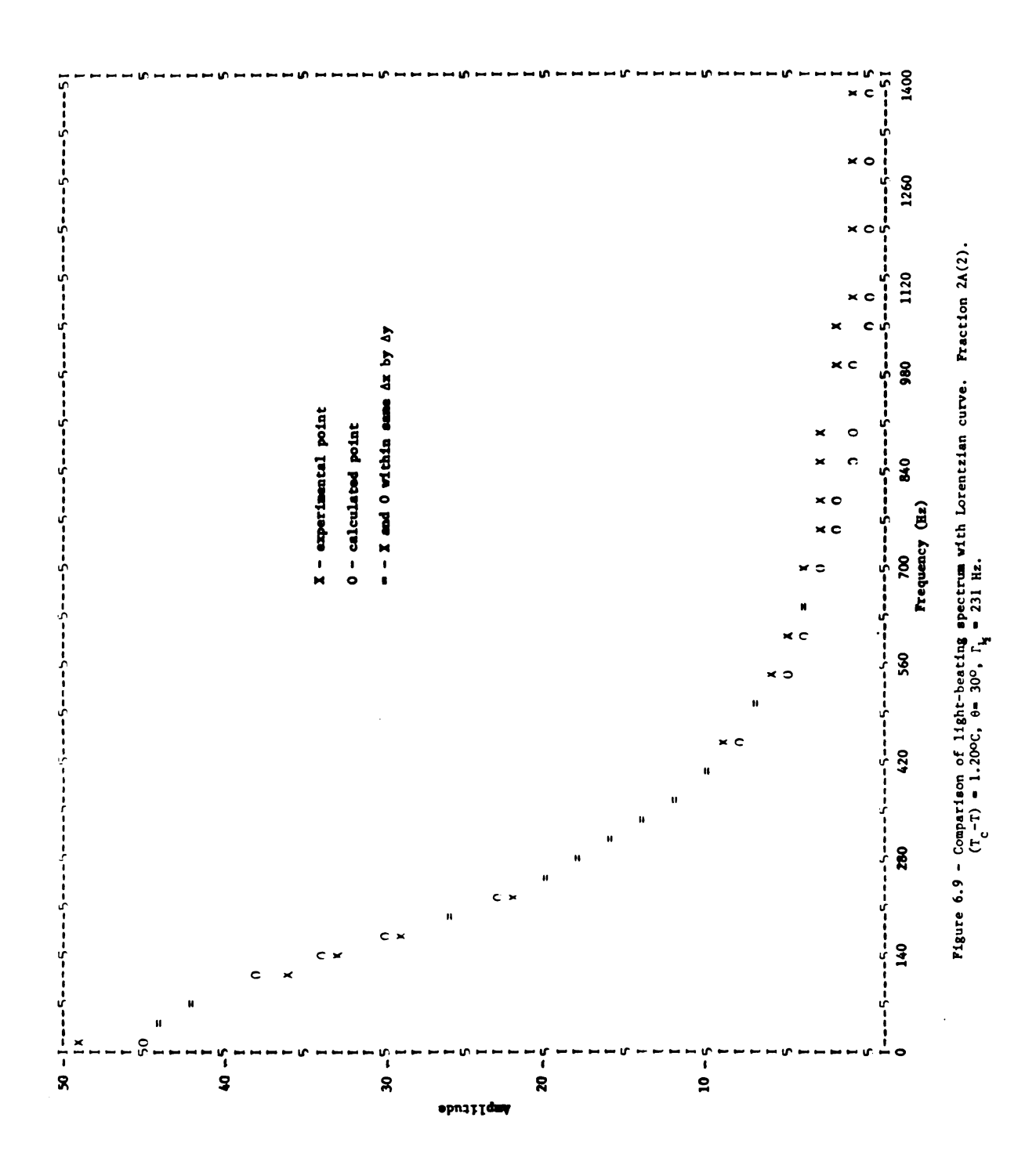


Figure 6.8 - Light beating spectra. Fraction 2A(2)



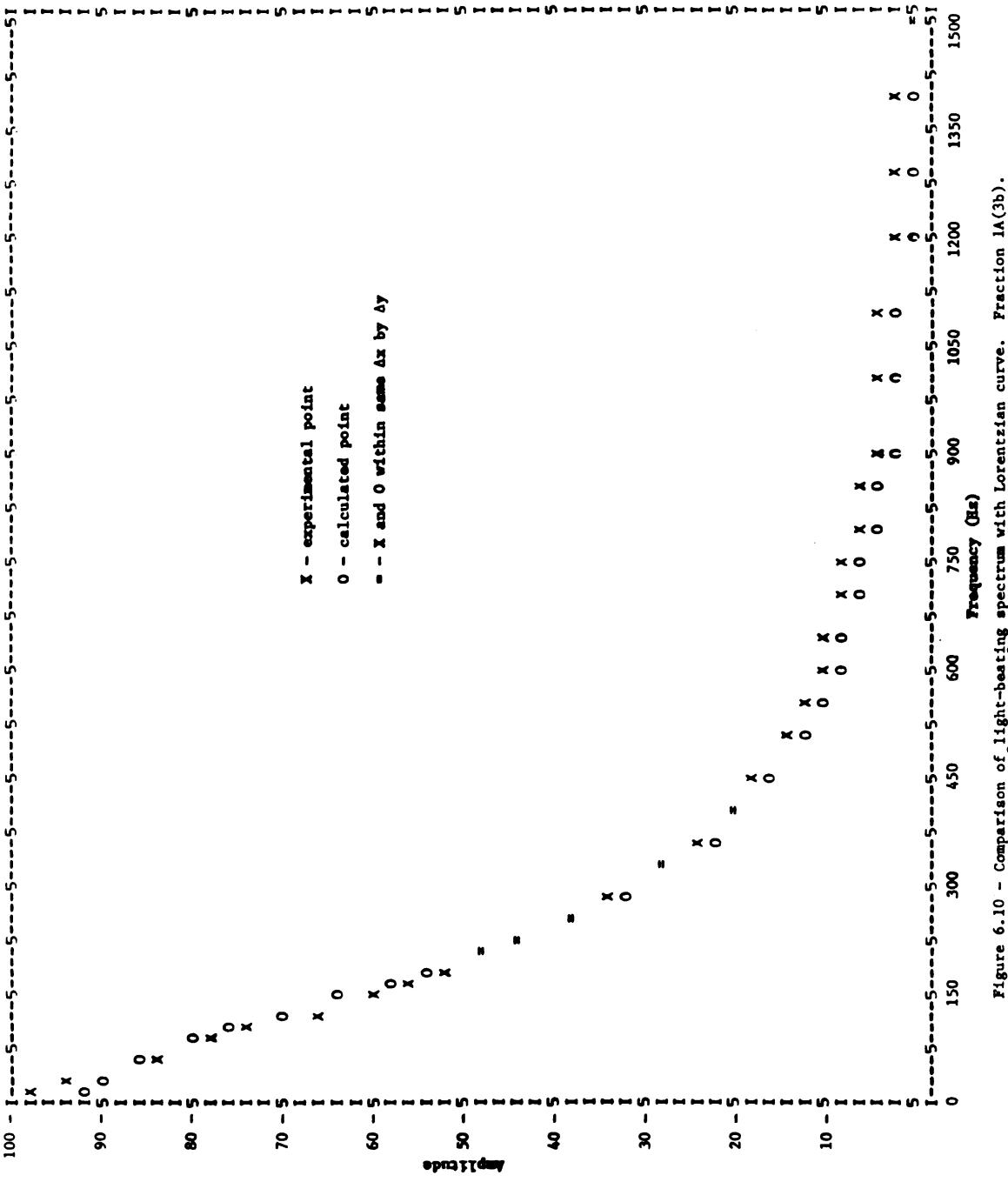
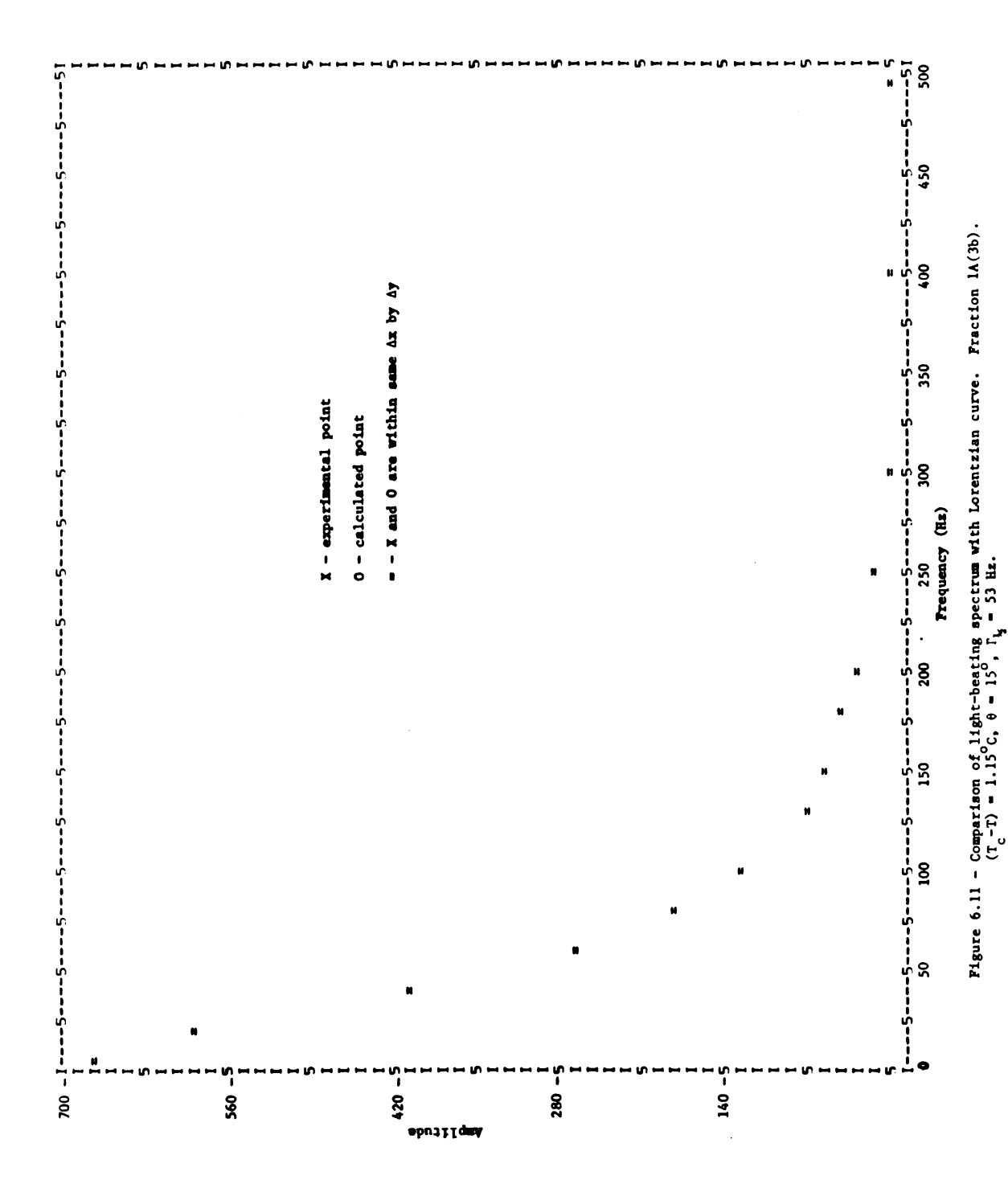


Figure 6.10 - Comparison of light-beating spectrum with Lorentzian curve. Fraction 1A(3b). (T_c-T) = 1.15°C, θ = 30°, $\Gamma_{k_{\rm s}}$ = 218 Hz.

The strong angular dependence of the light-beating spectrum near the critical point is illustrated by Figures 6.7 and 6.8. At angles between 0° and 30°, where the scattered intensity was high, the observed spectra were extremely narrow and exhibited good fit to a Lorentzian curve (Figure 6.11). At angles greater than 30°, the scattered intensity dropped sharply and the spectra broadened to an extent that accurate measurements were difficult. The poor fit to a Lorentzian curve, which was typically observed at higher scattering angles, is illustrated in Figure 6.12. At angles of observation beyond 60°, the amplitude of the light-beating signal was too low to be differentiated from detector shot noise, and a spectrum could not be obtained.

Furthermore, the shape of the light-beating spectrum was also found to be molecular weight dependent, with the lower molecular weight fractions exhibiting less intense scattering and broader spectra. Therefore, the spectral distribution of the light scattered from the highest molecular weight fraction (1A(2a)) could be measured with moderate accuracy between angles of 30° and 60° , although similar experiments on lower molecular weight fractions were limited to 45° and, in some instances, 30° .

The values for the spectral halfwidth which were measured at several angles and temperatures for the three polymer fractions are listed in Tables 6.3, 6.4, and 6.5 and are plotted as a function of $\sin^2\left(\frac{\theta}{2}\right)$ in Figures 6.13 through 6.15. The graphs show moderately good linearity, which is indicative of Lorentzian behavior. Deviations observed at higher scattering angles resulted from the low light-beating signal intensity relative to the shot noise of the detector, as previously discussed.



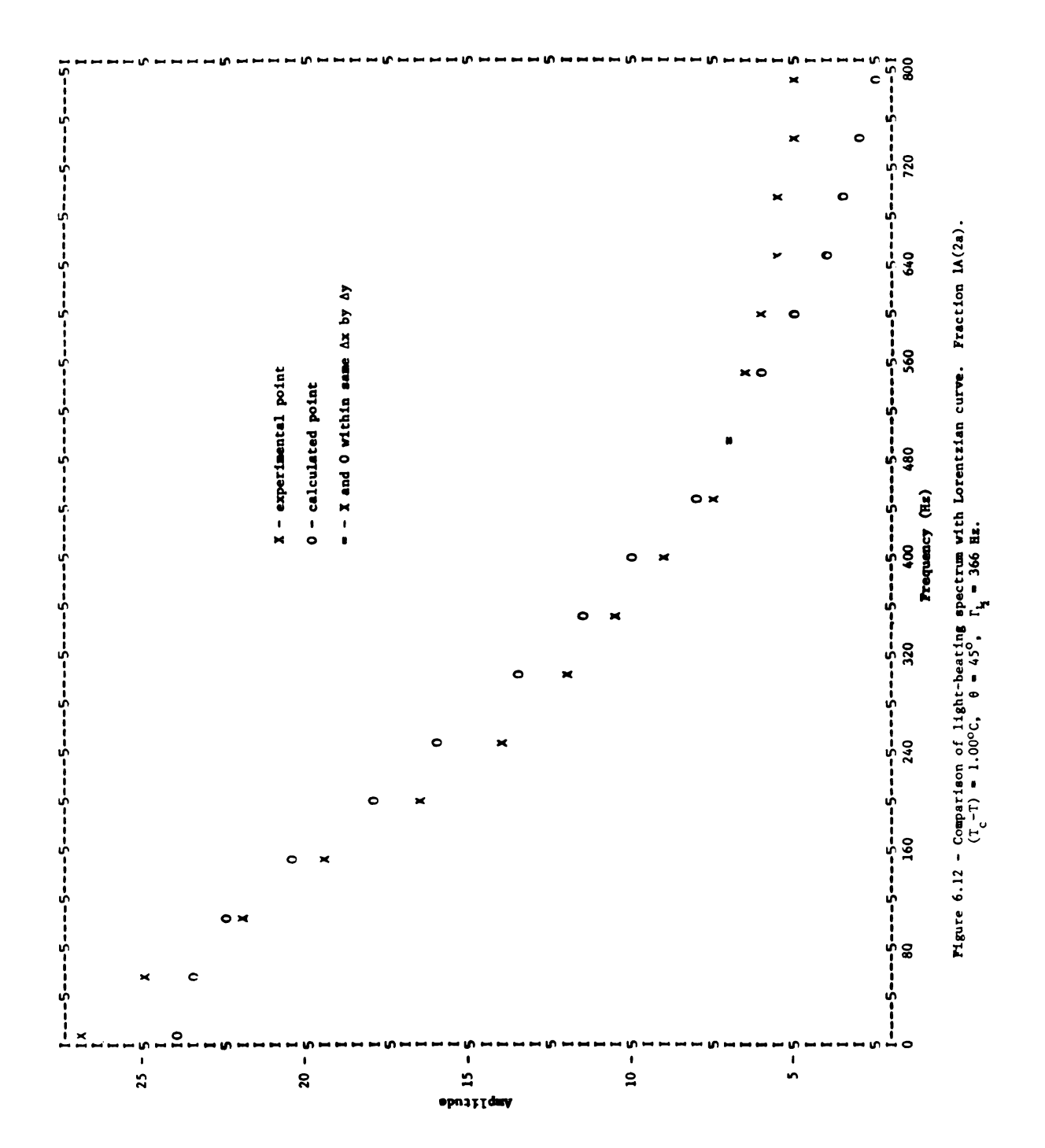


TABLE 6.3 - Angular Dependence of Spectral Halfwidth
Fraction 1A(2a)

(Tc-T)	θ	Γ _{1,2}
(°c)	(deg)	(Hz)
1.70	15	43 ± 8
	30	225 ± 12
	45	470 ± 33
	60	665 ±89
1.00	15	30 ± 7
	30	178±11
	45	366 ±27
	60	560 ±65
0.55	15	20 ± 6
	30	145 ± 9
	45	308 ± 24
	60	497±35
0,25	15	12± 6
	30	105± 8
	45	252 ± 13
	60	415±30

TABLE 6.4 - Angular Dependence of Spectral Halfwidth

Fraction 1A(3b)

(Tc-T)	θ	$\Gamma_{rac{1}{2}}$
(°c)	(deg)	(Hz)
1.95	15	62 ± 8
	30	274 ± 14
	45	535 ± 42
	60	
1.15	15	53 ± 8
	30	218 ± 12
	45	430 ±29
	60	600 ±78
0.65	15	39 ± 7
	30	150 ± 9
	45	335 ±24
	60	546 ±72
0.35	15	18 ± 6
	30	124 ± 8
	45	270 ±15
	60	433 ±31
		-

TABLE 6.5 - Angular dependence of Spectral Maliwidth
Fraction 2A(2)

(Tc-T)	θ	$\Gamma_{rac{1}{2}}$
(°c)	(de g)	(Hz)
2.30	15	60 ±15
	30	550 ±93
	45	
	60	
1.45	15	47 ± 8
	30	322 ± 21
	45	620 ± 73
	60	
1.20	15	26 ½ 8
	30	231 ± 14
	45	480 ± 35
	60	w. w. e
0,65	15	14 ± 6
	30	150 ± 9
	45	396±28
	. 60	~

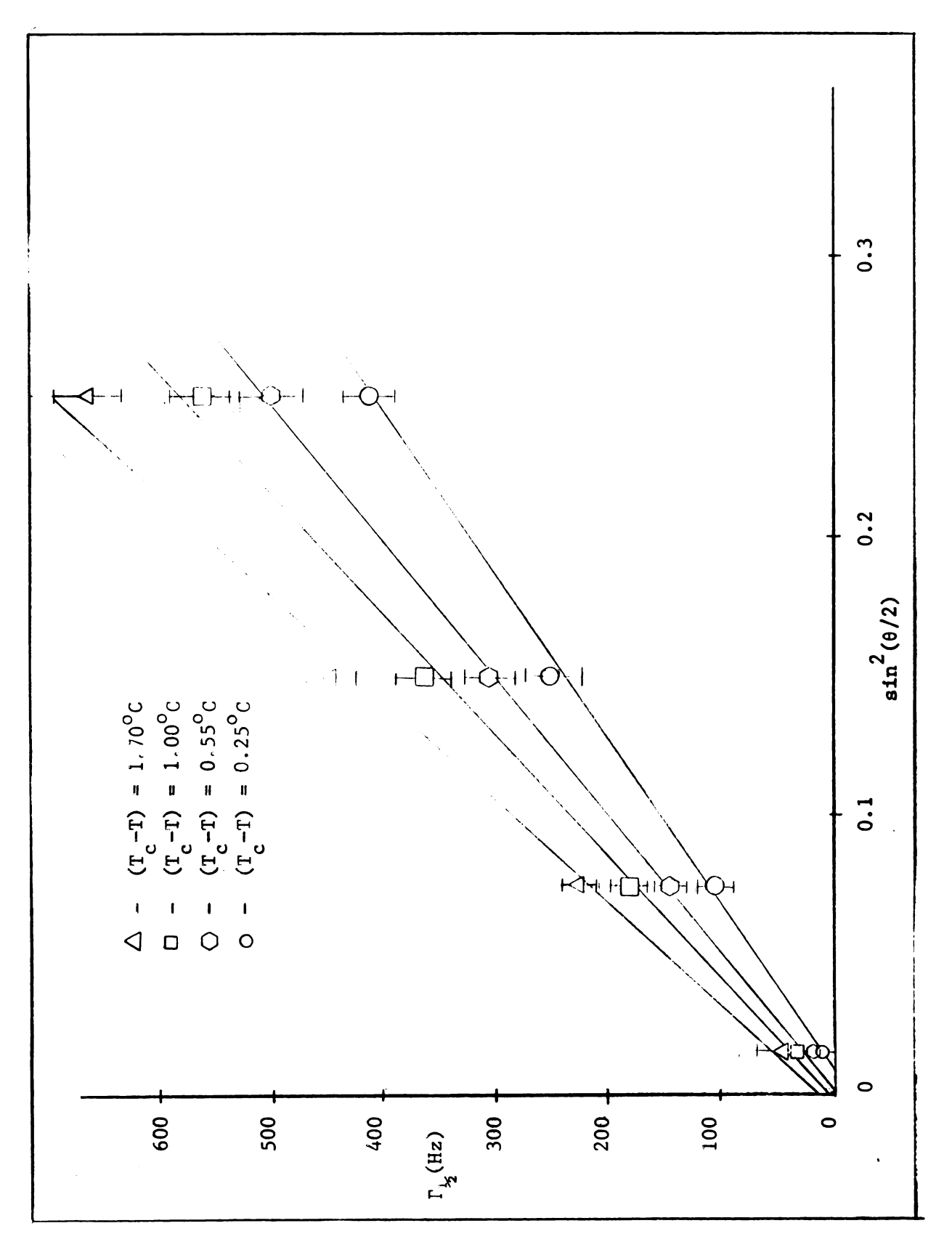


FIGURE 6.13 - Angular Dependence of Spectral Halfwidth. Fraction 1A(2a).

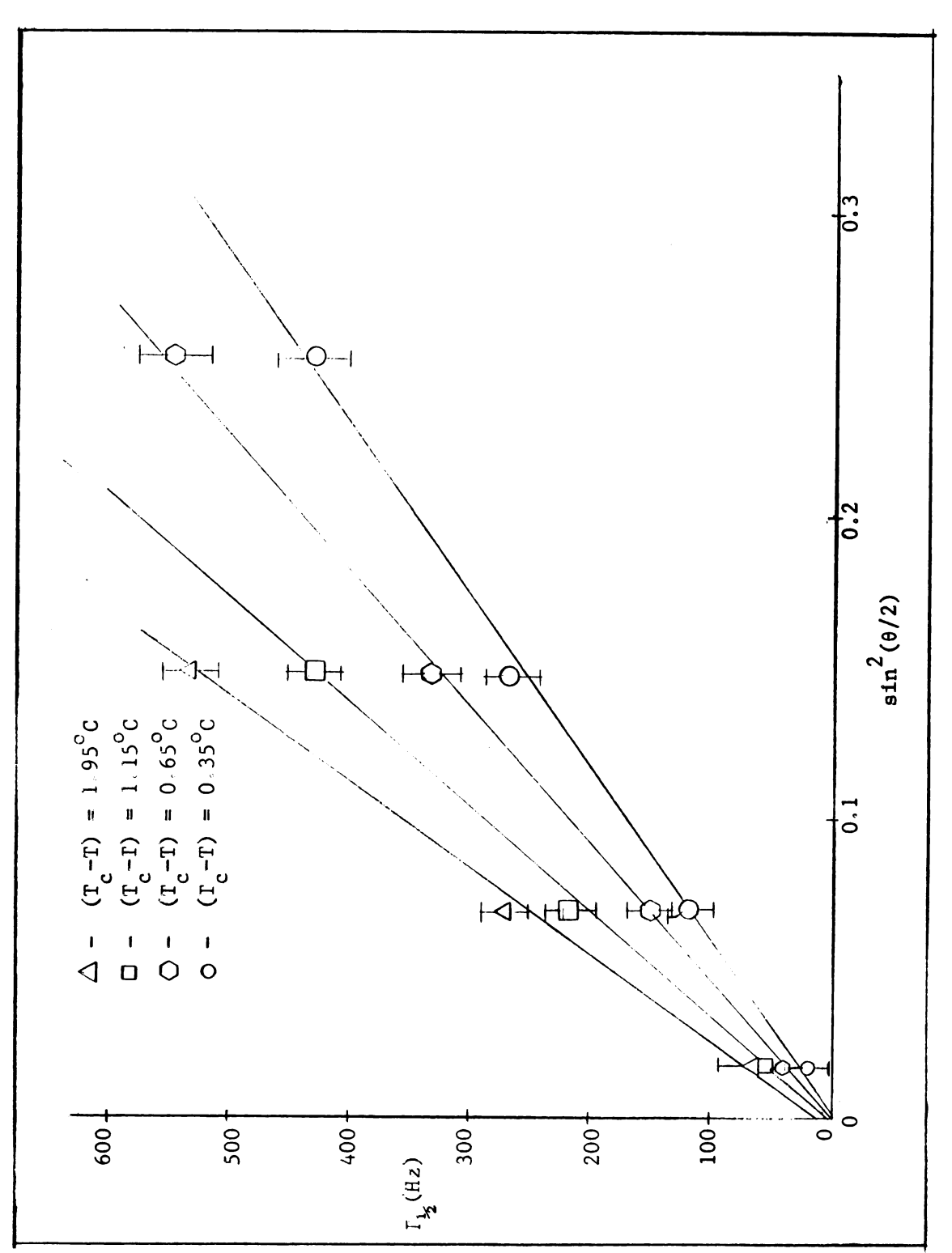


FIGURE 6.14 - Angular Dependence of Spectral Halfwidth. Fraction 1A(3b).

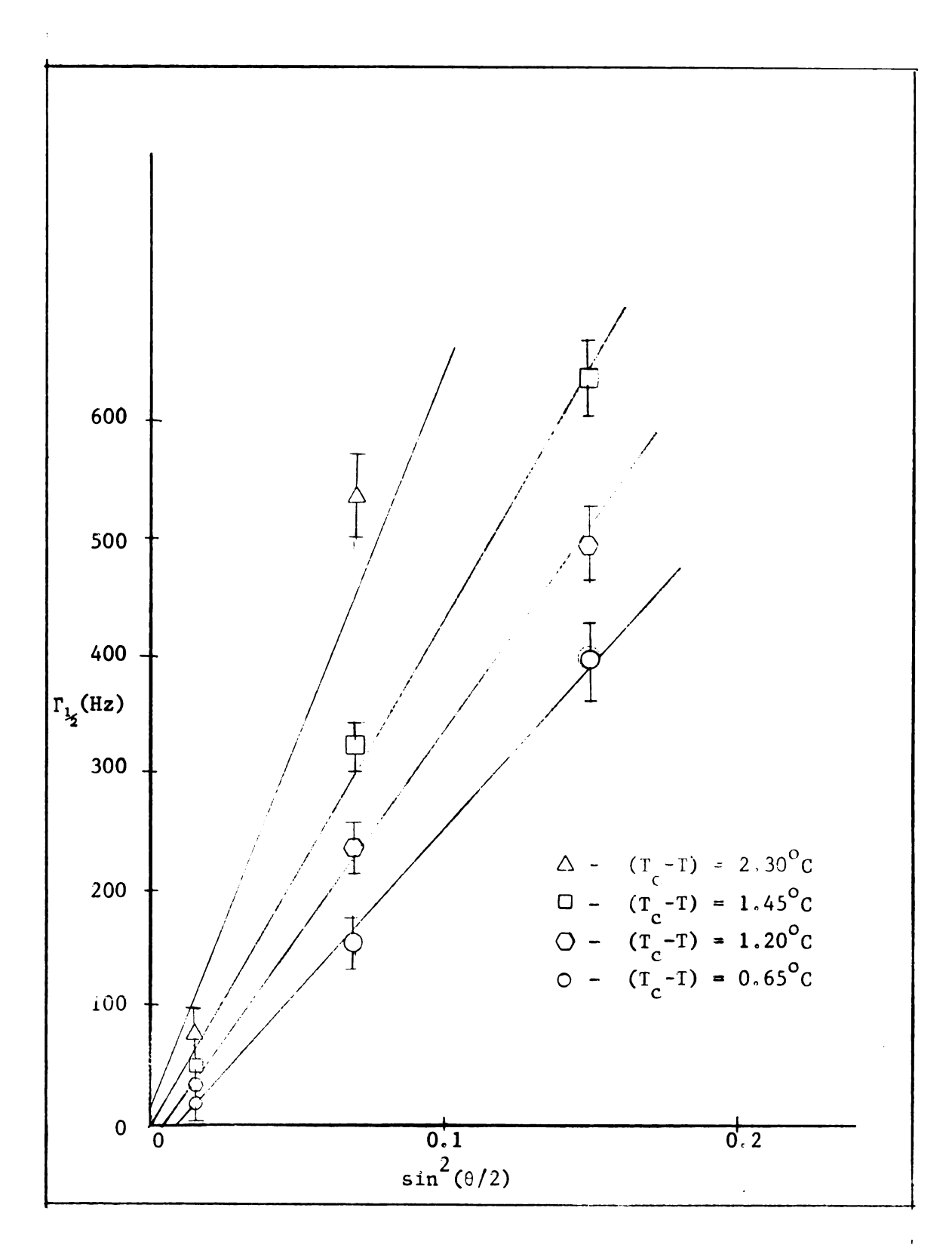


FIGURE 6 15 - Angular Dependence of Spectral Halfwidth. Fraction 2A(2).

Deviations from linearity observed at low scattering angles (15° or less) were attributed to the extreme narrowness of the spectra relative to instrumental broadening. For example, the halfwidths of the power spectra obtained for the three polymer fractions at the critical point were all less than 20 Hz (Tables 6.3, 6.4, and 6.5), which is not substantially greater than the instrumental linewidth (8 Hz). In view of the fact that the local oscillator signal obliterates most of the spectral information between 0 and 25 Hz, linewidth measurements under these conditions would be difficult, if not impossible, to obtain with reasonable precision if it were not for the fact that the square root of the power spectrum, rather than the power spectrum itself, is recorded. The former spectrum, it will be recalled, is identical in shape to the latter but has twice the width. Hence, the standard deviation of measurments at low scattering angles was moderately low (±8%) at temperatures removed from the critical point, but increased to approximately .±30% for measurements in the vicinity of the critical temperature.

Diffusion coefficients for the polyisobutylene/n-pentane systems were calculated from the least-squares slopes of the lines in Figures 6.13 through 6.15, and the results listed in Tables 6.6, 6.7, and 6.8. The temperature dependence of the diffusion coefficient was examined in terms of equation (2.19) which was modified slightly to correspond to lower critical point rather than upper critical point measurements

$$D \alpha \left(\frac{T_{c}-T}{T_{c}}\right)^{\gamma} \tag{2.19}$$

The results, which are graphically illustrated in Figure 6.16, demonstrate that the same relationship exists for high molecular weight polymer solutions in the lower critical temperature region that were observed by Chu¹⁹

TABLE 6.6 - Temperature Dependence of the Diffusion Coefficient for Fraction 1A(2a). $T_c = 76.75^{\circ}C$

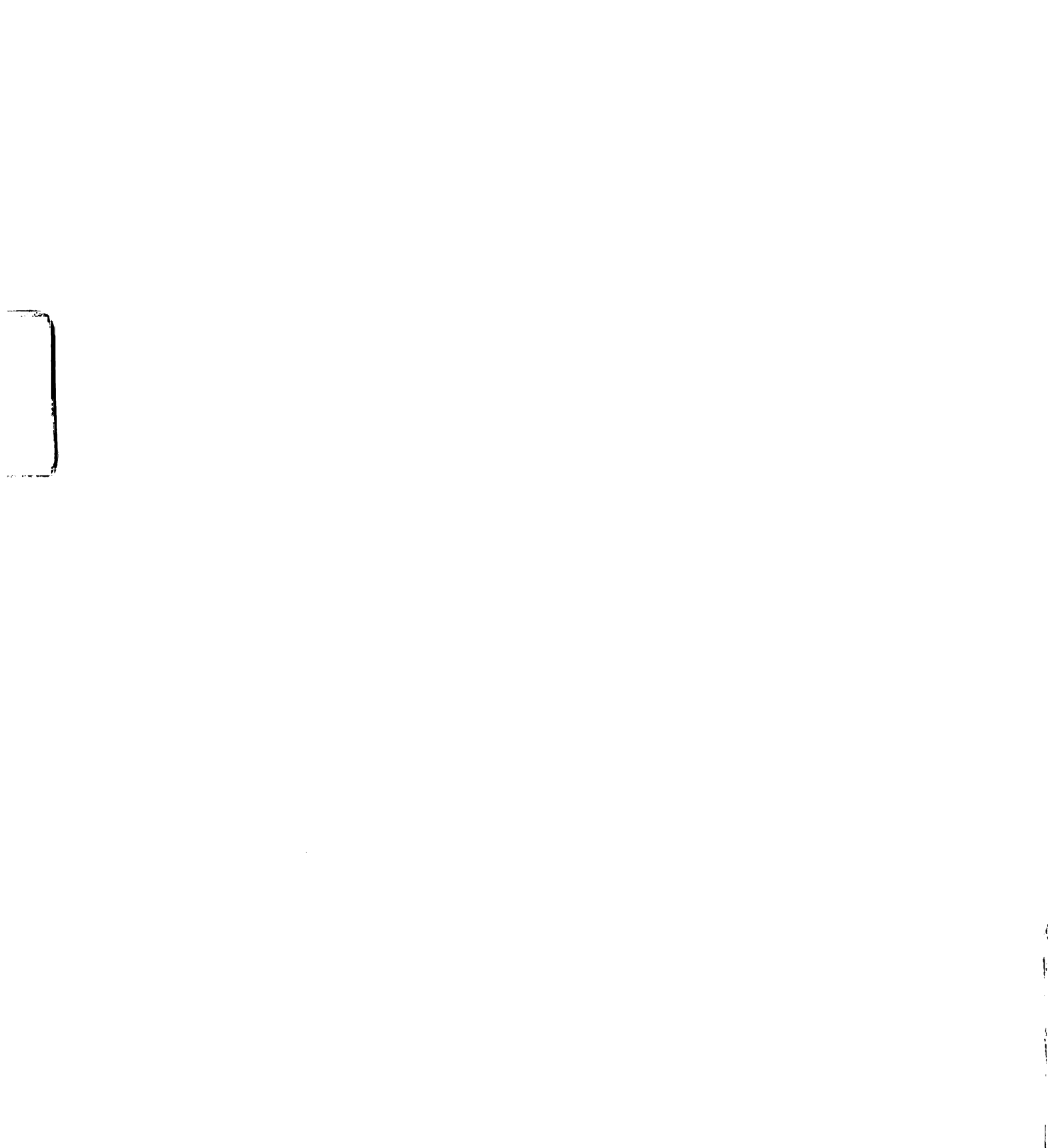
T _c -T (deg)	$-\log \frac{T_{c}^{-T}}{T_{c}}$	$D \times 10^{7}$ $(cm^{2}sec^{-1})$	-log D
1.70	1.65	1.1 + 0.1	6.98
1.00	1.88	0.90 + 0.07	7.05
0.55	2.16	0.81. + 0.04	7.09
0.25	2.45	0.69 ± 0.01	7.16

TABLE 6.7 - Temperature Dependence of the Diffusion Coefficient for Fraction 1A(3b). $T_c = 77.60^{\circ}C$

T _c -T (deg)	$-\log \frac{\frac{T_{c}-T}{T_{c}}}{\frac{T_{c}}{T_{c}}}$	D x 10 ⁷ (cm ² sec ⁻¹)	-log D
1.95	1.60	1.4 + 0.1	6.84
1,15	1.82	1.2 + 0.1	6.94
0.65	2.08	0.87 0.03	7.06
0.35	2.35	0.71-0.01	7.15

TABLE 6.8 - Temperature Dependence of the Diffusion Coefficient for Fraction 2A(2). $T_c = 77.85^{\circ}C$

T _c -T (deg)	$-\log \frac{T_{c}-T}{T_{c}}$	$D \times 10^{7}$ $(cm^{2}sec^{-1})$	-log D
2.30	1.52	2.8 + 0.6	6.55
1.45	1.75	1.7 ± 0.4	6.76
1.20	1.82	1.4 ± 0.1	6.86
0,65	2.08	1.2 + 0.1	6.92



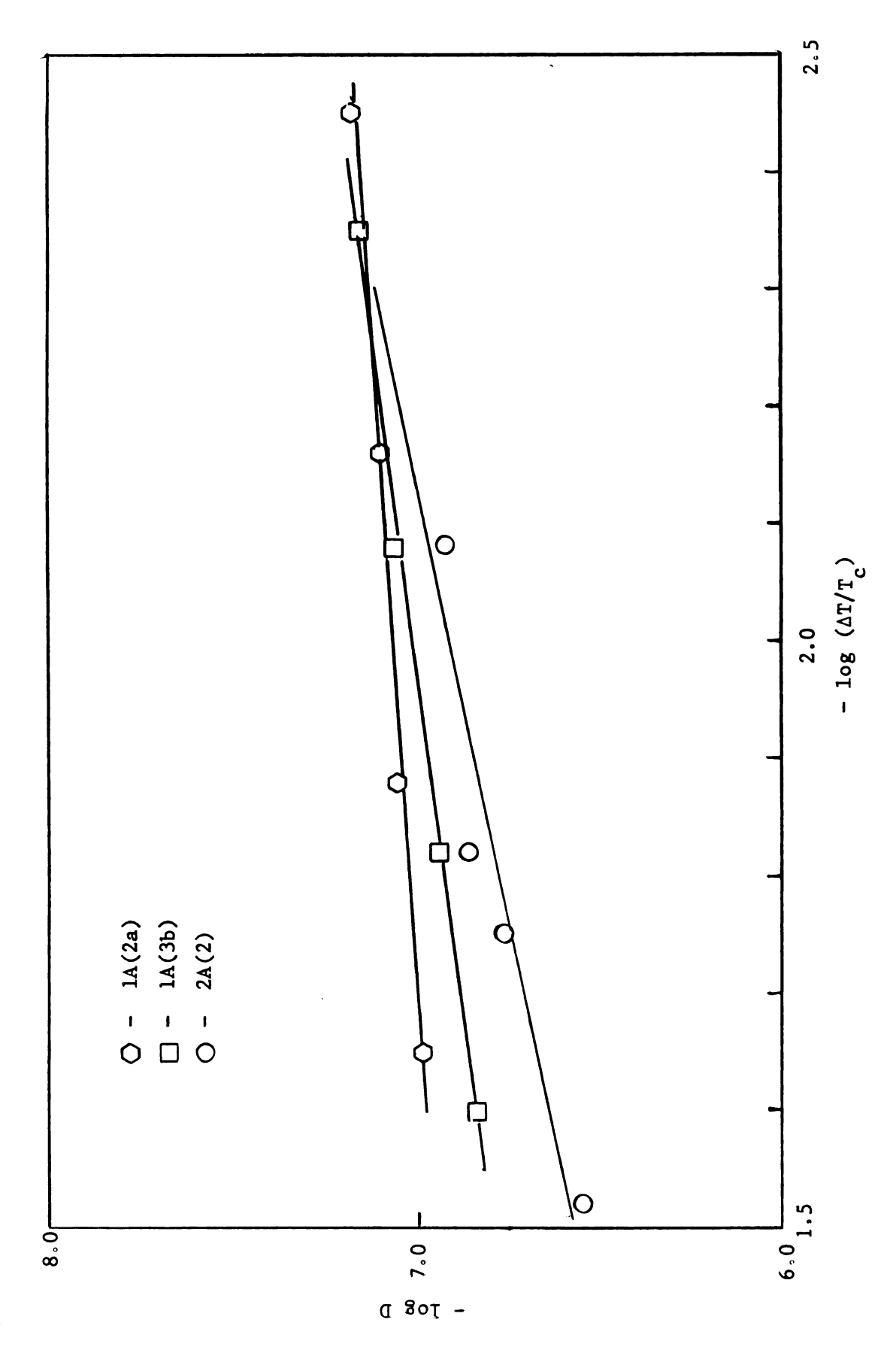


FIGURE 6.16 - Temperature Dependence of the Diffusion Coefficient

near the upper critical temperature of a polystyrene/cyclohexane system.

The values for the critical exponent, γ , were determined from the least-squares slopes of the graphs in Figure 6.16. They are 0.21±0.01, 0.42±0.02, and 0.66±0.03 for fractions 1A(2a), 1A(3b), and 2A(2), respectively. The value for the lowest molecular weight fraction (2A(2)) is comparable to that observed for systems of small molecules 19 and for the polystyrene/cyclohexane system studied by Chu.

The data in Tables 6.3, 6.4, and 6.5 was also analyzed with an applied correction for long range molecular interactions, as illustrated in Figures 6.17 and 6.18 for fractions 1A(2a) and 1A(3b), respectively. The data for fraction 2A(2) exhibited excessive scatter when graphed in this manner and was not given further consideration. The data at first appears to be more closely represented by the conventional analysis (Figures 6.13, 6.14, and 6.15), which would indicate that the influence of long range molecular correlation on the spectral measurements is minor. However, except for the values obtained at low scattering angles where instrumental contributions are most dramatic, the data is generally fit to within experimental error in Figures 6.17 and 6.18. Furthermore, the values for the correlation length, ξ_{Γ} , which were determined from the data (Table 6.9), are comparable to those determined by Chu^{19} for a polystyrene/cyclohexane system in which long range correlation was observed in the vicinity of the upper critical temperature. Therefore, long range correlation does quite probably occur for the polyisobutylene systems in the vicinity of the lower critical temperature, although detection is being hindered by instrumental limitations. The experimental conditions of the study must also be considered, as is explained in the following chapter.

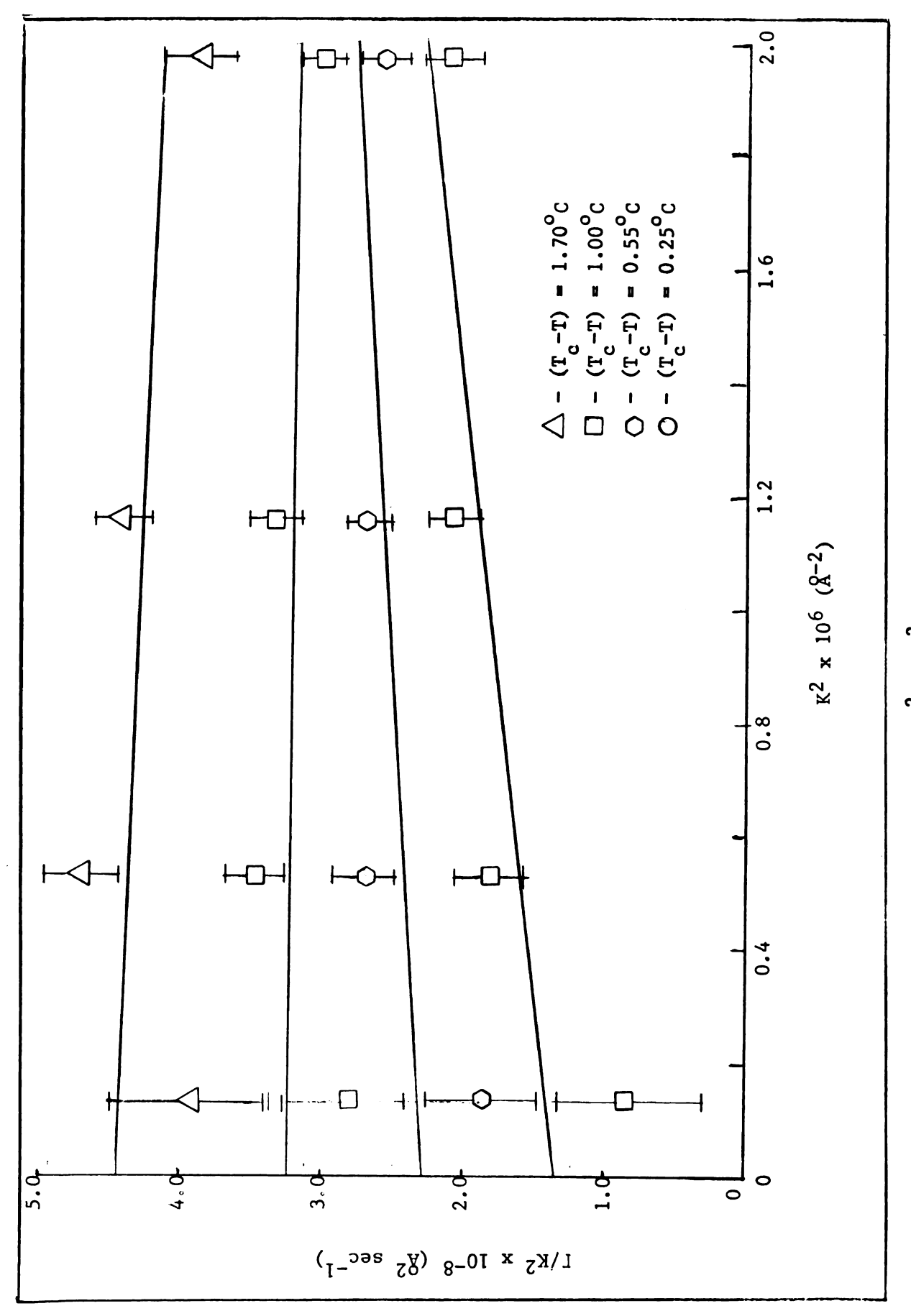


Figure 6.17 - Plot of Γ/K^2 vs K^2 for Fraction 1A(2a)

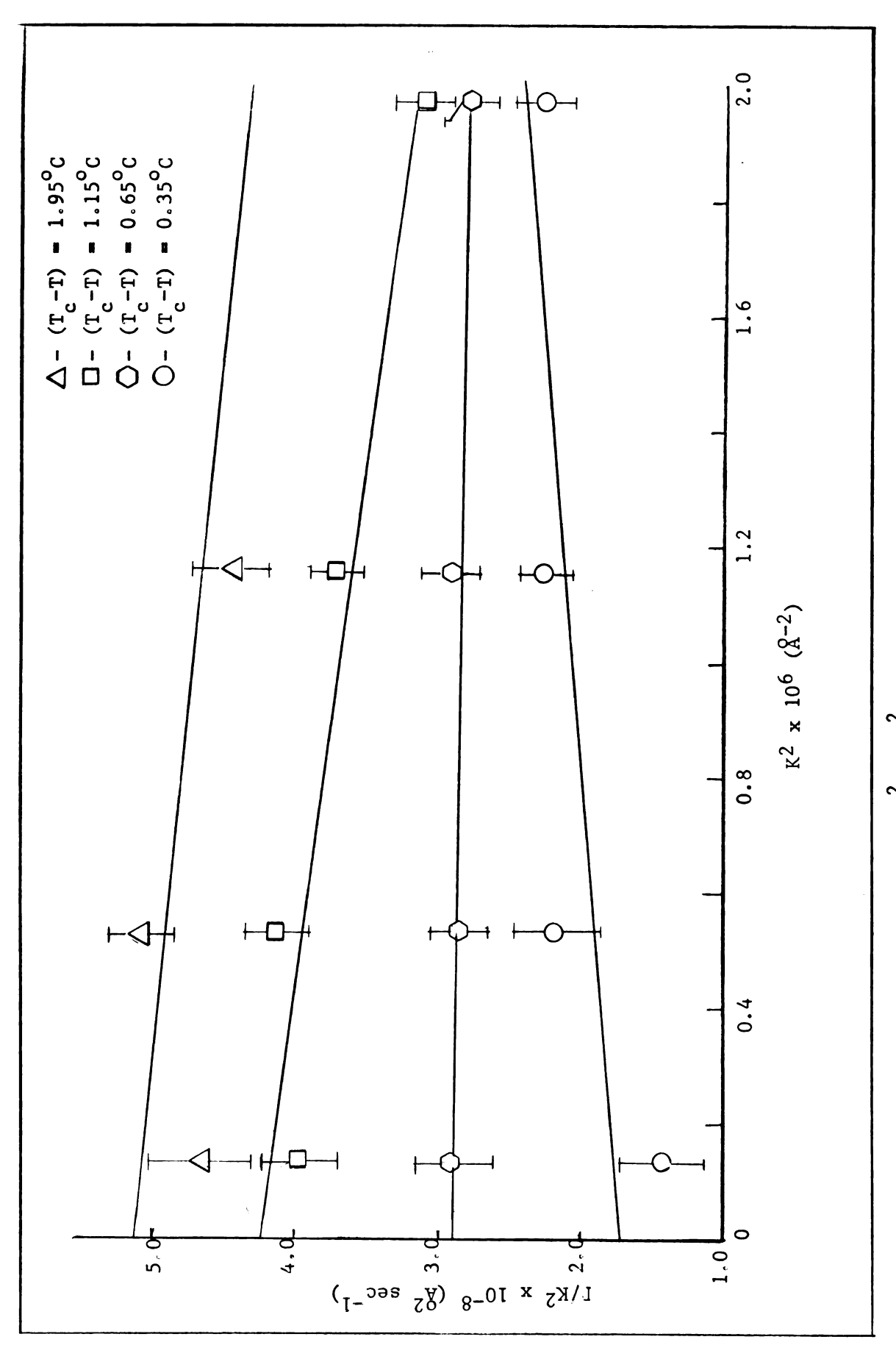


Figure 6.18 - Plot of Γ/K^2 vs K^2 for Fraction 1A(3b)

TABLE 6.9 - Diffusion Coefficients and Correlation Lengths with Correction for Long Range Correlation Applied

Fraction 1A(2a)

(T _C -T)	D x 10 ⁻⁸ (Å ² sec ⁻¹)	ξ _Γ × 10-2 (Å)	ξ _Γ Κ (θ=30°)
1.70	4.4±0.4	(-)	
1.00	3 , 2± 0 , 4	2.6±0.7	0.13
0.55	2.2±0.4	4,6±0.9	0.23
0.25	1.3±0.3	6.6±0.8	0.34

Fraction 1A(3b)

1.95	5.1±0.2	(-)	
1.15	4.2±0.2	(-)	
0.65	2,9±0,4	2.2±0.7	0.11
0.35	1.8±0.3	4.6±0.8	0.23

The values for ξ_{Γ} in Table 6.9 were calculated from the ratio $\xi_{\Gamma} = (\text{slope/intercept})^{\frac{1}{2}}$ for each of the least squares graphs in Figure 6.17 and 6.18. The negative values were also observed by Chu at temperatures removed from the critical point, and have been interpreted as a lack of long range correlation under these conditions.

A least squares fit to the data in Figures 6.17 and 6.18 yielded the diffusion coefficient from the intercept value (equation 2.19) as a function of temperature. The results are listed in Table 6.9 and plotted in log-log form in Figure 6.19.

Summary

A light-beating spectrometer of the homodyne type was designed and constructed for examination of the spectral distribution of the light quasi-elastically scattered from high molecular weight polymer solutions near the lower critical temperature as a function of scattering angle and temperature.

The performance of the instrument was tested by measuring the diffusion coefficients for polystyrene latex particles in water, a relatively ideal and strongly scattering system. The results clearly demonstrated that the instrument was functioning properly.

Solutions of three different molecular weight fractions of polyisobutylene in n-pentane were prepared for investigation. Light-beating spectra were obtained at several angles as the temperature of the sample approached the critical solution point.

In general, the power spectra exhibited good fit to a single Lorentzian curve. Deviations from Lorentzian behavior which were

observed could be attributed to instrumental limitations. The angular dependence of the spectral halfwidth appeared to be more closely represented by a plot of Γ vs K^2 rather than by a plot of Γ/K^2 vs K^2 , although there were definite indications of the presence of long range molecular interactions in the vicinity of the critical temperature. The diffusion coefficient was shown to exhibit the same temperature dependence that had been observed for polymer solutions and systems of small molecules in the vicinity of an upper critical solution point.

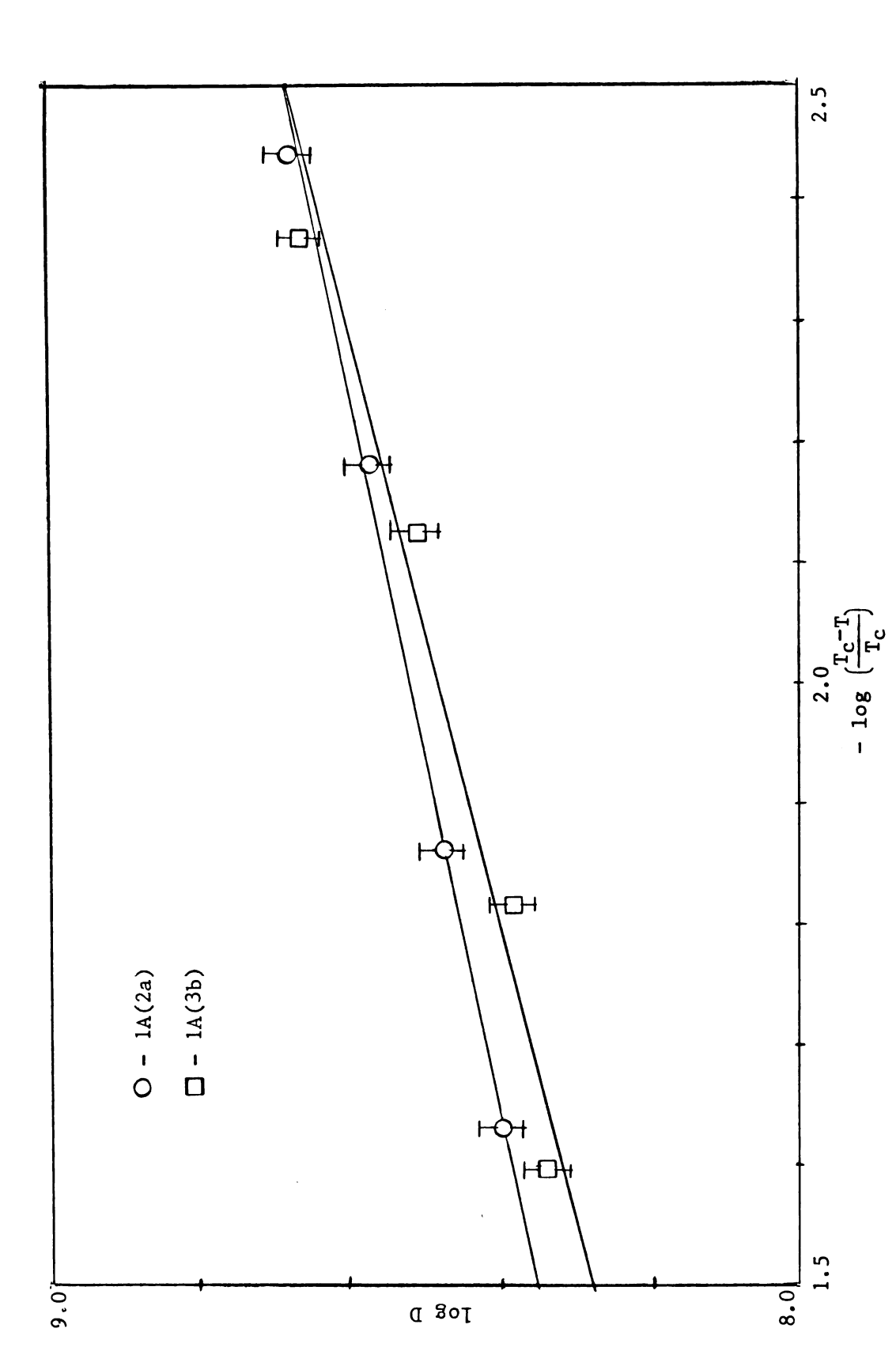


Figure 6.19 - Temperature Dependence of Diffusion Coefficient with Correction for Correlation Applied

CHAPTER VII

CONCLUSIONS

The results given in Figures 6.13, 6.14, and 6.15 indicate that the polyisobutylene/n-pentane systems which were studied exhibit Lorentzian behavior in the region of the critical solution point. Deviations from Lorentzian behavior were generally observed under conditions where instrumental contributions were important, i.e., at large scattering angles (greater than 30°) and in the higher frequency regions of the spectra (greater than $0.8 \rightarrow 1 \text{kHz}$) where the amplitude of the light-beating signal was low compared to detector shot-noise. Also, accurate measurements were difficult to obtain at very low scattering angles (150 or less) and at temperatures very near the critical point where the width of the light-beating spectrum approached the resolving power of the spectrometer. Hence, it is believed that the nonlinear behavior observed under these conditions (Figures 6.13, 6.14, and 6.15) was the result of instrumental factors and not a phenomenon characteristic of the scattering system. However, the questionable data should be re-examined under higher instrument sensitivity to clarify its interpretation. Methods for accomplishing this are discussed in the next section.

Binary diffusion coefficients for polyisobutylene/n-pentane system which were obtained from Figures 6.13 through 6.15 exhibited values

comparable to those reported for similar polymer/solvent systems 44. The critical exponents determined from the slopes of the log-log graphs exhibit a definite molecular weight dependence, as illustrated in Figure 6.16. The values for the lowest molecular weight fraction, 0.66, is comparable to that determined by Chu 18,19 for a polystyrene/cyclohexane solution of slightly lower molecular weight. The critical exponents for fractions 1A(2a) and 1A(3b) represent the first reported measurements of this type for high molecular weight polymer systems by this technique.

Comparison of Figures 6.17 and 6.18 with Figures 6.13 through 6.15 indicates that the data is more closely fit without the correction for long range correlation. In the strict sense, however, equation 2.18 is applicable only when the distance from the critical temperature is less than approximately 0.5° C, and ξ_{Γ} K<<1. It was generally observed that at temperatures closer to the critical point than those specified in Tables 6.3, 6.4, and 6.5, the light-beating spectra became unreliable due to fluctuating scattered intensity. For this reason more than half of the measurements had to be made at temperatures greater than $(T_{C}-T) = 0.5^{\circ}$ C. Similar investigations of a polystyrene/cyclohexane system by Chu^{19} were carried out from $(T-T_{C}) = 0.1^{\circ}$ C to $(T-T_{C}) = 5.0^{\circ}$ C, with good linearity exhibited out to $(T-T_{C}) = 0.75^{\circ}$ C.

Values for ξ_{Γ} and, consequently, $\xi_{\Gamma}K$ (Table 6.9) agree precisely with those determined by Chu for a system in which the effects of long range correlation were observed. Negative values for ξ_{Γ} observed at temperatures greater than $(T_{C}-T)=1^{\circ}C$ were also observed by Chu at $(T-T_{C})=1.50^{\circ}C$, and are indicative of the lack of correlation at these temperatures.

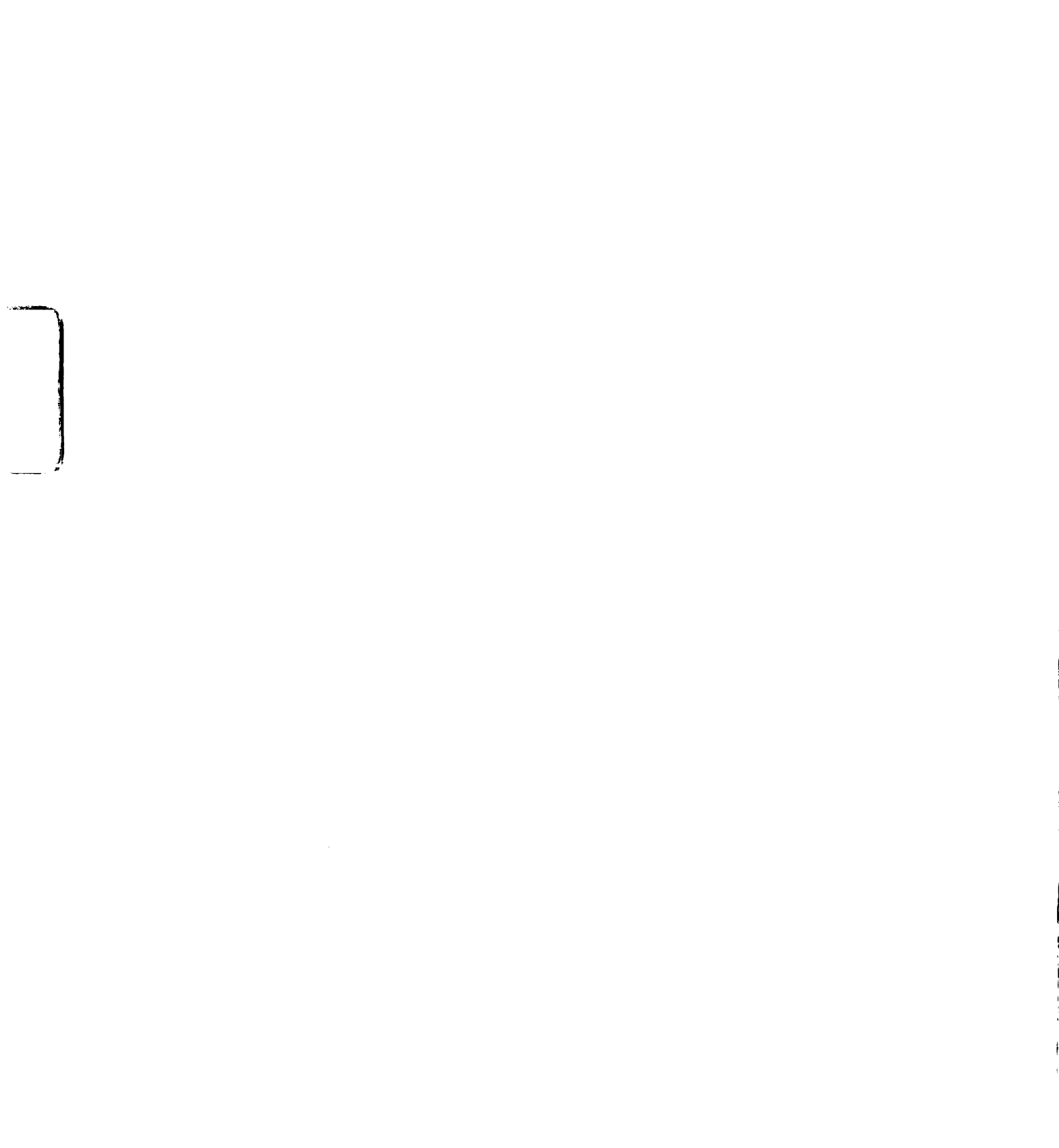
In conclusion, it is believed that long range molecular correlation is present at temperatures less than 1°C from the lower critical solution point for the systems studied, and that the correlation length increases as the critical temperature is approached and as the size of the polymer molecule increases. At temperatures greater than 1°C from the critical point, it is not believed that the effects of long range correlation were evident.

Suggestions for Future Research

It is difficult to obtain precise line broadening measurements for a high molecular weight polymer solution near a phase transition temperature because of the inherent polydispersity of the system. While the method of controlling the temperature of the sample described in Chapters III and IV was considered adequate, it was felt that the thermal lag which existed between the heating element and the sample was detrimental to precise, direct control of the samle temperature. It is believed that if the temperature control of the sample were improved by implementation of a thermostatic bath, and if a relatively less polydisperse system could be obtained, then the effects of long range correlation could be studied more conclusively.

It is recommended that the sensitivity of the spectrometer be improved and that the measurements made under conditions of low signal intensity be repeated. This can be accomplished by incorporating a more intense laser, by optimizing the beating efficiency, or by resorting to a heterodyning detection technique.

Conventionally, 15-20 mwatt lasers have been employed in lightbeating experiments, while the output power of the laser used in the



present study was only 4 mwatts. It is believed that incorporation of a more intense laser source would eliminate the problem of insufficient signal intensity without having to resort to methods 2 or 3 which are not as straight forward. However, when incorporating a more intense source, a high beating efficiency is still required to maintain a high signal to noise ratio at the detector. While stopping down the receiver slit increases the spatial coherence in the scattered light, and, hence, the beating-efficiency, it also reduces the amount of light reaching the detector. As previously mentioned, the optimum receiver slit width must be a compromise between the two considerations. However, the coherence length is a function of the angular spread in the scattered light (equation 3.1) so that coherence may be increased by a different choice or arrangement of optical components in the light collection system.

Resorting to a heterodyne detection technique should increase the signal-to-noise ratio significantly, although it would introduce other experimental difficulties discussed in an earlier chapter.

Furthermore, the light-beating power spectrum is obtained with the heterodyning technique rather than the square root of the power spectrum. Although the two spectra have the same shape, the former has half the width of the latter and measurements of extremely narrow spectra such as are found at the critical point would be more difficult.

It is also recommended that the method of data collection be modernized. This would involve incorporation of photon counting techniques with data analysis by an on-line computer, or as an

alternative, a multi-channel analyzer could be used. Either system would allow more rapid collection of data than can be obtained with a wave analyzer and recorder. Not only would the accuracy of measurements be improved because measurements are made over a shorter period of time, but also the difficulties associated with polymer sedimentation which were discussed earlier could be circumvented in that the time required to obtain a spectrum would no longer be a limiting factor. Furthermore, spectrum averaging techniques could be employed to eliminate noise and improve the accuracy of shape determination. Finally, with less time required for analysis of data, more time could be spent on the collection of data.

REFERENCES

- 1. Forrester, A.T., W.E. Parkins, and E. Gerjuoy, Phys. Rev., <u>72</u>, 728 (1947).
- 2. Griffith, L., Phys. Rev., 73, 922 (1948).
- 3. Gerjuoy, E., A.T. Forrester, and W.E. Parkins, Phys. Rev., 73, 922 (1948).
- 4. Forrester, A.T., R.A. Gudmundsen, and P.O. Johnson, Phys. Rev., 99, 1691 (1955).
- 5. Forrester, A.T., J. Opt. Soc. Amer., <u>51</u>, 253 (1961).
- 6. Cummins, H.Z., N. Knable, and Y. Yeh, Phys. Rev. Lett., 12, 150 (1964).
- 7. Ford, N.C., and G.B. Benedek, Phys. Rev. Lett., 15, 649 (1965).
- 8. Alpert, S.S., in <u>Proceedings of the Conference on Phenomena in the Vicinity of Critical Points</u>, National Bureau of Standards, Washington, D. C., April, 1965.
- 9. Rimai, L., J.T. Hickmott, T. Cole, and E.B. Carew, Biophys. J., 10, 20 (1970).
- 10. Dubin, S.B., N.A. Clark, and G.B. Benedek, J. Chem. Phys., <u>54</u>, 5158 (1971).
- 11. Schaefer, D.W., and G.B. Benedek, J. Chem. Phys., 55, 3884 (1971).
- 12. Cummins, H.Z., F.D. Carlson, T.J. Herbert, and G. Woods, Biophys. J., 9, 518 (1969).
- 13. Dubin, S.B., J.H. Lunacek, and G.B. Benedek, Proc. N.A.S., <u>57</u>, 1165 (1967).
- 14. Pecora, R., J. Chem. Phys., 43, 1562 (1965).
- 15. Ford, N.C., and G.B. Benedek, in <u>Proceedings of the Conference on Phenomena in the Vicinity of Critical Points</u>, National Bureau of Standards, Washington, D. C., April, 1965.
- 16. Debye, P., Phys. Rev. Lett., 14, 783 (1965).
- 17. White, J.A., J.S. Osmundson, and B.H. Ahn, Phys. Rev. Lett., 16, 639 (1966).

- 18. Chu, B., N. Kuwahara, and D.V. Fenby, Phys. Letters, 32A, 131, (1970).
- 19. Kuwahara, N., D.V. Fenby, M. Tamsky, and B. Chu, J. Chem. Phys., 55, 1140 (1971).
- 20. Landau and Lifschitz, <u>Fluid Mechanics</u>, Addison-Wesley Publishing Co., Inc., Reading, Mass., 1959, 226.
- 21. Landau and Lifschitz, <u>Statistical Physics</u>, Addison-Wesley Publishing Co., Inc., 1958.
- 22. Prigogine, I., and R. Defay, <u>Chemical Thermodynamics</u>, Longmans Green and Co., London, 1954.
- 23. Jacobs, M.H., <u>Diffusion Processes</u>, Springer-Verlag New York, Inc., New York, 1967, 96.
- 24. Chu, B., and F. Schones, J. Coll. and Interface Sci., <u>27</u>, 424, (1968).
- 25. Kittle, C., Elementary Statistical Physics, Wiley and Sons, New York, 1958, 136.
- 26. Cummins, H.Z., and H.L. Swinney, in <u>Progress in Optics</u>, Vol. VIII, E. Wolf, ed., North Holland Publishing Co., Amsterdam, 142.
- 27. Landau and Lifschitz, <u>Electrodynamics of Continuous Media</u>, Addison Wesley, New York, 1966, 392.
- 28. Chu, B., Phys. Rev. Lett., 18, 200 (1967).
- 29. Orstein, L.S., and F. Zernike, Proc. Roy, Acad. Sci Amsterdam, 17, 793 (1914).
- 30. Debye, P., Electromagnetic Scattering, ed. by M. Kerker, MacMillan & Co., New York (1963).
- 31. Landau, L., and G. Placzek, Physik Z. Sowjetunion, 5, 172 (1934).
- 32. Fixman, M., Pontifica Academia Scientarium Scripta Varia 31 on the Molecular Forces, Pontifical Academy of Science, Vatican City, Italy, 329 (1966).
- 33. Felderhof, B.U., J. Chem. Phys., 44, 602 (1966).
- 34. Kadanoff, L.D., and J. Swift, Phys. Rev., 166, 89 (1968).
- 35. Widom, B., J. Chem. Phys., 39, 842 (1963).

- 36. Klein, M.V., Optics, J. Wiley & Sons, New York, 1970, 272.
- 37. Sorenson and Campbell, Preparatory Methods of Polymer Chemistry, Interscience Publishing Co., 2nd ed., 1966, 266.
- 38. Thomas, R.M., W.J. Sparks, P.K. Frolich, M. Otto, and M. Mueller-Cunradi, J.A.C.S., <u>62</u>, 276 (1940).
- 39. Kamide, K., and C. Nakayama, Makromolekulare Chem, 129, 289 (1969).
- 40. Kamide, K., T. Ogawa, and C. Nakayama, Ibid., 135, 9 (1970).
- 41. Kamide, K., K. Sugamiya, T. Ogawa, C. Nakayama, N. Buba, Ibid., 135, 23 (1970).
- 42. Koningsveld, R., and A.J. Staverman, J. Polymer Sci., 6, Part A-Z, 367 (1968).
- 43. Kamide, K., T. Ogawa, C.Nakayama, and T. Kawai, Bull. Chem. Soc. Japan.
- 44. Brandrup, J., and E.H. Immergut, Polymer Handbook, Interscience Publishers, New York, 1966, IV-163.
- 45. Ibid, IV-2.
- 46. Fox, T.G., J.C. Fox, and R.J. Flory, J.A.C.S., 73, 1901 (1951).
- 47. Miller, G.A., I. San Fillipo, and D. Carpenter, Macromolecules, 3, 125 (1970).
- 48. Miller, G.A., and C.S. Lee, J. Phys. Chem., 71, 2305 (1967).
- 49. Gaumer, S.J., Doctoral Thesis, Michigan State University, Dept. of Chemistry, 1972.
- 50. McCoy, J.H., Doctoral Thesis, Michigan State University, Dept. of Chemistry, 1963.
- 51. Stamm, R., J. Opt. Soc. Amer., <u>40</u>, 788 (1950).
- 52. Dye, J., and V.A. Nicely, J. Chem. Ed., 48, 443 (1971).
- 53. Lee, S.P., W.Tscharnuter, and B. Chu, J. Polymer Sci., 10, 2453 (1972).
- 54. Dubois, M., and P. Berge, Phys. Rev. Lett., 26, 121 (1970).

APPENDICES

RESTEM

```
PROGRAM RESTEM (INPUT, OUTPUT, TAPE 60=INPUT, TAPE 61=OUTPUT)
           100 FORMAT (F7.4, F9.7, F5.3)
           101 FORMAT (F7.4)
           102 FORMAT (F10.4,5X,F6.3)
5
                READ (60,100) RO, ALPHA, DELTA
                A = 0.0001492
               B = 1.01492
             1 READ (60,101) RT
               KOUNT = 1
10
                C = (RT - RO) / (ALPHA*RO)
                T = (-B - SQRT (B**2 - 4.0*A*C)) / (2.0*A)
               WRITE (61,102)RT,T
                KOUNT = KOUNT + 1
                IF (KOUNT .LE. 28) GO TO 1
15
                STOP
                END
```

TEMF

```
PROGRAM TEMF (INPUT, OUTPUT, TAPE 60 = INPUT, TALE 61 = OUTPUT)
    DIMENSION X1 (6500), X2 (6500)
    ITIME \neq 0
    DP 1 IT = 1,6500,1
     ITIME = ITIME + 1
    T = 20.00 + FLOAT (IT) / 100
    E = 0.243969E-01 + 0.367094E-01*T + 0.674673E-04*T**2
    *- 0.147089E-10*T**5
    X1(IT) = T
 1 \quad X2(IT) = E
    WRITE (61,100) (X1 (I), X2 (I), I = 1, ITIME)
100 FORMAT (F5.2,2X,F6.4,4X,F5.2,2X,F6.4,4X,F5.2,2X,F6.4,4X,F5.2,2X,
     *F6.4,4X,F5.2,2X,F6.4,4X,F5.2,2X,F6.4,4X,F5.2,2X,F6.4,4X,F5.2,2X,
     *F6.4,4X)
     STOP
    END
```

EMFFT

```
PROGRAM EMFFT (INPUT, OUTPUT)
    DIMENSION T(100), E(100), X (6.100), W(100), A(7,7), SIGMA (7), B(7),
    1Y (100), DEV (100)
2 READ 10, NOPT
10 FORMAT (15)
    IF (NOPT.EQ.0) GO TO 1
    DO 3 I = 1, NOPT
    READ 20, T(I), E(I)
20 FORMAT (F6.3, F7.4)
3 CONTINUE
   PRINT 30
30 FORMAT (1HI)
   PRINT 40
40 FORMAT (*,*,*TEMPERATURE*,3X,*EMF*)
    DO 4 I = 1, NOPT
   PRINT 50, T(I), E(I)
4 CONTINUE
50 FORMAT (*,*,F10.4,2X,F10.4)
   DO 5 K = 1, NOPT
    X(1,K) = T(K)
    X(2,K) = T(K) * T(K)
    X(3,K) = T(K) * T(K) * T(K)
    X(4,K) = T(K) * T(K) * T(K) * T(K)
    X(5,K) = T(K) * T(K) * T(K) * T(K)
    X(6,K) = E(K)
   W(K) = 1.0
 5 CONTINUE
   N \doteq 6
   M = NOPT
    NPLUS = 7
    CALL MULTREG (X,W,N,M,NPLUS,A,SIGMA,B,SB,Y,DEV,IPRINT)
    GO TO 2
 1 CONTINUE
    END
```

